LBL-6824
c.2

Energy and Environment Division

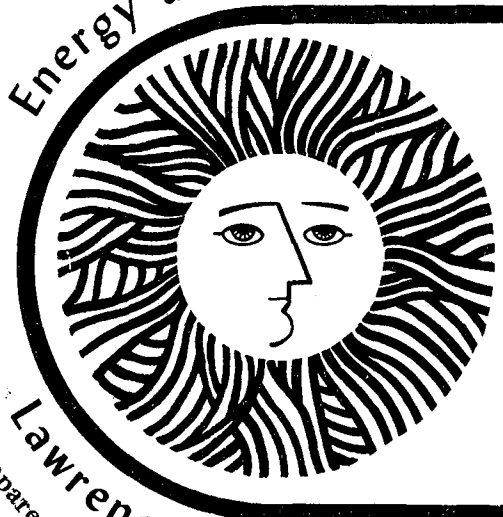

Stochastic Acceleration By A Single Wave In A Magnetized Plasma

Gary Richard Smith

Ph.D. Thesis

September 22, 1977

Lawrence Berkeley Laboratory University of California/Berkeley

Prepared for the U. S. Energy Research and Development Administration under Contract No. W-7405-ENG-48

LBL-6824
c.2

Stochastic Acceleration by a Single Wave in a Magnetized Plasma

Gary Richard Smith

Department of Physics and
Lawrence Berkeley Laboratory,
University of California,
Berkeley, CA 94720

September 22, 1977

ABSTRACT

Simple dynamical systems displaying complicated behavior are found in fields as diverse as biology, fluid dynamics, and space physics. In plasma physics a number of problems exhibit stochastic motion which is attributed to the overlap of resonances. These problems include superadiabaticity in mirror machines, destruction of maghetic surfaces in toroidal systems, and lower hybrid heating.

A particularly simple problem exhibiting stochasticity is the motion of a charged particle in a uniform magnetic field and a single wave. Our detailed studies of this wave-particle interaction show the following features. An electrostatic wave propagating obliquely to the magnetic field causes stochastic motion if the wave amplitude exceeds a

certain threshold. The overlap of cyclotron resonances then destroys a constant of the motion, allowing strong particle acceleration. A wave of large enough amplitude would thus suffer severe damping and lead to rapid heating of a particle distribution. The stochastic motion resembles a diffusion process even though the wave spectrum contains only a single wave.

The motion of ions in a nonuniform magnetic field and a single electrostatic wave is treated in our study of a possible saturation mechanism of the dissipative trapped-ion instability in a tokamak. A theory involving the overlap of bounce resonances predicts the main features found in our numerical integration of the equations of motion. Ions in a layer near the trapped-circulating boundary move stochastically. This motion leads to nonlinear stabilization mechanisms which are described qualitatively.

Work performed under the auspices of the U. S. Energy Research and Development Administration.

Acknowledgments

My thesis adviser, Allan Kaufman, inspired me to enter plasma theory by means of his clear classroom presentations of the basic material. During this research his many good ideas and constant encouragement have been of great value.

Thanks are also due to Wulf Kunkel for his leadership of the fusion research program at Lawrence Berkeley Laboratory and for his assistance and instruction at many stages of my graduate career. Charles Birdsall supervised my education in plasma simulation which helped greatly in developing a physical understanding of plasma phenomena.

Several young physicists aided the development of my ideas. Particularly helpful were extensive discussions of my work with John Krommes, Nino Pereira, and Bruce Cohen. In addition, the following people gave time to listen and contribute to my work: Dwight Nicholson, Mike Mostrom, Shayne Johnston, Bill Nevins, Harry Mynick, Jim **Hammer, John Cary, and Bill Sharp.**

Barbara Moog skillfully typed all of the equations in the thesis. Assistance with other typing jobs was provided by Georgella Perry, Chris Graham, Dessa Bucksbaum, and Valerie Kelly.

For her interest in my daily activities and her unflagging moral support, I am especially grateful to my wife, Peg.

Table of Contents

1. Introduction

A. Overlapping resonances, destruction of constants of the motion, divergence of neighboring trajectories, stochastic motion

Problems in which only one resonance occurs are well known in physics. An example in plasma physics is the one-dimensional motion of an electron in a Langmuir wave, in which the resonance condition is $\omega = kv$. Here, as elsewhere in this thesis, a particle is in resonance if it maintains its phase relation in the wave. Exact solutions for the motion of such systems can be found in general. O'Neil[1] wrote down the equations describing the motion of an electron in a Langmuir wave of given amplitude and frequency and used those equations to study the Landau damping of the wave. More recent work[2] has attempted to incorporate the amplitude and frequency shifts of the wave and calculate the evolution of the wave and the motion of the electrons self-consistently. We ignore the problem of self-consistency (the problem actually does not occur in the situations mentioned in Section 2A); we study instead the extremely complicated motion which occurs when multiple resonances overlap.

The presence of multiple resonances which do <u>not</u> overlap does not lead to fundamental complications. Near each resonance the motion is similar to the motion found in a problem with only one resonance. The "far away" resonances produce high-frequency oscillations in the motion, which are unimportant in the problems we treat.

When two or more resonances overlap (the criterion for overlap

will be discussed in Section 2F), the motion changes qualitatively and becomes incredibly complicated. Numerical solutions of the motion of such systems show a complexity which clearly cannot be described analytically; we cannot write, for example, an equation describing the evolution of a distribution of particles when two resonances overlap.

One characteristic of systems with overlapping resonances is the destruction of constants of the motion. As resonances grow wider and overlap, constants which restrict the motion to a certain space disappear, allowing motion in a space of higher dimension. For example, particles restricted to move on a two-dimensional surface in phase space might move on a three-dimensional surface when resonances overlap. The entropy and energy of a set of particles may then change in time irreversibly, as we will demonstrate in Section 2J. In this work we use extensively the characteristic of destruction of constants of the motion.

Another characteristic of systems with overlapping resonances is the divergence of neighboring trajectories. Roughly speaking, trajectories initially close together in phase space are found[3] to separate in time linearly if resonances do not overlap but exponentially if they do overlap. Zaslavskii and Chirikov[4] (page 558) point out that this local instability is neither a necessary nor a sufficient condition for the destruction of constants of the motion. We have made little use of the divergence of neighboring trajectories.

The term which has come into use to describe motion in the presence of overlapping resonances is "stochastic." This term generally

means "random" or "almost random." For the systems we will treat, the motion is more precisely described as "pseudorandom", since differential equations without randomness determine the motion, but a very slight change in initial conditions leads to a large change in the conditions (referred to as "final") at a later time. When almost all initial conditions are unstable in this way, the motion tends to be mixing,[4] and correlations between initial and final conditions decay rapidly. Initial conditions, which are never known precisely in reality, cannot predict final conditions, and the motion is therefore random in practice.

B. Synopsis of thesis

In this thesis we describe several problems involving stochastic motion, and we treat in detail two such problems which are of interest in plasma physics. In Section 1C, we discuss (in Subsections 1 through 5) problems involving stochasticity which are of direct interest to the magnetic fusion energy program. In Subsection 1C6 we describe some of the problems which have interested researchers in stochasticity theory since the important work by the astronomers Hénon and Heiles in 1964. In Subsection 1C7 we write the Hamiltonian of a very general oscillator system and show how it relates to our specific problems. Section 1C ends with a discussion of the possible implications of stochasticity for the foundations of statistical mechanics. Section 1D mentions the striking behavior observed in some dissipative systems which arise in fields far removed from plasma physics.

Chapters 2 and 3 of the thesis treat the first of our specific problems, the overlap of cyclotron resonances. Sections 2A, 2B, and 2C introduce the problem and the variables we use. In Section 2D we find some results which are valid when resonances do <u>not</u> overlap. In Section 2E we find the behavior, in certain limits, of quantities which we later study numerically; the behavior is the same whether resonances overlap or not. In Section 2F we apply a simple analytical criterion for the onset of stochasticity. To prepare for the description of our numerical results we discuss the method of numerical integration (in Section 2G), some related Hamiltonian systems (Section 2H), and the surface of section method (Section 2I). Section 2J discusses our

numerical results, and in Section 2K we further illuminate some of those results by studying a mapping. Section 2L discusses some electrostatic waves which could cause strong ion acceleration due to the overlap of resonances. Section 2M calculates the distortion of the tail of a Maxwellian distribution in the presence of such a wave. In Chapter 3 we discuss some theoretical ideas bearing upon an analytic description of the diffusion process observed in Chapter 2. Section 3D contains the conclusions of our study of the overlap of cyclotron resonances.

Chapter 4 treats the second of our specific problems, the motion of an ion in the presence of a trapped-ion mode in a tokamak. Sections 4A and 4B introduce the problem and the variables we use. In Section 4C we obtain a simplified model for ion motion in a tokamak in the absence of the mode. Section 4D contains the full Hamiltonian which we study, and Section 4E mentions several other problems described by the same Hamiltonian. In Section 4F we again apply the simple stochasticity criterion. Section 4G discusses the results of our numerical integrations of this problem. In Section 4H we relate our work to that of some other authors. The implications of stochastic motion for the saturation of the trapped-ion instability are treated in Section 4I. Section 4J contains the conclusions of Chapter 4.

The supplementary material includes appendices, references, a list of first authors referenced, tables, figures, and their captions.

Note on the numbering of sections and equations. Sections of this thesis are referred to by giving the number of the chapter followed by the section number. For example, Section 2F refers to section F of Chapter 2. For subsections we append the number of the subsection (e. g., Subsection 1C7). Equation numbers appear in parentheses. The number of the equation is preceded by a period and the number of the chapter in which it appears. The chapter number is omitted if the equation and the reference to it appear in the same chapter. For example, a reference to equation (2.7) appears as (7) within Chapter 2.

C. Problems involving stochastic motion

Stochastic motion, caused by overlapping of resonances, occurs in many physical problems. Some of these problems occur in plasma physics, where stochastic effects have importance for the fusion program (and possibly also for space physics). In this section we mention some of the problems involving overlap of resonances, to indicate areas of possible application of the ideas discussed later.

1. Particle in a magnetic field perturbed by an obliquely propagating wave

A very basic concept in plasma theory is the interaction between a wave and a charged particle. A strong interaction occurs if the particle is in resonance with the wave. In an unmagnetized plasma, in which a single sinusoidal wave is propagating, the resonance condition is $\omega = \underline{k}\cdot\underline{v}$, where ω is the wave frequency, $\underline{k}$ is the wave vector, and $\underline{v}$ is the particle's velocity. We write the condition for resonance as

$$\omega = \dot{\phi}_1 + \dot{\phi}_2 + \dot{\phi}_3 \ , \tag{1}$$

where the three frequencies $\dot{\phi}_i$ are $k_i v_i$. A qualitative change in the resonance condition occurs when a magnetic field is applied to the plasma. Now the resonance condition is

$$\omega = \ell_1\dot{\phi}_1 + \ell_2\dot{\phi}_2 + \ell_3\dot{\phi}_3 \ , \tag{2}$$

where ℓ_i denotes any integer and the frequencies $\dot{\phi}_i$ have more complicated forms than before. From (1) and (2) we see that the

magnetic field allows resonance to occur for values of ℓ_i other than $\ell_1 = \ell_2 = \ell_3 = 1$. The existence of these multiple resonances is crucial for the stochastic effects discussed in this work.

a. Overlap of cyclotron resonances

The simplest magnetic field in which we can study overlap of resonances is a uniform, magnetostatic field $\underline{B} = B_o \hat{z}$. In this case, the resonance condition (2) becomes

$$\omega = k_z v_z - \ell\Omega \quad , \tag{3}$$

where $\Omega \equiv eB_o/mc$ is the cyclotron (or gyro-) frequency of the particle of charge e and mass m, and ℓ is any integer. The resonances (3) are responsible for cyclotron-harmonic[5] (or gyro-resonant) damping and growth of waves in a uniformly magnetized plasma. Cyclotron-harmonic waves, which are called Bernstein[6] waves in the limit $k_z \to 0$, owe their existence to the resonances (3). Chapter 2 is devoted to a detailed treatment of the motion of a particle in the presence of overlapping cyclotron resonances.

b. Overlap of bounce resonances

In a magnetic field with nonuniformity along a field line new effects arise because a particle can bounce between magnetic mirrors. Sometimes the frequency ω_b of bouncing is comparable to the wave frequency ω but both are much less than the gyrofrequency Ω. Then resonance condition (2) reduces to

$$\omega = n\omega_b \quad , \; n = 1, \; 2, \; 3, \; \ldots \quad . \tag{4}$$

These resonances are important in the theory of trapped-particle instabilities[7] in tokamaks. Chapter 4 contains a study of the motion of a particle in the presence of overlapping bounce resonances. Many other problems of current interest, which we discuss in Section 4E, involve the overlap of bounce resonances.

2. Magnetic moment jumps, superadiabaticity, and Arnold diffusion

An approach to thermonuclear fusion, initiated in the early years of the program, is to confine plasma in a magnetic mirror machine. A minimum requirement for this approach to be useful is that individual ions be confined long enough to have an opportunity to undergo a fusion reaction. In modern mirror machines the escape of an ion represents a loss of plasma density and energy content which must be replaced by injection of an energetic atom. If ions are lost too quickly, a given injection capability will be able to maintain too low a density and temperature, or for a given thermonuclear output too large an injection facility (and therefore an uneconomic value of Q = thermonuclear output power / injected power) will be required.

Mirror machines are in the class of open magnetic confinement systems in which the plasma (or at least some of it in a field-reversed mirror) is on magnetic field lines which lead directly to the walls of the machine. The regions of large magnetic field (the mirrors) prevent ions from moving along the field lines as long as the magnetic moment μ

is conserved. The magnetic moment, defined in terms of the magnitude B of the field $\underline{B}$ and the velocity $v_\perp$ perpendicular to $\underline{B}$ by $\mu \equiv \frac{1}{2} m v_\perp^2/B$, can change for several reasons. Changes caused by Coulomb collisions are reduced as the temperature is raised. Changes caused by fluctuating electric fields can be reduced by suppressing the instabilities which lead to the fluctuating fields. Even if these changes are reduced to a negligible level, the magnetic moment still suffers changes because it is not an exact constant of the motion in a nonuniform magnetic field.

The changes suffered by the magnetic moment take the form of sudden jumps which occur in some, but not all, field configurations at the points of minimum magnetic field. As shown in Fig. 1, a plot of μ vs. time also shows rapid oscillations which are largest when the particle is near a point where a jump occurs. Fig. 1 is strikingly similar to behavior seen in our Fig. 21 for the problem of overlap of cyclotron resonances. In Section 2J we ascribe the jumps to constructive interference of terms in the equations of motion. Fig. 1 is strong evidence that constructive interference occurs for a particle moving in a nonuniform magnetic field. The utility of our constructive interference picture and its relation to other pictures of the jumps in μ can be decided only by further research.

Kruskal[8] showed that the magnetic moment can be redefined so that it is conserved to all orders in a small parameter ε, which measures, roughly speaking, the particle's energy and the nonuniformity of the field. Changes of μ proportional to $\exp(-C/\varepsilon)$, where C is

a constant, are not ruled out by theory and have been observed in numerical calculations[9,10] of particle trajectories performed over a period of almost twenty years. The magnitude of the jumps in the magnetic moment can now be calculated analytically[10] very accurately.

Jumps in μ sufficiently large to cause loss of a deeply trapped ion are of course serious, but moderate changes of μ do not, by themselves, imply serious loss of particles from a mirror machine. Successive changes might be correlated so that the magnetic moment would remain near its initial value for all time. Such <u>eternal</u> confinement of a particle in an <u>exactly</u> axisymmetric machine was proved rigorously by Arnold[11] for sufficiently small values of ε. Arnold's theorem does not say how small ε must be, but Chirikov[12] used the criterion of overlapping resonances to find an expression for ε below which eternal confinement could be expected. He found fair agreement between his expression and both a computer[9] and a laboratory[13] experiment. Coulomb collisions, ignored in Ref. 11, prevent strictly eternal confinement in a mirror machine, but in a thermonuclear plasma collisional diffusion may be negligibly slow.

The word "superadiabaticity" refers to the eternal confinement discussed above. The correlations necessary for superadiabaticity can be destroyed by nonuniformity of the magnetic field (too large an ε) or by fluctuating electric fields resulting from instabilities. Using a very simple model, Rosenbluth[14] found the amplitude of fluctuating fields necessary to prevent superadiabaticity and guessed that a mirror reactor might be in the superadiabatic regime. For fluctuating fields

of much higher amplitude, Aamodt and Byers[15] observed a transition back to superadiabaticity by numerically calculating particle trajectories. Timofeev[16] reviewed the work on the effect of fluctuating fields on particle motion and concluded that stochastic motion occurs for moderate fluctuation levels but not for low or high levels. To our knowledge, no comparison has appeared in the literature of the superadiabaticity conditions determined by nonuniformity of the magnetic field and by fluctuating electric fields.

Jaeger, Lichtenberg, and Lieberman[17] and Lieberman and Lichtenberg[18] studied the heating of electrons in a mirror machine by application of an electromagnetic field resonant with the electron gyrofrequency. They found the motion of electrons to be stochastic, leading to higher and higher energies until an adiabatic barrier (analogous to the superadiabaticity conditions mentioned above) was reached which prevented further energy increase. Related work on radio-frequency plugging of a mirror machine was done by Lichtenberg and Berk.[19]

If collisional diffusion is negligible and superadiabaticity conditions are satisfied, good confinement in an axisymmetric mirror machine can be expected. An asymmetric machine has worse confinement because Arnold diffusion can occur. Chirikov[20] has studied this little-known process in considerable detail and predicts a sharp increase in diffusion rates as ϵ is increased. His estimates do not contradict the results of an experiment[21] showing an abrupt decrease in the confinement time of electrons as ϵ is increased. Since

asymmetry is required in mirror machines to prevent MHD instabilities, research on the unavoidable process of Arnold diffusion seems desirable.

3. Destruction of magnetic surfaces in toroidal systems

The major approaches to thermonuclear fusion by means of magnetic confinement include both open and closed systems. In closed systems magnetic field lines in the region occupied by the plasma hopefully remain always within the plasma. Unavoidable errors in coil construction, which allow field lines to reach the walls of the vacuum chamber, are hopefully small enough that the macroscopic behavior of the plasma is not seriously degraded. The errors allow particles, which move along field lines easily, to strike the walls of the chamber, thereby being lost to the plasma and also releasing impurities from the walls into the plasma.

Toroidal systems, of which the tokamak is the most important example, are usually treated theoretically under the assumption that the errors in coil construction are negligible. The field lines then generate a set of nested toroidal magnetic surfaces, except where a field line happens to connect up on itself.

Destruction of these surfaces (also known as magnetic braiding or stochasticity of field lines) by coil construction errors is due to the overlap of resonances. This phenomenon has been studied for stellarators with[22] an Ohmic heating current and without[23-25] such a current and for a levitron[26-28] (also known as a spherator). Very

small errors can often cause large-scale destruction of magnetic surfaces. In Ref. 26, for example, a tilt of the levitated ring by 0.1° was found to be a serious error.

In Ref. 28 on the FM-1 spherator, spatial variations in the plasma density were shown to result from construction errors in the levitated ring. The current in the ring was not centered at exactly the same point in the ring's cross section for different azimuthal angles; the center of the current distribution deviated by at most 30 mils (less than one millimeter), but these errors led to density variations up to 30%. The density variations were attributed to the presence of wide magnetic islands, which allowed rapid radial transport of particles and heat along field lines. Each chain of magnetic islands results from a single resonance. If different chains of islands (multiple resonances) overlap, destruction of magnetic surfaces results. In Ref. 28 destruction of surfaces was not thought to be a prevalent effect.

In the absence of coil construction errors destruction of magnetic surfaces can still occur because of current perturbations in the plasma. The current perturbations grow to large amplitudes because of instabilities of certain plasma modes. These modes include internal kink modes (described either by ideal MHD[29] or by resistive[30] equations) and tearing modes (which also occur in several collisionality[31] regimes).

In Fig. 2 we have sketched tokamak magnetic surfaces in a poloidal cross section (i. e., at a particular toroidal angle). In Fig. 2a we show the magnetic surfaces in the absence of current

perturbations. The nested toroidal surfaces are represented by concentric circles, each labeled by the value of the safety factor q on the surface. (On the surfaces for which q is rational [for example, q=2], a field line connects up on itself [after two circuits around the torus the long way and one the short way], and, strictly speaking, the line does not generate a surface.) In Fig. 2b we show the magnetic surfaces when current perturbations are present near the minor radii where q=2 and 3. Note the formation of chains of islands near those radii.

Finn[32] has studied the hypothesis that the very serious disruptive instability observed in tokamak experiments[33] is caused by destruction of magnetic surfaces. He computed the trajectories of field lines in a tokamak (modeled as a cylinder) in the presence of certain perturbations: two current perturbations with different poloidal mode numbers or one current perturbation interacting with the poloidal variation of the toroidal field. In the former case, the intensity of the two current perturbations necessary for destruction of surfaces was found to be comparable to intensities thought to be present just prior to the disruptive instability. Stix[34,35] has expressed ideas very similar to those of Finn.[32] Recently, Finn[36] has pointed out the difficulty of satisfying the instability conditions for two tearing modes with different poloidal mode numbers in a given discharge. The tearing instability is thus unlikely to produce two island chains which can overlap, but Finn[36] has studied an otherwise stable tearing mode with poloidal mode number m=3 which is <u>driven</u> to large amplitudes by coupling to an unstable m=2 mode.

Rechester and Stix[37] studied the destruction of magnetic surfaces when tearing modes with m=2 and 3, for example, have amplitudes too low to cause overlap of their magnetic islands. In this case, the destroyed surfaces are the ones represented in Fig. 2b by the moon-shaped outer contours of the islands near q=2. These surfaces are destroyed by the overlap of bounce resonances, in complete analogy with the problem studied in Chapter 4. Rechester and Stix[37] found, for appropriate tokamak parameters, that the area of the islands near q=2 effectively shrinks by 30% as a result of destruction of the outer contours of the islands.

The destruction of magnetic surfaces allows rapid radial transport in the parts of the plasma cross section where resonances overlap. Besides causing expansion of the plasma column and flattening of the temperature profile, this transport tends to eliminate the current perturbations which caused the destruction of surfaces in the first place. Thus stochasticity of field lines in a plasma tends to be self-limiting, as pointed out by Stix.[34] We can thus expect current perturbations to hover near the intensities necessary for the onset of stochasticity. At these intensities the trajectories of field lines are more difficult to treat analytically than either of the cases of very weak or very strong stochasticity.

Theoretical calculations of the trajectories of field lines begin with the equations giving the directions of a field line:

$$dr/d\zeta = RB_r/B_\zeta \tag{5a}$$

$$d\theta/d\zeta = RB_\theta/rB_\zeta \ . \tag{5b}$$

Here, r measures the distance from the magnetic axis of a large-aspect-ratio tokamak, θ is the poloidal and ζ the toroidal angle. R is the distance from the axis of symmetry to the point (r,θ,ζ). The right sides of (5) are functions of r,θ,ζ and are periodic in θ and ζ. Equations (5) thus have the form

$$\dot{r} = \sum_{m,n} F_{mn}(r) \exp i(m\theta - n\zeta) + c.c. \tag{6a}$$

$$\dot{\theta} = \sum_{m,n} G_{mn}(r) \exp i(m\theta - n\zeta) + c.c. , \tag{6b}$$

where the dot denotes differentiation with respect to ζ. The toroidal angle ζ takes the place of the usual time variable; ζ is the independent variable in the set (6) of two coupled ordinary differential equations for the dependent variables r and θ. Equations (6) have the same form as the Hamiltonian equations which we study in detail in this thesis, but (6) are not derivable, in general, from a Hamiltonian. Hamiltonians describing trajectories of field lines were used for an axisymmetric field[27] and for a special, helically symmetric model for a stellarator field.[24] It seems impossible, however, to describe an arbitrary magnetic field in terms of a single scalar function (the Hamiltonian).

In the absence of current perturbations, all coefficients F_{mn} and G_{mn} are zero except $G_{oo} = 1/2q$, so (6) reduces to

$$\dot{r} = 0, \quad \dot{\theta} = 1/q(r).$$

Of all the terms representing the perturbations, the <u>resonant</u> terms in (6) are those that vary slowly with ζ, that is, those for which

$$m\dot{\theta} - n \approx m/q(r) - n \approx 0 \quad .$$

Determining[27,32] the width (in r) of the resonances and their

separation, one derives a criterion for overlap of the magnetic islands due to current perturbations. Overlap of the islands implies destruction of magnetic surfaces near the chosen r.

The status of work on the disruptive instability at present seems to be the following. It is well established by the theoretical work of Finn[32] and the experimental work of Karger, et al.[38] (in which the disruption was induced by currents in external helical coils), that overlap of magnetic islands is involved in the disruptive instability. It is not yet clear, however, what physical processes lead to the observed islands or how to predict the maximum size of the islands theoretically.

4. Lower hybrid heating

A charged particle may move stochastically in an obliquely propagating ($k_z \neq 0$) wave, as mentioned in Subsection 1B1 and shown by detailed studies in Chapters 2 and 4. Stochastic motion may also occur for a wave which propagates perpendicularly ($k_z = 0$) to a uniform magnetic field. We give in Appendix A the equations describing the transition between oblique and perpendicular propagation. Here we review the work which has studied the possibility of stochastic effects in lower hybrid heating of a tokamak.

Karney and Bers[39] have numerically integrated the equations of motion for an ion in a perpendicularly propagating wave of frequency ω. A rapid increase in the ion's energy occurs if the perpendicular

velocity $v_\perp \lesssim \omega/k$. Ref. 39 interprets this increase as due to trapping by the wave during a time short compared to a gyroperiod. For larger perpendicular velocities a transition to stochastic motion is observed as the wave amplitude is increased. When stochasticity occurs, ions in the tail of the perpendicular distribution can be accelerated to high energies by the wave.

Fukuyama, et al.[40] have studied, both analytically and numerically, the motion of an ion in a wave with frequency ω close to a harmonic $L\Omega$ of the gyrofrequency. In a wave of small amplitude the perpendicular velocity of an ion is confined between values at which $kv_\perp/\Omega$ is a zero of the Bessel function J_L.[41] Ref. 40 shows, as was speculated in Ref. 16, that this confinement is spoiled when the wave amplitude becomes large. Ion motion becomes stochastic because of the overlap of certain resonances, and ions are accelerated to high perpendicular velocities. The analytical methods used in Ref. 40 are very similar to those used by us in Chapter 4.

5. Applicability of quasilinear and resonance broadening theory

In plasma physics one often uses quasilinear theory or its "renormalized" version, resonance broadening theory, to describe the interaction between particles and a spectrum of waves. A check of the most fundamental requirement for validity of these theories is rarely done, however. This requirement is that a set of resonances overlap.

Quasilinear and resonance broadening theory both describe

evolution of a distribution function using a diffusion equation. This description is always valid if the spectrum is continuous. In reality, however, there are always boundary conditions which make the spectrum discrete; the separation between resonances is non-zero. If the energy in the wave spectrum is great enough, the resonances may be wide enough to overlap each other. Then a diffusion equation is likely to be a good description. On the other hand, if the wave spectrum contains insufficient energy to cause overlap of resonances, a constant of the motion will exist which prevents diffusion. In this case, completely erroneous results would be obtained by using quasilinear or resonance broadening theory. This point has been made also by Tetreault.[42]

Since the onset of stochasticity marks a radical change in the behavior of a system, it seems likely to us that systems will be found to hover in the vicinity of the stochastic threshold. For example, the energy in a wave spectrum would be sufficient to make resonances overlap marginally. The dynamics of the system is incredibly complicated in such a situation, as illustrated, for instance, by our Fig. 18. In the presence of such complexity a description using a simple diffusion equation cannot claim rigorous validity but may be accurate enough to answer practical, qualitative questions.

6. Other Hamiltonian systems

a. Hénon-Heiles and Barbanis systems

The pioneering work of Hénon and Heiles,[43] in which important numerical methods were introduced for the study of stochastic motion, was motivated by astronomical considerations. The stars in a galaxy produce a gravitational potential in which those stars move. The total energy (kinetic plus potential) of a given star is conserved in the absence of close encounters. In an axisymmetric galaxy the angular momentum is also conserved. The existence of a third conserved quantity (the third integral) could neither be proved nor disproved despite many attempts, and observations of the distribution of stellar velocities near the sun suggested existence of the third integral. The dispersion of velocities in the direction of the galactic center and in the direction perpendicular to the galactic plane have a ratio of roughly two to one; such anisotropy implies existence of a third conserved quantity. Hénon and Heiles convincingly showed, using numerical experiments, that the third integral may or may not exist depending on the strength of a perturbation.

The motion of a star in an axisymmetric galaxy may be reduced to a Hamiltonian system with two degrees of freedom. As a model problem, not directly related to any astronomical system, Hénon and Heiles[43] studied the Hamiltonian

$$H(x,y,p_x,p_y) = T(p_x,p_y) + U(x,y) \tag{7a}$$

$$T = \frac{1}{2}\,(p_x^2 + p_y^2) \tag{7b}$$

$$U = \frac{1}{2}(x^2 + y^2) + x^2y - \frac{1}{3}y^3 \quad . \tag{7c}$$

Eqs. (7) represent the motion of a particle in a non-axisymmetric two-dimensional potential well. Equipotential lines (U = constant) of this well are shown in Fig. 3a. Near the bottom of the well the equipotential lines are almost circular, but the degree of asymmetry increases as U increases, until at $U = \frac{1}{6}$ the equipotential line is an equilateral triangle. A particle with a low total energy E (= the constant numerical value of the Hamiltonian function (7a)) is confined to the nearly symmetric part of the well. A particle with a high E can reach parts of the well where the triangular asymmetry is strong.

In writing (7) a certain choice of units has been made so that all quantities are dimensionless. Before making this choice of units we can write (7) as

$$H = (p_x^2 + p_y^2)/2m + \frac{1}{2}k(x^2 + y^2) + \varepsilon(x^2y - \frac{1}{3}y^3) \quad .$$

We see that the quantities in (7) are to be measured in a system of units in which

unit of mass = m

unit of length = k/ε

unit of time = $(m/k)^{\frac{1}{2}}$

unit of energy = k^3/ε^2 .

A particle of given dimensional (i. e., physical) energy C, moving in a well with given k, has a large value of the dimensionless energy $E = C\varepsilon^2/k^3$ if ε is large. A large value of E is thus seen to imply importance of the triangular asymmetry of the potential well (the term

proportional to ε), a result deduced above by examining the equipotentials of U.

Lunsford and Ford[44] showed that the Hénon-Heiles Hamiltonian describes a three-mass system which could model the dynamics of a small molecule or, in a cruder approximation, a solid. They considered three equal masses, each having just one degree of freedom, linked in a chain obeying periodic boundary conditions. Possible chains of this type are sketched in Fig. 4. The potential energy of the springs, assumed to be identical, was taken to be

$$V(x) = \frac{1}{2} x^2 - \frac{1}{6} x^3.$$

Ref. 44 gave a canonical transformation which casts this three-mass system into the form (7).

It is instructive to express the Hénon-Heiles system in terms of other canonical variables. In a polar coordinate system the coordinates, r and θ, and the canonical momenta, p_r and p_θ, are related to the Cartesian variables by

$$r^2 = x^2 + y^2, \quad \tan\theta = y/x \tag{8a}$$

$$p_r = (xp_x + yp_y)/r \tag{8b}$$

$$p_\theta = xp_y - yp_x \ , \tag{8c}$$

or, inversely, by

$$x = r\cos\theta, \ y = r\sin\theta \tag{9a}$$

$$p_x = (xp_r - yp_\theta/r)/r \tag{9b}$$

$$p_y = (yp_r + xp_\theta/r)/r \ . \tag{9c}$$

That (8) or (9) defines a canonical[45] transformation can be verified by checking the appropriate Poisson bracket relations. Alternatively, one can derive the transformation given by (8) or (9) from a generating function,[45] which guarantees that the transformation is canonical. Possible generating functions are

$$F_2(x,y,p_r,p_\theta) = p_r(x^2 + y^2)^{\frac{1}{2}} + p_\theta \tan^{-1}(y/x)$$

or

$$F_3(r,\theta,p_x,p_y) = -r(p_x \cos\theta + p_y \sin\theta) \quad .$$

In terms of the polar variables Hamiltonian (7) becomes

$$H(r,\theta,p_r,p_\theta) = T(r,p_r,p_\theta) + U(r,\theta) \tag{10a}$$

$$T = \frac{1}{2}\,[p_r^2 + (p_\theta/r)^2] \tag{10b}$$

$$U = \frac{1}{2}\,r^2 + \frac{1}{3}\,r^3 \sin 3\theta \quad . \tag{10c}$$

The triangular asymmetry of the potential U shows clearly in (10c). We also see that the Hamiltonian is independent of θ in the limit $r \to 0$, which suggests using p_θ as the first approximation to a constant of the motion, if such a constant is known to exist.

Often, it is best for analytic purposes to express a Hamiltonian in action-angle variables. These variables are related to the Cartesian variables by

$$J_i = \frac{1}{2}\,(p_i^2 + x_i^2) \tag{11a}$$

$$\phi_i = \tan^{-1}(x_i/p_i) \quad , \tag{11b}$$

where i=1 refers to x and i=2 to y. The inverse relationships are

$$x_i = (2J_i)^{\frac{1}{2}} \sin \phi_i \tag{12a}$$

$$p_i = (2J_i)^{\frac{1}{2}} \cos \phi_i \quad . \tag{12b}$$

The generating function

$$F_1(x_i,\phi_i) = \frac{1}{2} x_i^2 \cot \phi_i$$

produces the canonical transformation (11) or (12).

In terms of the action-angle variables Hamiltonian (7) appears

$$H(\phi_1,\phi_2,J_1,J_2) = H_o(J_1,J_2) + V(\phi_1,\phi_2,J_1,J_2) \tag{13a}$$

$$H_o = J_1 + J_2 \tag{13b}$$

$$V = 2(2J_2)^{\frac{1}{2}} \sin \phi_2 (J_1 \sin^2\phi_1 - \frac{1}{3} J_2 \sin^2\phi_2) \tag{13c}$$

$$= (2J_2)^{\frac{1}{2}} \{\frac{1}{2} J_1[\sin(2\phi_1 - \phi_2) - \sin(2\phi_1 + \phi_2) + 2 \sin \phi_2]$$

$$+ \frac{1}{6} J_2[\sin 3\phi_2 - 3 \sin \phi_2]\} \quad . \tag{13d}$$

Note that H_o is the Hamiltonian of two harmonic oscillators with equal frequency:

$$\dot{\phi}_1 = \partial H_o/\partial J_1 = \dot{\phi}_2 = \partial H_o/\partial J_2 = 1 \quad .$$

In contrast to the Hamiltonian systems treated in detail in this thesis, in the Hénon-Heiles system the resonance condition

$$\ell_1\dot{\phi}_1 + \ell_2\dot{\phi}_2 = 0$$

is independent of J_1 and J_2, since $\dot{\phi}_1$ and $\dot{\phi}_2$ are constant. In

addition the resonant term $\sin(\phi_1 - \phi_2)$ is absent from the perturbation V . These characteristics prevent us from applying the first-order perturbation theory which is applicable to most problems, including the ones treated in detail in this thesis. The Hénon-Heiles system is thus a special (not generic) type of Hamiltonian system and is more difficult to treat.

A Hamiltonian system very similar to the Hénon-Heiles system was chosen for numerical studies by Barbanis[46] after theoretical work had been carried out by Contopoulos and Moutsoulas.[47] The Barbanis system is given by (7a)-(7b) and

$$U = \frac{1}{2}(x^2 + y^2) - xy^2 \quad . \tag{14}$$

In terms of the polar variables (8a), (14) becomes

$$U = \frac{1}{2} r^2 + \frac{1}{4} r^3 (\cos 3\theta - \cos\theta) \quad . \tag{15}$$

The equipotential lines of the well given by (14) or (15) are shown in Fig. 3b. In terms of the action-angle variables (11), the Barbanis system is given by Hamiltonian (13a) and (13b) but with

$$V = \frac{1}{2} J_2 (2J_1)^{\frac{1}{2}} [\sin(\phi_1 - 2\phi_2) + \sin(\phi_1 + 2\phi_2) - 2\sin\phi_1] \, . \tag{16}$$

Since (16) has fewer terms than (13d), the Barbanis system would probably be less tedious to treat analytically than the Hénon-Heiles system.

Other Hamiltonians similar to those of Hénon-Heiles and

Barbanis have been studied[48] extensively. In particular, the term y^2 in (14) was multiplied by a constant (e. g., $\frac{1}{4}$ or $(\frac{3}{4})^{\frac{1}{2}}$), thereby making unequal the frequencies of the oscillators described by H_0. Contopoulos[49] and Gustavson[50] have given procedures for calculating terms in a formal series approximating a constant of the motion (the third integral). Contopoulos[51] has compared his methods to those of von Zeipel, Whittaker, Cherry, and Birkhoff. The formal series obtained by these methods generally have very complicated terms which must be found by tedious high-order perturbation methods. A simple and elegant method for calculating a formal series was given by Dunnett, Laing, and Taylor,[52] who ignored the desire of earlier authors to have each term in the series be a polynomial in x_i and p_i. This method is applicable to the problems of primary interest to us and will be discussed in Section 2D. The method is possibly not applicable to the problems of this subsection, because the resonance condition is independent of J_1 and J_2.

Hénon and Heiles[43] showed that, in the potential well of Fig. 3a, motion changes <u>qualitatively</u> as the total energy of the particle is increased. They represented the motion in two dimensions using a technique invented by Poincaré[53] in the nineteenth century. This technique, which is called the surface of section method, will be discussed in Section 2I. Briefly, the surface of section method allows us to represent a four-dimensional particle trajectory as a set of points on a plane while retaining information describing the long-time behavior of the trajectory.

In Fig. 5, based on figures in Ref. 43, we show the changes in motion which occur as the particle's energy is increased. For low energies, like $E = \frac{1}{12}$, the points representing a given trajectory are found always to lie on a curve. For high energies, like $E = \frac{1}{6}$, almost all trajectories have points filling an area rather than lying on a curve. For intermediate energies, like $E = \frac{1}{8}$, the nature of a trajectory depends on the values of the positions and velocities at $t=0$.

The three plots in Fig. 5 allow us to observe the disappearance of a constant of the motion as the energy is raised. For low energies E, this constant restricts the motion of the particle to one-dimensional curves in the plane. For high energies E, this constant has disappeared, allowing the particle to visit points in a two-dimensional region of the plane.

Further discussion on the nature and importance of the disappearance of constants of the motion is contained in Section 2F.

Mo[54] gave a method based on projection-operator techniques which allowed her to calculate analytically the energy E at which widespread stochasticity should occur. The analytical values of E were found to agree very accurately with the values determined by numerical experiments.

Finally, we note that the Hénon-Heiles and Barbanis systems were studied using the methods of <u>quantum</u> mechanics by Nordholm and Rice.[55] Their desire was to determine if a small quantum mechanical system, like

an isolated molecule, shows effects analogous to those seen in Fig. 5, for which classical mechanics was used. The quantum problem was found to be more difficult, both conceptually and computationally. Nordholm and Rice computed energy levels and the corresponding eigenstates for several Hamiltonians, including those of Hénon-Heiles and Barbanis. For some systems, but not for others, they found a tendency for low-energy eigenstates to be localized, which is analogous to existence of a constant of the motion, and for high-energy eigenstates to be global, analogous to nonexistence of the constant. It seems to us that Ref. 55 does not give a definitive answer regarding the existence of stochastic effects in quantum mechanics.

b. Restricted problem of three bodies

A famous problem in the history of physics is the motion of three masses interacting by their mutual gravitation. Extensive numerical studies by Hénon[56-58] of a restricted three-body problem suggest that the general three-body problem is analytically insoluble.

Hénon studied the most restricted form of the three-body problem. The mass of the third body, whose motion is studied, is infinitesimal compared to the mass of the other two bodies, so the motion of the first two bodies is given by the well-known solution of Kepler. The first two bodies revolve about the center of mass in circular (not elliptical) orbits. The initial position and velocity of the third body lie in the plane of motion of the first two bodies; the motion of all three bodies is thus restricted to this (fixed) plane.

The total mass of the system is taken as the unit of mass, the distance between the first two bodies as the unit of length, and the angular frequency of rotation of those bodies as the unit of frequency. One uses a synodical coordinate system, which rotates with the first two bodies and which has the origin at the center of mass of those bodies. The motion is described by the Hamiltonian

$$H(x, y, p_x, p_y) = \frac{1}{2}(p_x^2 + p_y^2) - (xp_y - yp_x) - (1 - \mu)/r_1 - \mu/r_2 ,$$

where μ is the mass of the second body and

$$r_1 \equiv [(x + \mu)^2 + y^2]^{\frac{1}{2}}, \quad r_2 \equiv [(x - 1 + \mu)^2 + y^2]^{\frac{1}{2}} .$$

The numerical value of the Hamiltonian (times -2) is called the Jacobi constant and is given by

$$C = x^2 + y^2 + 2(1 - \mu)/r_1 + 2\mu/r_2 - \dot{x}^2 - \dot{y}^2 .$$

Hénon found the restricted three-body problem to be qualitatively similar to the Hénon-Heiles system; surface of section plots show regions where a constant of the motion (in addition to the Jacobi constant) exists and other regions where it does not exist. As the numerical value of the Jacobi constant is decreased, the regions of existence of the additional constant are found to shrink. This behavior is shown in Fig. 6, which is taken from Ref. 56, which treated the case $\mu = \frac{1}{2}$ (equal masses of the first two bodies). In later work Hénon found similar behavior in the limiting[57] case $\mu \to 0$ and for intermediate[58] values of μ .

c. Størmer problem

The motion of a charged particle in a magnetic dipole field, the simplest approximation to the earth's field, is interesting because of possible applications to radiation belt phenomena. This problem, named in honor of Størmer, has been discussed in an excellent article by Dragt and Finn.[59] Here we review briefly the results found in Ref. 59 and give our interpretation of them.

The Hamiltonian describing motion in a dipole field can be reduced to two degrees of freedom and written, in a certain system of units, as

$$H = \frac{1}{2}(p_z^2 + p_\rho^2) + V(z,\rho)$$

$$V = \frac{1}{2}[\rho^{-1} - (\rho/r^3)]^2$$

$$r \equiv (z^2 + \rho^2)^{\frac{1}{2}} \quad .$$

Here z and ρ are ordinary cylindrical coordinates: ρ is the distance of the particle from the axis of the dipole field and z is its distance from the equatorial plane. The potential energy $V(z,\rho)$ contains a well in which particles with appropriate initial conditions can be trapped. The corresponding particles in the earth's magnetic field are the ones observed in the radiation belts. In the potential well the motion consists of coupled oscillations representing gyration about a field line and bouncing along it.

The analysis of this problem by Dragt and Finn begins with a clear description of what is meant by a homoclinic point. They show that a time-independent Hamiltonian system with two degrees of freedom

which has a homoclinic point cannot have an analytic constant of the motion other than the Hamiltonian. Numerical evidence is then presented which strongly suggests the existence of a homoclinic point for the Størmer problem. This implies that there exists no analytic expression, valid throughout phase space, for a particle's magnetic moment in the presence of a dipole field.

The nonexistence of an additional constant of the motion has been observed by us in the problems treated in detail in this thesis. In Chapter 4 we study the disappearance of a constant in the vicinity of a separatrix, where a constant of the motion can be destroyed by an arbitrarily small perturbation. This behavior near a separatrix prevents existence of a constant of the motion valid throughout phase space.

In applications to physical problems it is important to determine the extent of the region near the separatrix in which a constant is destroyed. (In Chapter 4 this extent is referred to as the width of the stochastic layer.) If this region is extremely small, it cannot be important in applications. Unfortunately, the extent of this region cannot be found by any mathematically rigorous technique. The extent of the complementary region, in which an additional constant of the motion does exist, has been shown by Braun,[60] using methods developed by Moser, to have at least a certain extremely small, but nonzero, size. Numerical studies of dynamical systems seem to indicate a much larger size for this complementary region. However, in numerical integrations it is not possible to reach the long confinement times

observed for radiation belt particles, and numerical studies thus cannot show definitively whether a constant of the motion exists or not.

Nevertheless, we speculate that the good confinement of radiation belt particles results from the existence of a constant of the motion in a large region of phase space, the regions of nonexistence either being very small or being located in regions of phase space not occupied by radiation belt particles.

d. Elastic pendulum

Considerable attention[61-63] has been directed recently to the motion of a mass attached to a spring which can swing in a fixed, vertical plane. With a certain[61] choice of units this system is described by the Hamiltonian

$$H(x, z, p_x, p_z) = \frac{1}{2}(p_x^2 + p_z^2) - gz + \frac{1}{2}(r - 1)^2 \quad , \tag{17}$$

where $r \equiv (x^2 + z^2)^{\frac{1}{2}}$. Interest has centered on the case $g = \frac{1}{3}$ for which the two natural frequencies (stretching and swinging) occur in a ratio of two to one.

Hitzl[61] investigated the periodic orbits, some of them rather complicated, which occur for this system, and also he found an increasing fraction of aperiodic (i. e., stochastic) orbits as he increased the total energy. Hitzl's results are thus qualitatively similar to those of Hénon and Heiles,[43] which we discussed above. Expanding (17) about the equilibrium point ($x=0$, $z=\frac{4}{3}$), Olsson[63] wrote down a dynamical system which happens to be identical to one studied[49]

by Contopoulos.

7. General oscillator system

In this subsection we will show that the Hamiltonian systems studied in detail in this thesis are of a form which is found under very general conditions and therefore in many other conservative systems. The results of our work should therefore be applicable, with only minor modifications, to many other problems.

Physical systems often take the form of coupled one-dimensional oscillators each described by a time-independent Hamiltonian $H_o^{(i)}(x_i, p_i)$. The coupling occurs through an interaction energy $\varepsilon V(x_1, p_1, x_2, p_2, \ldots, t)$. The equations of motion for a particular oscillator (i=1) involve the dynamical variables of the other oscillators only through εV, which is often small compared to $H_o^{(1)}$. A valid approximation is then obtained by replacing $x_2, p_2, \ldots$ by the explicit functions of time derived from the Hamiltonians $H_o^{(2)}, \ldots$. The Hamiltonian describing oscillator 1 takes the form

$$H(x, p, t) = H_o(x, p) + \varepsilon V(x, p, t) \quad . \tag{18}$$

As noted by Chirikov,[20] this reduction to the study of one-dimensional oscillators eliminates the possibility of Arnold diffusion, which can only be important if the stronger effects due to overlapping resonances are absent.

Frequently, we study the motion of a particle in a force field

dependent only on x and t. The potential energy U, which produces the force field, can sometimes be Fourier analyzed in x and t:

$$U(x, t) = \Sigma_{k\omega} U_{k\omega} \cos\ (kx - \omega t + \eta_{k\omega}). \tag{19}$$

If boundary conditions force the values of k and ω to be multiples of a fundamental wavenumber k_o and frequency ω_o, then (19) takes the form

$$U(x, t) = \Sigma_{n\ell} U_{n\ell} \cos\ (nk_o x - \ell\omega_o t + \eta_{n\ell}), \tag{20}$$

where n and ℓ are integers. The corresponding Hamiltonian,

$$H(x, p, t) = p^2/2m + U(x, t), \tag{21}$$

is a particularly simple example of the general form (18) and has exactly the form of (2.45) if the coefficients $U_{n\ell}$ are zero for $n \neq 1$. In Section 2H we note that Hamiltonian (2.45) displays the main feature (stochastic motion due to resonance overlap) displayed by the Hamiltonian ((2.3),(2.4), and (2.9)) of a particle in a uniform magnetic field and an oblique electrostatic wave.

If the Fourier coefficients $U_{n\ell}$ differ in size, or their relative importance differs because the particle is nearer the resonant velocities $\ell\omega_o/nk_o$ of some terms in (20) than of others, it may be possible to study motion in the presence of only a few terms from (20). In the presence of only one term, the motion would be described by the Hamiltonian

$$H_o(x, p, t) = p^2/2m + U_{n_o\ell_o} \cos(n_o k_o x - \ell_o \omega_o t + \eta_{n_o\ell_o}). \tag{22}$$

After a change of reference frame and a choice of convenient units, (22) takes the form

$$H_o(x, p) = \frac{1}{2}p^2 - \cos x ,$$

which is the Hamiltonian for the well-known problem of a (nonlinear) pendulum. The exact solutions of this problem are given in Section 4C. In the presence of <u>two</u> terms from (20), the particle moves according to

$$H(x, p, t) = H_o(x, p) - \varepsilon \cos (\lambda x - \Omega t) , \tag{23}$$

where appropriate definitions of ε, λ, and Ω are to be used. Chapter 4 includes a study of (23) for the particular choice $\lambda = \frac{1}{2}$.

For theoretical work, it is most convenient to express (18) in terms of variables for which the unperturbed Hamiltonian H_o depends only on the canonical momentum and not on the coordinate. Such variable transformations have been performed in sections 2B and 4B. In terms of the new variables, which we denote by ϕ and J, (18) has the form

$$H(\phi, J, t) = H_o(J) + \varepsilon V(\phi, J, t) . \tag{24}$$

If ϕ is an angle variable, V must be periodic in ϕ. If V is also periodic in t, then

$$V(\phi,J,t) = \Sigma_{n\ell} V_{n\ell}(J) \cos (n\phi - \ell\omega t + \eta_{n\ell}) . \tag{25}$$

We note here the close analogy between (21) and (20) on one hand and (24) and (25) on the other. A term in (25) is slowly varying in time (i. e., resonant) if

$$n\dot{\phi} \approx n\omega_b(J) \approx \ell\omega,$$

where $\omega_b \equiv \partial H_o/\partial J$. The resonant values of J are determined by the integers n and ℓ, and, in general, form a set whose members are distributed along the real number line as the rational numbers are distributed. We treat the simpler cases in which either n is always unity, leading to a resonance condition of the form (3), or ℓ is always unity, leading to (4). Ref. 20 contains a treatment (pp. 55-62) of the more difficult, general case.

For the purpose of studying the overlap of resonances, a time-dependent system of one degree of freedom and a time-independent system of two degrees of freedom are equivalent. The latter type of system in fact includes the former type, since $H(x,p,t)$ can be transformed to

$$K(x,p,\theta,I) = H(x,p,\theta/\omega) + I\omega \tag{26}$$

using the generating function

$$F_2(x,p',I,t) = xp' + I\omega t \ .$$

Most of Chapter 2 deals with a time-independent system, but we feel that a time-dependent system exhibits the overlap of resonances more cleanly than a time-independent one. A time-dependent system contains no variable analogous to I in (26) and is thus free of the effects of changes in I, which are not directly relevant to stochasticity.

8. Possible implications for statistical mechanics

Many-body problems in physics are usually described adequately using the methods of statistical mechanics. The fundamental postulate of statistical mechanics, upon which all of its results are based, is that an isolated system be found with equal probability in any of its accessible states, that is, in any part of the energy (hyper)surface. The few-body problems traditionally studied in classical mechanics courses generally have constants of the motion in addition to the energy which restrict the motion to a subspace of the energy surface. More typical behavior is seen in numerical studies, like ours, of dynamical systems with quite simple Hamiltonians but with very complex motion. These studies show that additional constants of the motion can be destroyed by a sufficiently large perturbation. The perturbation strengths required for destruction of the additional constants are generally quite high in the two-degree-of-freedom problems which have been most extensively studied. Possibly, the required perturbation strengths decrease as the number of degrees of freedom increases. Evidence for this behavior has been given by Froeschlé and Scheidecker.[64]

The possibilities of discovering the reasons for the empirical success of statistical mechanics or of proving the fundamental postulate have naturally led to much work by both mathematicians and physicists. A number of excellent review articles have appeared. The most comprehensive (book-length) treatment, written from a physicist's viewpoint, is by Chirikov.[20] Written in a similar, dense style and

containing many of the same results is the article by Zaslavskii and Chirikov.[4] Farquhar[65] gives a very readable introduction to the concepts of modern ergodic theory. Other reviews of note are by Lebowitz,[66] Lebowitz and Penrose,[67] Galgani and Scotti,[68] Ford, [69-71] and Walker and Ford.[72]

D. Complicated behavior in simple dissipative dynamical systems

The dynamical systems mentioned in the previous section were all conservative systems, derivable from a Hamiltonian. Simple dissipative systems can also exhibit incredibly complicated behavior, as we will show in this section by giving several examples. We do not believe that overlap of resonances is responsible for every (or even any) aspect of the behavior of dissipative systems. We include these examples because the behavior is sometimes strikingly similar to that observed in conservative systems.

1. Population levels in biology

The number of individuals in a species, that is, the population, obeys a complicated set of equations, in general. In a few situations, however, an adequate approximation may be given by the so-called logistic equation

$$dN/dt = rN(1 - N/K) \quad .$$

Here N is the population level, K the carrying capacity, and r is the growth rate of the species. If the generations of the species are non-overlapping, as in the 13-year periodical cicada, then one uses a nonlinear difference equation

$$N_{t+1} = N_t \exp[r(1 - N_t/K)] \tag{27}$$

for the population at time $t+1$ in terms of the population at time t.

The difference equation (27) has radically different behavior depending on the value of r, as shown in Fig. 7, which comes from Ref. 73. Plot (a), for r=1.8, shows the population N leveling off at the carrying capacity K after initial transients have died out. Plot (b), for r=2.3, shows a stable two-point cycle in which the population oscillates between a low and a high level each generation. Plot (c), for r=2.6, shows a stable four-point cycle. Plots (d) and (e) have the same value of r, 3.3, but different initial population levels. In (d) the motion appears to have lost any regularity, but in (e) the motion appears quasiperiodic with period three. In plot (f), for r=5, the motion is characterized by large isolated spikes in the population level.

Ref. 74 can be consulted for recent work on a dynamical system similar to (27). May[75] notes that similar types of equations occur also in economics and sociology and the same type of dynamics might occur in those fields as well.

2. Rikitake dynamo

The earth's magnetic field is known to have changed its polarity at seemingly random intervals during the past ten million years. The observations of the polarity intervals are shown in Fig. 8, which is taken from Cox.[76] One might think that the apparent randomness is due to the complexity of the earth's core. However, there exist <u>very simple</u> models which lead to apparently random changes in the polarity of the

magnetic field.

Such a model[77] is known as the Rikitake two-disk dynamo. In Fig. 9 is shown a schematic picture of this dynamo. The equations which describe the system are

$$\begin{cases} L\dot{I}_1 + R I_1 = M\Omega_1 I_2 \\ L\dot{I}_2 + R I_2 = M\Omega_2 I_1 \\ C\dot{\Omega}_1 = C\dot{\Omega}_2 = G - M I_1 I_2 \quad . \end{cases} \tag{28}$$

In (28) I_1 and I_2 are the currents in the two loops of wire, L and R are the inductance and resistance of each loop, M is the mutual inductance between one loop and the opposite disk, Ω_1 and Ω_2 are the angular velocities of the two disks, C is the moment of inertia of each disk, and G is the (common) couple which drives each disk.

In Fig. 10 is shown a typical time evolution of the current I_1, as calculated by Cook and Roberts.[78] Note the variable interval between reversals of the sign of I_1; sometimes there are many of the rapid oscillations before I_1 changes sign, sometimes I_1 changes sign only very briefly. This behavior is similar to the observational data shown in Fig. 8. We stress the fact that the complicated motion seen in Fig. 10 results from a simple set of three nonlinear differential equations.

3. Fluid motion between cylinders

In this subsection and the next we discuss two classical problems in fluid mechanics which have been the subject of renewed interest in recent years. The first problem is the motion of a fluid between two coaxial cylinders, the inner one of which is rotating with respect to the other. The name "Couette flow" describes the motion of the fluid when the rotational velocity is very small. This system is thought to be described accurately by the Navier-Stokes equation

$$\frac{\partial \underline{u}}{\partial t} + (\underline{u} \cdot \nabla)\,\underline{u} = \frac{1}{\rho}\nabla p + \nu \nabla^2 \underline{u}$$

and the incompressibility condition $\nabla \cdot \underline{u} = 0$.

The theoretical picture of turbulence developed by Landau[79] many years ago states that the level of turbulence gradually increases as the rotational velocity of the inner cylinder increases. More recently, a new theoretical picture of turbulence was proposed by Ruelle and Takens,[80] who state that the onset of turbulence is sudden.

Experimental results are available which support the picture of Ruelle and Takens. In Fig. 11 are shown the results of an experiment[81] on fluid motion between cylinders. On the left side of the figure we see the variation with time of a certain component of the fluid velocity. That data has been Fourier analyzed on the right to yield a power spectrum. The rotational velocity of the inner cylinder is parametrized by the reduced Reynolds number R* which increases from top to bottom in the figure. At a low rotational velocity, the motion is periodic at a frequency f_1. As the rotational velocity is

increased, new frequencies f_2 and f_3 appear. At a certain velocity the spectrum changes abruptly from discrete to continuous, indicating a sudden onset of turbulence. This sudden qualitative change in the spectrum reminds us of the change in the motion of a Hamiltonian system when the initial condition is displaced from an ordered region of phase space into a stochastic region. In an ordered region the motion is quasiperiodic (has a discrete spectrum), while in a stochastic region the motion is aperiodic (has a continuous spectrum).

4. Rayleigh-Bénard heat convection problem and the Lorenz model

Another classical problem in fluid mechanics is the Rayleigh-Bénard problem of heat convection through a layer of fluid heated from below. A theoretical approach[82] to this problem starts by writing the fluid equations describing the system. The equations are Fourier analyzed and all but a few modes are discarded. A very crude model[83] retains only three modes, denoted by x, y, and z, which obey the system of equations

$$\begin{cases} \dot{x} = \sigma(y - x) \\ \dot{y} = rx - y - xz \\ \dot{z} = -bz + xy \quad . \end{cases} \tag{29}$$

The parameters σ and b are unimportant for the present discussion, but we think of r as a measure of the stress on the system due to the temperature gradient. For small r, (29) has solutions corresponding to heat <u>conduction</u> . For intermediate r, the solutions correspond to

laminar convection, and for large r to turbulent convection. For large r the motion in the three-dimensional xyz-space has a very intriguing nature. For any initial condition whatever of the dynamical system (29), the motion is found to converge rapidly to a two-dimensional surface embedded in the three-dimensional space. This two-dimensional surface, which is called a strange attractor , has a very complicated structure, which is difficult to represent on paper. There exist systems of lower dimensionality, however, for which the strange attractor can easily be shown. Such a system is the subject of the next subsection.

Before leaving the Lorenz model (29) we mention three noteworthy comments of Lorenz.[83] He argued for large r that all solutions of (29) are aperiodic, except for a set of periodic solutions of measure zero. He observed all solutions to be unstable to small modifications, or in other words, slightly differing initial conditions led to greatly differing final conditions. These two characteristics of the dissipative system studied by Lorenz are identical to characteristics of conservative systems with overlapping resonances studied by us and by many others.

Lorenz' third comment is that the inevitable inexactness of meteorological observations (initial conditions) makes long-range weather prediction (knowledge of final conditions) impossible.

5. Mapping with a strange attractor

A two-dimensional mapping with a strange attractor was discovered recently by Hénon.[84] The mapping is defined by specifying the coordinates of a point on the xy-plane at time $i+1$ in terms of the xy-coordinates at an earlier time i:

$$\begin{cases} x_{i+1} = y_i + 1 - ax_i^2 \\ y_{i+1} = bx_i \end{cases} . \tag{30}$$

For many initial points (x_0,y_0), the points defined by the mapping rapidly converge to the attractor, which is the curve shown in the upper left part of Fig. 12. The structure of this attractor is indeed very strange, as we see by blowing up the small square in the upper left picture to produce the picture at the upper right. The four lines which were visible under low resolution can now be seen to consist of at least seven lines. Continuing clockwise around Fig. 12, we see successive blowups in which more and more lines can be resolved. It seems that the structure of the attractor will appear complicated at whatever resolution we choose to use. Conservative systems also show complications at all resolutions, a phenomenon we have observed to a limited extent by numerically calculating particle trajectories in certain electromagnetic fields.

2. Overlap of Cyclotron Resonances

A. Choice of model

Stochastic instability is possible if a set of resonances exists and the resonances can overlap. In plasma physics such a set of resonances occurs when a uniform magnetic field is present. A particle is in (exact) resonance with a sinusoidal wave of frequency ω if the Doppler-shifted wave frequency is a multiple of the gyrofrequency $\Omega \equiv eB_o/mc$:

$$\omega - k_z v_z = -\ell\Omega , \quad \ell = 0, \pm 1, \pm 2, \ldots . \tag{1}$$

From (1) we find the set of resonant parallel velocities

$$v_z = (\omega + \ell\Omega)/k_z \ ; \tag{2}$$

these velocities are finite if $k_z \neq 0$. The resonances have a non-zero width when the wave amplitude is not infinitesimal and the gyroradius is finite ($k_\perp \rho > 0$). Overlap of the resonances is thus possible if the wave propagates at an oblique angle to the magnetic field: $k_z, k_\perp \neq 0$. Published accounts of our early work on the overlap of cyclotron resonances appear in Refs. 85 and 86.

Our work assumes the wave spectrum is so narrow that a single wave is a good representation of the spectrum. This situation is easiest to treat analytically and leads to the most striking results. Having studied the single-wave situation, we will be able to understand the nature of stochastic motion in many-wave problems more clearly.

We usually assume that the wave is electrostatic ($\underline{k} \parallel \underline{E}$). An electromagnetic wave can also cause stochastic acceleration since the same resonances occur as in the electrostatic case. The widths of the resonances are different and, as is shown in Appendix B, a wave amplitude large enough to cause overlap of the resonances is more difficult to achieve in the electromagnetic case.

Appendix C mentions the analytical complications which would arise if we relaxed our assumption that the wave is sinusoidal.

Finally, we assume that the amplitude Φ_o of the electrostatic wave is constant in time. An antenna which launches a wave in a steady-state plasma will produce a constant wave amplitude. If, instead, the wave is due to an instability, then an equilibrium will be reached in which the linear growth rate γ_ℓ balances the nonlinear damping rate $\gamma_s(\Phi_o)$ caused by stochastic acceleration of the particles. The amplitude Φ_o is then given by

$$\gamma(\Phi_o) = \gamma_\ell - \gamma_s(\Phi_o) = 0 \quad .$$

(We assume here that stochastic acceleration saturates the instability before any other nonlinear effect is important; this assumption must be investigated separately for each physical situation.) We will find that stochastic acceleration is a very rapid process (characteristic rates comparable to the gyrofrequency Ω). Therefore, even a variation in the wave amplitude at a quite rapid ($\sim 0.1)\Omega$) rate will not alter our results qualitatively.

B. Choice of variables

To describe the motion of a particle in a uniform magnetic field and a wave, we could use the Cartesian variables (x, y, z, v_x, v_y, v_z). Our work is simplified and the generalization to a nonuniform magnetic field made clearer by choosing other variables. We use a Hamiltonian formulation so we can utilize many results of Hamiltonian theory. The simplest Hamiltonian formulation is found by choosing generalized coordinates $\underline{q}$ and momenta $\underline{p}$ such that the motion in the magnetic field with no wave is described by a Hamiltonian depending on the momenta only: $H_o = H_o(\underline{p})$.

We derive the uniform magnetic field $B_o \hat{z}$ from the vector potential

$$\underline{A}_o(y) = -B_o y \hat{x} \quad .$$

The unperturbed (i. e., $\Phi_o = 0$) Hamiltonian is

$$H_o(y, p_x, p_y, p_z) = \frac{1}{2}mv^2 = (\underline{p} + m\Omega y \hat{x})^2/2m \quad .$$

We see that we need to transform the perpendicular variables (x, y, p_x, p_y) to a new set of variables which describe, it turns out, the position of the guiding center and the gyration about it. We use the variables

$$\underline{q} = (z, \phi, Y)$$
$$\underline{p} = (p_z, p_\phi, m\Omega X) \quad ,$$

where ϕ is the gyrophase, p_ϕ the canonical angular momentum of

gyration, and X and Y the components of the guiding center. These variables are defined in terms of the Cartesian variables by

$$\phi \equiv \tan^{-1} [(p_x + m\Omega y)/p_y]$$

$$p_\phi \equiv [(p_x + m\Omega y)^2 + p_y^2]/2m\Omega$$

$$Y \equiv - p_x/m\Omega$$

$$X \equiv x + p_y/m\Omega \quad .$$

The requirements for these variables to be canonical are easily verified by computing the Poisson brackets

$$[\phi, p_\phi] = [Y, m\Omega X] = 1$$

$$[\phi, Y] = [\phi, X] = [p_\phi, Y] = [p_\phi, X] = 0 \quad .$$

Alternatively, we can transform

$$(x, y, p_x, p_y) \rightarrow (\phi, Y, p_\phi, m\Omega X)$$

using the generating function[45]

$$F_1(x, y; \phi, Y) = m\Omega[\tfrac{1}{2}(y - Y)^2 \cot \phi - x Y] \quad .$$

The gyroradius ρ, the perpendicular velocity $v_\perp$, and the magnetic moment μ are defined in terms of p_ϕ by

$$p_\phi \equiv \tfrac{1}{2}m\Omega\rho^2 \equiv mv_\perp^2/2\Omega \equiv (mc/e)\mu \quad .$$

We write

$$\phi = \sin^{-1}(- v_x/v_\perp) = \cos^{-1} (- v_y/v_\perp)$$

$$Y = y + \rho \sin \phi$$

$$X = x - \rho \cos \phi$$

to show that we have named ϕ, ρ, X, and Y according to their conventional meanings. We illustrate in Fig. 13 the definition of the gyrophase ϕ which we have adopted.

The unperturbed Hamiltonian is now written

$$H_o(p_z, p_\phi) = p_z^2/2m + p_\phi \Omega \quad . \tag{3}$$

In terms of the chosen variables the unperturbed motion is extremely simple:

$$\dot{H}_o = \dot{p}_z = \dot{p}_\phi = \dot{X} = \dot{Y} = 0$$

$$\dot{z} = p_z/m = v_z$$

$$\dot{\phi} = \Omega \quad .$$

(The dot denotes time differentiation.)

C. Hamiltonian

The Hamiltonian for a particle in a uniform magnetic field and an electrostatic wave is

$$H = H_o + V \quad , \tag{4}$$

where H_o is the unperturbed part discussed above and V is the perturbation due to the wave. We use canonical variables which measure the position $z' = z - (\omega/k_z)\, t$ and the parallel momentum $p_z' = p_z - m\omega/k_z$ in the wave frame. This reference frame moves with velocity $(\omega/k_z)\,\hat{z}$ with respect to the center of mass of the plasma. The canonical

transformation, given in Appendix A, to the wave frame variables is a mathematical, not a physical (Galilean) transformation, and there is no requirement, as noted by Palmadesso,[87] that $\omega/k_z << c$. Nevertheless, we apply the transformation only to waves for which $\omega/k_z << c$, because these slow waves seem to lead to the strongest stochastic effects. For simplicity of notation we henceforth drop the primes on the wave frame variables.

In the wave frame the perturbation due to the sinusoidal electrostatic wave is

$$V = e\Phi_o \sin (\underline{k} \cdot \underline{x}) . \tag{5}$$

We choose the direction of the x-axis so that

$$\underline{k} = k_z \hat{z} + k_\perp \hat{y}, \; k_\perp > 0 \quad .$$

Then, in terms of the variables discussed above

$$V = e\Phi_o \sin (k_z z + k_\perp Y - k_\perp \rho \sin\phi) \; .$$

We redefine the origin of z by performing a canonical transformation to the new variables

$$z' = z + k_\perp Y/k_z \; , \quad p_z' = p_z$$

$$Y' = Y, \quad X' = X - k_\perp p_z/k_z m\Omega \quad .$$

Since Y' and X' do not appear in the transformed Hamiltonian, they are each constants of the motion. Y' is constant because there is no E_x to cause an $\underline{E} \times \underline{B}$ drift of the guiding center in the y-direction. X' is constant because the electric field components E_y and E_z,

which are related by $k_z E_y = k_\perp E_z$, cause, respectively, an $\underline{E} \times \underline{B}$ drift in the x-direction and an acceleration in the z-direction. The constancy of X' and Y' has been shown earlier[88] using less powerful methods. We drop the primes on the new variables and write the perturbation in the final form

$$V(z, \phi, p_\phi) = e\Phi_o \sin (k_z z - k_\perp \rho \sin\phi) \quad . \tag{6}$$

The Hamiltonian given by (3),(4), and (6) does not depend on time; therefore

$$H(z, \phi, p_z, p_\phi) = p_z^2/2m + p_\phi \Omega + e\Phi_o \sin (k_z z + k_\perp Y - k_\perp \rho \sin\phi) \tag{7}$$
$$= E = \text{const},$$

the particle's energy in the wave frame is constant. In the plasma frame (7) becomes

$$\frac{1}{2} m [(v_z - \omega/k_z)^2 + v_\perp^2] + e\Phi_o \sin (\underline{k} \cdot \underline{x} - \omega t) = \text{const}.$$

This result has been noted previously by several authors.[87,89]

D. Particle motion in a small-amplitude wave

Stochastic acceleration occurs when the wave amplitude is large. (The Chirikov criterion tells us how large; this criterion will be discussed and applied to the present problem in Section 2F.) We prepare for our discussion of stochastic acceleration by studying here the case of a small-amplitude wave.

We use the Bessel-function identity

$$\exp\ (i\, a \sin\phi) = \sum_{\ell=-\infty}^{\infty} J_\ell(a) \exp\ (i\ell\phi) \tag{8}$$

to write the perturbation (6) as

$$V = e\Phi_o\ \Sigma_\ell\ J_\ell\ (k_\perp \rho)\ \sin\ (k_z z - \ell\phi)\ . \tag{9}$$

Most of the terms in this sum over ℓ vary rapidly in time and are not expected, on physical grounds, to have a significant effect on the particle motion. We identify the rapidly varying terms by substituting into (9) the expressions

$$z = v_{zo}t + z_o,\ \phi = \Omega t + \phi_o,\ \rho = \rho_o\ , \tag{10}$$

derived from the unperturbed Hamiltonian H_o. (In (10) the subscript naught denotes the value of a quantity at $t=0$.) We find that (9) contains the oscillating functions

$$\sin\ [(k_z v_{zo} - \ell\Omega)t + k_z z_o - \ell\phi_o]\ .$$

The particle is in exact resonance with the ℓth component of the wave if

$$k_z v_{zo} = \ell\Omega\ . \tag{11}$$

This condition is the same as (1) but is expressed in terms of the parallel velocity in the wave frame instead of the plasma frame.

If v_{zo} is far from satisfying (11) for any ℓ, then all the terms in (9) vary rapidly and the unperturbed motion, (10) together with

$$v_z = v_{zo} \quad ,$$

is a reasonable approximation to the exact motion.

If v_{zo} is close to satisfying (11) for a particular $\ell = L$ but far from satisfying it for all other ℓ, then the motion is approximately that given by the Hamiltonian

$$H_L = H_o + e\Phi_o J_L \sin(k_z z - L\phi) \quad .$$

Two constants of the motion exist in this approximation. Since H_L is independent of time, one constant is H_L itself. The coordinates z and ϕ appear only in the combination $k_z z - L\phi$, so we can trivially derive the second constant by transforming to new variables using the generating function

$$F_2(z, \phi, p_\psi, I_L) = (k_z p_\psi + mL\Omega/k_z)\, z + (I_L - Lp_\psi)\phi \quad .$$

In terms of the old variables, the new ones are

$$\psi = \partial F_2/\partial p_\psi = k_z z - L\phi, \quad \phi' = \partial F_2/\partial I_L = \phi$$
$$p_\psi = (p_z - mL\Omega/k_z)/k_z, \quad I_L = p_\phi + Lp_\psi \quad . \tag{12}$$

The Hamiltonian is

$$H_L(\psi, p_\psi, I_L) = H_o(p_\psi, I_L) + e\Phi_o J_L \sin\psi \quad ,$$

which is independent of ϕ', showing that I_L is a constant of the motion. Other constants, combinations of the two constants H_L and I_L, have been derived previously[87,90] using other methods.

We now derive a measure of the width of the resonance L,

i. e., how close v_{zo} must be to $L\Omega/k_z$ for the Lth term in (9) to be slowly varying in time. We write the approximate Hamiltonian H_L as

$$H_L(\psi, p_\psi) = p_\psi^2 k_z^2/2m + e\Phi_o J_L \sin\psi \quad , \tag{13}$$

where we have suppressed the dependence on I_L and dropped constant terms. Equation (13) gives the Hamiltonian found in several other familiar problems, e. g., the one-dimensional motion of a particle in a Langmuir wave and the motion of a (nonlinear) pendulum. A separatrix divides the ψp_ψ-plane into regions in which the motion is qualitatively different. Inside the separatrix the particle is "trapped": ψ repeatedly takes on values in a subset of the interval $(0, 2\pi)$ during the motion. Outside the separatrix the particle is "untrapped": ψ increases (or decreases) monotonically in time. The separatrix has

$$H_L = e\Phi_o J_L \quad .$$

On the separatrix the maximum deviation of p_ψ from zero is

$$\Delta p_\psi = 2 \left| me\Phi_o J_L \right|^{\frac{1}{2}}/k_z \quad .$$

Using (12), we derive $2\Delta v_z = 2\Delta p_z/m \equiv w_L$, which we refer to as the trapping width:

$$w_L = 4 \left| e\Phi_o J_L(k_\perp \rho)/m \right|^{\frac{1}{2}} \quad . \tag{14}$$

Near the stable equilibrium point ($\psi = \pm \frac{1}{2}\pi$, if $e\Phi_o J_L \lesssim 0$) the particle has a bounce frequency

$$\omega_L = k_z \left| e\Phi_o J_L(k_\perp \rho)/m \right|^{\frac{1}{2}} = \frac{1}{4} k_z w_L \quad . \tag{15}$$

In the above development we have eliminated terms from the complete Hamiltonian by using our physical intuition that rapidly varying terms do not significantly affect the particle motion. This elimination can be done rigorously using any of several averaging methods, as discussed by Nayfeh.[91] Higher-order effects of the rapidly varying terms can be computed using these methods.

We end our discussion of particle motion in a small-amplitude wave by presenting a method, given by Taylor and Laing,[92] for computing an asymptotic expansion for a constant of the motion. The method is based on the fact that a function I of the canonical variables satisfies the Poisson bracket equation

$$\dot{I} = [I, H] \equiv \frac{\partial I}{\partial q} \cdot \frac{\partial H}{\partial p} - \frac{\partial I}{\partial p} \cdot \frac{\partial H}{\partial q} \quad .$$

A function I which is constant during the motion satisfies

$$0 = [I, H] \quad . \tag{16}$$

H and I are each expanded in a series using a small parameter ε:

$$H = H_0 + \varepsilon H_1 \tag{17a}$$

$$I = I_0 + \varepsilon I_1 + \varepsilon^2 I_2 + \ldots \quad . \tag{17b}$$

Equations (17) are substituted into (16) and terms containing the same powers of ε are collected. The coefficients of each power of ε must vanish identically:

$$0 = [I_0, H_0] \tag{18}$$

$$0 = [I_{n+1}, H_o] + [I_n, H_1], \quad n = 0, 1, 2, \ldots \quad . \tag{19}$$

Knowing the Hamiltonian H, we can, in principle, solve the partial

differential equations for the I_n in succession and find as many terms in I as we desire. The series obtained will generally be asymptotic: the series is divergent but, if truncated, the series can approximate the value of I as closely as desired by making ϵ small enough. Nevertheless, the series obtained may be singular; near certain points in phase space, I_1 may become infinite faster than I_0. Dunnett, Laing, and Taylor[52] developed a method for ensuring that I_1 is no more singular than I_0, that is, for making the first two terms of the asymptotic series uniformly valid.[91]

Applying this method to our problem, Taylor and Laing[92] choose units of mass, length, and time such that

$$m = k_z = \Omega = 1 \quad , \tag{20}$$

and write our Hamiltonian as

$$H = \frac{1}{2} p_z^2 + p_\phi + \epsilon \, \Sigma_\ell J_\ell \sin (z - \ell\phi) \tag{21a}$$

$$\epsilon \equiv k_z^2 \, e\Phi_o / m\Omega^2 \quad . \tag{21b}$$

For brevity in the equations below, we drop the subscript on p_z. Equation (18) is then

$$0 = p \frac{\partial I_o}{\partial z} + \frac{\partial I_o}{\partial \phi} \quad ,$$

the solution of which is an arbitrary function of p, p_ϕ, and $z - p\phi$. A sufficiently general solution is an arbitrary function $I_o(p)$ of p alone; for details, see Ref. 52. Equation (19) for $n=0$ is then

$$p \frac{\partial I_1}{\partial z} + \frac{\partial I_1}{\partial \phi} = \frac{dI_o}{dp} \frac{\partial H_1}{\partial z} = \frac{dI_o}{dp} \Sigma_\ell \, J_\ell \cos (z - \ell\phi) \quad ,$$

which has the solution

$$I_1 = \frac{dI_o}{dp} \Sigma_\ell \, J_\ell \, \frac{\sin (z - \ell\phi)}{p - \ell} \quad .$$

In general, I_1 is singular at

$$p = \ell, \; |\ell| = 0, 1, 2, \ldots \quad .$$

The singularities can be removed by choosing

$$I_o = \cos \pi p \quad .$$

The first two terms of the uniformly valid asymptotic series for I are thus

$$I = \cos \pi p - \epsilon \pi \sin \pi p \, \Sigma_\ell \, J_\ell \, \frac{\sin (z - \ell\phi)}{p - \ell} \quad . \tag{22}$$

Knowing the two constants of the motion H and I, we can illustrate the particle motion by drawing in the zp_z-plane contours of constant I for given H. We choose a value of ϕ ($= \pi$, here) and eliminate p_ϕ between $H(z, p_z, p_\phi)$ and $I(z, p_z, p_\phi)$ to obtain $I(z, p_z, H)$. (Note that p_ϕ appears in the argument $k_\perp \rho$ of the Bessel functions.) The actual computational algorithm exploits the simplification of (21a) for $\phi = \pi$:

$$H = \frac{1}{2} p_z^2 + p_\phi + \epsilon \sin z \quad .$$

This is solved for p_ϕ , which is used to calculate the argument of J_ℓ in (22). Values of I are computed at all points on the zp_z-plane which satisfy $p_\phi > 0$, and a plotting program draws the contours. The contour plots thus obtained show some of the features revealed by "surface of section" plots, discussed in Section 2I, which are computed

by time-consuming integration of the equations of motion. Some features of the particle motion are not revealed by contour plots of I, most importantly whether a constant of the motion I actually exists or not!

Shown in Fig. 14 is a sample contour plot of I. We see that near each resonance the contours of I are topologically different from those between resonances: the contours are closed curves instead of open ones. These topological differences lead to the singularities in the expansion (17) for I. Taylor and Laing[92] have shown how to remove the singularities while retaining the topological differences.

E. "Diffusion" and correlations in a linear theory

In later sections we will present numerical calculations showing diffusion and decay of correlations when resonances overlap. Here we define the diffusion coefficient and correlation function which we study, and show that, for short times, "diffusion" and "decay of correlations" can occur regardless of whether resonances overlap or not. True diffusion and decay of correlations, for long times, are possible only when overlapping resonances cause loss of memory of initial conditions. The results of this section allow us to properly interpret the numerical calculations to be presented later.

We choose to study the autocorrelation function of the parallel acceleration:

$$C(\tau, t') \equiv \langle \dot{v}_z (t' + \tau) \dot{v}_z (t') \rangle \quad . \tag{23}$$

The brackets denote an average over the phases $k_z z_o$ and ϕ_o,

$$\langle A \rangle \equiv \int_0^{2\pi} \frac{d(k_z z_o)}{2\pi} \int_0^{2\pi} \frac{d\phi_o}{2\pi} A \ , \tag{24}$$

with the subscript naught indicating the value of a variable at $t=0$. This average mimics the situation often found in the laboratory; the initial phases cannot be chosen by the experimenter and are uniformly distributed over the physically distinct values.

To calculate (23) we use, in this section, the unperturbed ($\Phi_o = 0$) orbits (10). These are the orbits used in linear theory (e. g., to find a dispersion relation), and it is clearly impossible to describe nonlinear effects, like resonance overlap, using them. The parallel acceleration is found from (9):

$$\dot{v}_z = -\frac{1}{m}\frac{\partial V}{\partial z} = -\frac{k_z e\Phi_o}{m} \Sigma_\ell J_\ell (a) \cos (k_z z - \ell\phi), \tag{25}$$

where $a \equiv k_\perp \rho_o$. Inserting (10) into (25) and calculating (23), we find

$$C(\tau) = C(0) \Sigma_\ell J_\ell^2(a) \cos[(k_z v_{zo} - \ell\Omega)\tau] \tag{26a}$$

$$= C(0) \cos (k_z v_{zo}\tau) J_o (2a \sin \tfrac{1}{2}\Omega\tau) , \tag{26b}$$

where $C(0) \equiv \frac{1}{2}(k_z e\Phi_o/m)^2$. Note that (26) is independent of t'. Formula (8.531.3) of Ref. 93 has been used to rewrite (26a) in the form (26b).

Many of our numerical calculations use $a=5$, so we study the shape of (26) for short times in the limit $a \gg 1$. For

$$\tau \lesssim 2\pi/\Omega , \tag{27}$$

(26b) yields

$$C(\tau) \approx C(0) \cos (k_z v_{zo} \tau) J_o (a\Omega\tau) . \tag{28}$$

For initial conditions such that

$$k_z v_{zo} << a\Omega = k_\perp v_{\perp o} , \tag{29}$$

(28) further simplifies, for $\tau \lesssim (k_z v_{zo})^{-1}$, to

$$C(\tau) \approx C(0) J_o (a\Omega\tau) . \tag{30}$$

From (30) we see that the correlation function falls to zero in the short time

$$\tau \approx 2.4/a\Omega \approx 0.5/\Omega$$

and then oscillates with a period

$$\tau_1 \approx 2\pi/a\Omega \approx 1.3/\Omega .$$

In Fig. 15 we compare the correlation function $C(\tau)$ found analytically from (26), the approximation (30), and $C(\tau, t' = 0)$ found from numerical integration (see Section 2G) of the equations of motion. The behavior predicted by the approximate expression (30) is indeed observed for sufficiently short times. Plots like Fig. 15 for other values of v_{zo} verify another prediction of (30): $C(\tau)$ is independent of v_{zo} when (29) holds.

In addition to the correlation function, we study the diffusion $\langle(\Delta v_z)^2\rangle$ in parallel velocity, where

$$\Delta v_z(t) \equiv v_z(t) - v_{zo} = \int_0^t dt'\ \dot{v}_z(t') \tag{31}$$

and the brackets are again defined by (24). From the definition (23) we have

$$\langle(\Delta v_z)^2\rangle \equiv \int_0^t dt' \int_{-t'}^{t-t'} d\tau\ C(\tau, t') \tag{32a}$$

$$= 2\int_0^t d\tau \int_0^{t-\tau} dt'\ C(\tau, t') \tag{32b}$$

$$= 2\int_0^t d\tau\ (t - \tau)\ C(\tau)\ . \tag{32c}$$

In (32b) we first used the symmetry property $C(\tau, t') = C(-\tau, t' + \tau)$ and then interchanged the order of the integrations.

To predict the time-dependence of $\langle(\Delta v_z)^2\rangle$ for short t, we again specialize to (29) and use (30). For <u>very</u> short times, $t \ll \tau_o \equiv (a\Omega)^{-1}$, (30) is nearly constant and (32c) yields

$$\langle(\Delta v_z)^2\rangle \approx C(0)t^2\ . \tag{33}$$

For

$$\tau_o < t < 2\pi/\Omega\,, \tag{34}$$

the main contribution to (32c) comes from $0 < \tau < \tau_o$, since $C(\tau)$ is small and rapidly oscillating for larger τ. Thus

$$\langle(\Delta v_z)^2\rangle \approx 2\ C(0)\ \tau_o t\,, \tag{35}$$

and the predicted "diffusion" coefficient is

$$D \equiv \langle(\Delta v_z)^2\rangle/2t \tag{36a}$$

$$\approx C(0)\tau_o = (k_z e\Phi_o/m)^2/2a\Omega \approx 0.1\ (k_z e\Phi_o/m)^2/\Omega\ . \tag{36b}$$

In Fig. 16 we compare $\langle(\Delta v_z)^2\rangle$ calculated analytically from (26) and (32) and from numerical integration of the equations of motion.

Tetreault[42] reached the same conclusion that "diffusion" can occur for short times even though motion is not stochastic. He pointed out the role in this "diffusion" of the nonresonant terms in (25). Each term causes constant acceleration of the particle, which would lead to the quadratic behavior seen in (33), but the number of nonresonant terms decreases as $1/t$, resulting in the linear behavior in (35).

For $k_z v_{zo} \approx a\Omega$, (28) predicts a different shape for $C(\tau)$ than (30) predicted in the limit (29). In the time interval (34) we use the large-argument formula

$$J_o(a \to \infty) \to (2/\pi a)^{\frac{1}{2}} \cos\ (a - \tfrac{1}{4}\pi)$$

to find (after dropping a rapidly varying term)

$$C(\tau) \approx C(0)\ (2\pi a\Omega\tau)^{-\frac{1}{2}} \cos\ [(k_z v_{zo} - a\Omega)\tau + \tfrac{1}{4}\pi]\ .$$

There is now a significant contribution to (32c) from $\tau > \tau_o$, and $\langle(\Delta v_z)^2\rangle$ increases more rapidly than t in the interval (34). Evidence for this behavior has been observed in our numerical integrations.

F. Chirikov criterion for stochasticity

In Section 2D we treated particle motion in a wave of amplitude small enough that at most one term in the perturbation (9) was slowly varying in time. Two terms can be slowly varying if a particle lies within a trapping half-width of each of two adjacent resonances (11):

$$|v_z - \ell\Omega/k_z| < \tfrac{1}{2} w_\ell$$

for <u>both</u> $\ell = L$ and $L+1$. The constants of the motion H_L and I_L, found when only the term $\ell = L$ was retained, are not expected to remain constant when <u>two</u> terms are slowly varying. Numerical integrations of the equations of motion verify (see Section 2J) that, in large regions of phase space, no constant exists except the Hamiltonian, if the wave amplitude is large. The particle is thus free to move almost anywhere on the energy (hyper)surface. This freedom can result in important physical consequences; in the presence of a single, obliquely propagating wave, particles can be accelerated to high velocities (i. e., a distribution can be heated to high temperatures).

The criterion that resonances overlap has been studied extensively by Chirikov[20] and found to predict the disappearance of constants of the motion (i. e., the onset of stochasticity) with accuracy sufficient for physical applications. The criterion is simply that the sum of the half-widths of adjacent resonances exceed the separation δ between them:

$$\frac{1}{2}(w_L + w_{L+1}) > \delta . \tag{37}$$

The separation (in parallel velocity) follows from the resonance condition (11):

$$\delta = \Omega/k_z \ . \tag{38}$$

The Chirikov criterion for stochastic particle motion in an oblique, electrostatic wave is thus

$$2|e\Phi_o/m|^{\frac{1}{2}} \left[|J_L(k_\perp\rho)|^{\frac{1}{2}} + |J_{L+1}(k_\perp\rho)|^{\frac{1}{2}}\right] > \Omega/k_z. \tag{39}$$

If the Bessel functions have comparable amplitudes, then (39) can be replaced by the simpler formula

$$16|e\Phi_o \ J_L(k_\perp\rho)/m| > (\Omega/k_z)^2 \ . \tag{40}$$

We interpret (40) as follows. Particles with parallel velocity (in the wave frame) such that $|k_z v_z/\Omega - L| < \frac{1}{2}$ will tend to move stochastically if (40) is satisfied but nonstochastically if it is not. We compare (39) to the findings of our numerical experiments in Section 2J.

Criterion (40) gives the wave amplitude necessary for stochasticity to occur for most (roughly speaking, the majority) of particles with the specified velocity. For wave amplitudes much less than (40), stochasticity occurs only in thin layers surrounding the separatrices associated with the resonances (11). These stochastic layers can be understood as arising from the overlap of a different set of resonances, which we call bounce resonances and study in detail in Chapter 4. One might think that these bounce resonances are of more fundamental importance than the cyclotron resonances we are emphasizing in Chapters 2 and 3, and that a more accurate stochasticity criterion

could be derived by considering bounce resonances. The numerical results of Chapter 4 show however that, for some choices of parameters, the border of stochasticity is determined by the overlap of yet another set of resonances. We clearly cannot continue to ascend the infinite hierarchy of resonances forever, and it is probably best to apply the Chirikov criterion to the lowest set of resonances for which a sensible answer can be obtained.

G. Numerical integration of the equations of motion

To test various aspects of the theory of stochasticity as applied to particle motion in an oblique, electrostatic wave, we perform numerical integrations of the equations of motion. The equations are derived from Hamiltonian (7):

$$\dot{z} = \partial H/\partial p_z \,, \quad \dot{\phi} = \partial H/\partial p_\phi \,,$$
$$\dot{p}_z = -\partial H/\partial z \,, \quad \dot{p}_\phi = -\partial H/\partial \phi \,. \tag{41}$$

We choose units such that (20) holds and write (41) explicitly as

$$\dot{z} = p_z \tag{42a}$$
$$\dot{\phi} = 1 - \varepsilon k_\perp \rho^{-1} \sin\phi \cos\chi \tag{42b}$$
$$\dot{p}_z = -\varepsilon \cos\chi \tag{42c}$$
$$\dot{p}_\phi = \varepsilon k_\perp \rho \cos\phi \cos\chi \,, \tag{42d}$$

where ε is defined in (21b),

$$\chi \equiv z - k_\perp \rho \sin\phi \,,$$

and $\rho = (2p_\phi)^{\frac{1}{2}}$. We avoid taking a square root by replacing (42d) by

$$\dot{\rho} = \varepsilon k_\perp \cos\phi \cos\chi . \tag{42e}$$

The four equations of motion (42a,b,c,e) are integrated on a CDC 7600 computer. The integration scheme used (Gear-Hindmarsh) is described by Risk[94] and utilizes standard predictor-corrector methods. The order of the method and the size of the integration step are adjusted automatically to optimize the efficiency of the integration. The maximum order available is twelve. In our integrations, a typical order was eight and a typical integration step was $\Delta t \sim 0.05\,\Omega^{-1}$.

Several checks of the integration accuracy were made. Since the Hamiltonian is independent of the time, its numerical value should be nearly conserved during the integration. The percentage change in the value of the Hamiltonian was 0.0005% in a typical integration time of $50\,\Omega^{-1}$. A different integration scheme was used in the early stages of this work. During the changeover from the old to the new scheme we checked that the particle trajectories found by the two schemes were very close to each other. Also, the equations of motion could be integrated forward and then backward in time to see if the initial conditions were recovered. For stochastic trajectories, the most difficult ones to integrate, we could integrate forward for a time $\sim 10\Omega^{-1}$ and still recover the initial conditions fairly well.

All calculations were done in single-precision, which is about 14 decimal digits on the 7600. There was no point in reducing round-off errors by calculating in double-precision, because truncation errors in

the integration scheme were always much larger than round-off errors.

We could adjust the amount of truncation error per integration step which was tolerated by the integration subroutine. For nonstochastic trajectories it was easy to see when a sufficiently small tolerance had been chosen, since points on our surface of section plots then fell on smooth curves. If too large a tolerance had been chosen, the points would tend to spiral in or out from a central point, behavior known not to occur in conservative systems like ours. For stochastic trajectories it was generally found necessary to choose a smaller tolerance than for nonstochastic ones. We could check that a small enough tolerance had been chosen for a stochastic orbit only by integrating for two values of the tolerance and comparing the resulting orbits.

It is easy to understand why smaller tolerances are required for stochastic trajectories. A truncation error causes a displacement in phase space between the calculated trajectory and the "true" one defined by the equations of motion. Along a stochastic orbit this displacement tends to increase exponentially with time while the increase tends to be linear along a nonstochastic one. A smaller tolerance helps to keep the accumulated error of a stochastic orbit comparable to the error of a nonstochastic one.

The presence of numerical integration errors in our trajectories is thought to have little, if any, significance for the physics of the problem we are studying. A real particle does not obey (42) exactly because there will inevitably be small, perturbing terms in the

equations of motion, arising from physical effects not included in our model. The truncation errors mimic, to some extent, the effects we have ignored. These errors are small enough that a nonstochastic trajectory appears to be stochastic only in a relatively thin layer separating the stochastic and nonstochastic regions; outside this layer the stochastic or nonstochastic nature of a trajectory is unaffected by small integration errors. These empirical results can probably be understood using the mathematical ideas[4] of KAM stability for nonstochastic orbits and of structural stability for stochastic orbits.

H. Related Hamiltonian systems

Several Hamiltonians, closely related to (7) which we have studied in most detail, have also been found by us to exhibit stochastic motion.

Our numerical results with (7) sometimes show only small variation of the gyroradius from its initial value ρ_o and only small deviation of the gyrophase ϕ from the unperturbed trajectory given in (10). A dynamical system with these properties built in is described by the Hamiltonian

$$H(z, p_z, t) = \frac{1}{2}p_z^2 + \epsilon \sin \chi \tag{43a}$$

$$\chi \equiv z - k_\perp \rho_o \sin \phi \tag{43b}$$

$$\phi \equiv t + \phi_o . \tag{43c}$$

The computer programs developed for studying (7) could easily be adapted

to study (43) instead; the only necessary change was the replacement of order ε terms on the right-hand-sides of (42b) and (42e) by zeros. We observed qualitatively similar behavior with (7) and with (43) but did not attempt detailed comparisons.

Another Hamiltonian studied by us is

$$H(z, \phi, p_z, p_\phi) = \frac{1}{2}p_z^2 + p_\phi + \varepsilon \sum_{\ell=m}^{M} C_\ell \sin (z - \ell\phi) , \tag{44}$$

where the C_ℓ are constants. The closest relationship to (7) is achieved by taking

$$C_\ell = J_\ell(k_\perp \rho_o)$$

with m and M large enough that the coefficients $J_\ell(k_\perp \rho_o)$ of the terms omitted from the sum in (44) are very small. The same time variation (43c) of the gyrophase is found from (44) as from (43a). An undesirable feature of (44) is the behavior of $p_\phi(t)$ which is found using it: p_ϕ can become negative if p_z increases (in the presence of overlapping resonances) to a large value. Hamiltonian (7) does not allow this possibility because a decrease in p_ϕ reduces the values of the coefficients $J_\ell(k_\perp \rho)$, preventing an excessive increase in p_z.

A Hamiltonian with the good behavior of (43) but with the flexibility of (44) is

$$H(z, p_z, t) = \frac{1}{2}p_z^2 + \varepsilon \sum_{\ell=m}^{M} C_\ell \sin (z - \ell\phi) , \tag{45}$$

with the time appearing again through (43c). If only two terms of the sum in (45) are retained, we obtain a dynamical system equivalent in all important respects to the one studied in Chapter 4 (compare (4.28)).

If we specialize (45) by taking $M=-m=\infty$ and $C_\ell \equiv 1$, we find

$$H(z, p_z, t) = \frac{1}{2}p_z^2 + \varepsilon T \sin z \, \Sigma_n \, \delta(t - nT + \phi_o) , \tag{46}$$

using $T \equiv 2\pi$ and the identity

$$\sum_{\ell=-\infty}^{\infty} e^{i\ell t} = 2\pi \sum_{n=-\infty}^{\infty} \delta(t - 2\pi n) . \tag{47}$$

We choose the particular value $\phi_o = 0^-$, drop the subscript on p_z, and write the equations of motion resulting from (46):

$$\begin{aligned} \dot{z} &= p \\ \dot{p} &= -\varepsilon T \cos z \, \Sigma_n \, \delta(t - nT + 0^-) . \end{aligned} \tag{48}$$

The evolution of the system is seen to reduce to the discrete mapping

$$\begin{cases} p_{i+1} = p_i - \varepsilon T \cos z_i \\ z_{i+1} = z_i + p_{i+1} \, T . \end{cases} \tag{49}$$

This mapping is similar to mappings studied by Chirikov,[20] Froeschlé, [95] and others.

I. Surface of section method

A particle trajectory resulting from integration of (42) lies on

a three-dimensional energy surface which is contained in the four-dimensional phase space. Attempting to represent a trajectory by a curve in a three-dimensional space would be needlessly difficult and confusing. To answer the important physical question of whether motion is stochastic or not, we need trajectory information only at certain, well-separated instants of time. In this section we describe the technique, known as the surface of section method, for selecting these instants of time and for constructing a plot using the retained trajectory information; we also discuss the utility of the method.

Poincaré's[53] surface of section method considers the intersection of a trajectory with a cross-section of the phase space. The chosen cross-section must be crossed repeatedly by the trajectory; a convenient choice in our work is defined by the gyrophase $\phi = \pi$. The choice of any other constant instead of π is quite possible, but the choice of π was seen in Section 2D to lead to a desirable simplification in applying the Taylor-Laing method. The intersection of the trajectory with $\phi = \pi$ yields a set of points in a three-dimensional space with axes z, p_z, and p_ϕ. We then ignore the p_ϕ-coordinates of the points and plot the points in the zp_z-plane (i. e., we <u>project</u> them onto the plane).

As we integrate the equations of motion forward in time, successive points on the surface of section plot are generated roughly once each gyroperiod. The points are iterates of an area-preserving mapping of the zp_z-plane onto itself. Calculating the iterates using the Hamiltonian equations of motion is computationally time-consuming,

and past workers[20,43,95-97] have often replaced a Hamiltonian system by a discrete mapping thought to mimic more or less closely the actual physical systems of interest. These mappings display transitions from nonstochastic to stochastic behavior as a parameter is varied, just as Hamiltonian systems do. We use the mapping (49) in Section 2K to aid us in understanding our numerical results for the correlation function $C(\tau)$. Generally we prefer, however, to use the Hamiltonian equations of motion and thereby eliminate uncertainty about the relation between the given physical system and a chosen mapping.

By looking at a surface of section plot we can tell immediately whether a particular trajectory shows stochastic motion (nonexistence of a constant of the motion) or not. By examining plots for several values of the stochasticity parameter (our ε) and for various initial conditions we can quickly gain a comprehensive understanding of the dynamical system being studied.

The utility of a surface of section plot arises from its method of construction. If a constant of the motion I exists for a particular orbit, that orbit will be confined to a two-dimensional surface, the intersection of the energy hypersurface with the hypersurface I=const. The intersection of this two-dimensional surface with the surface of section $\phi = \pi$ is a curve in $zp_z p_\phi$-space, and projection onto the zp_z-plane yields a curve on which the set of trajectory points must lie. If <u>no</u> constant I exists, an orbit will visit a three-dimensional region of the energy hypersurface. That region intersects $\phi = \pi$ in a two-dimensional surface, which, after

projection, appears as an area of the zp_z-plane. Thus, a constant of the motion exists if trajectory points lie on a curve, while a constant does not exist if the points fill an area. Note that the surface of section method does not tell us the analytic form of the constant, if one exists.

Surface of section plots are very useful in determining the important resonances of a dynamical system, as shown by an example to be presented in the next section.

J. Discussion of numerical results

To validate the analytic work, we integrate (42) numerically, presenting many of the results as surface of section plots.

We first illustrate, in Fig. 17, three of the resonances (11) for a wave amplitude Φ_o small enough that the resonances do not overlap. The widths of the resonances (w_L for L=-1, 0, and 1) are indicated. The dashed lines are the limits on the motion of a particle with a given energy which follow from the positivity of the gyroradius.

Next, in Fig. 18, we plot trajectories when the wave amplitude is large enough for resonances to overlap. Points representing nonstochastic trajectories have been connected by smooth curves. This plot illustrates the "divided phase space" which occurs at intermediate values of the wave amplitude: regions in which a constant of the motion (in addition to the energy) exists are interspersed with regions in

which it does not exist. Referring to Fig. 14 we see that the shapes of some of the smooth curves in Fig. 18 were predicted accurately using the method of Taylor and Laing. Other curves, representing resonances other than (11), appear in Fig. 18 but were not predicted earlier. Near each of the three "primary" resonances (11) we see a set of five smooth curves; each set represents a single trajectory and is referred to as a chain of islands. Each chain shows the existence of a "secondary" or bounce resonance, which we study in detail in Chapter 4.

To demonstrate the possibility of heating a distribution of particles by applying a single, obliquely propagating wave, we use the plots in Fig. 19. The plots are constructed by the surface of section method, but in contrast to Figs. 17 and 18, the trajectory points are projected onto the $v_\perp v_z$-plane instead of the zp_z-plane. Fig. 19 shows the motion in velocity space (i. e., the acceleration) of a group of particles which is specified precisely in the figure caption; the group is chosen to represent particles with certain values of the perpendicular and parallel velocities at $t=0$. We consider a wave of frequency $\omega = 3.6\Omega$ and choose a value $v_z = -\omega/k_z$ for the parallel velocity (as measured in the wave frame). The chosen particles thus have zero parallel velocity (as measured in the plasma frame) at $t=0$.

Fig. 19 contrasts the particle acceleration in a wave of relatively small ($\varepsilon = 0.25$) or large ($\varepsilon = 0.75$) amplitude. In the small amplitude case no particles in the chosen group move stochastically, and the particle velocities remain near their initial values. In the large amplitude case all of the particles move stochastically, appearing to

diffuse throughout much of the semicircular annulus bounded by the dashed curves. The dashed curves give the limits on the particle motion which follow from conservation of energy (as measured in the wave frame): the wave can change the kinetic energy of a particle by $2e\Phi_o$ at most, giving curves at speeds $(v^2 \pm 4\, e\Phi_o/m)^{\frac{1}{2}}$, where v is the initial speed. The time-averaged value of a particle's kinetic energy, as measured in the plasma frame, increases substantially in the large amplitude case. The vertical axis at the far left of Fig. 19 helps us see the extent of the increase in parallel kinetic energy.

In Section 2L we give examples of electrostatic waves which could cause heating of a particle distribution. In Section 2M we consider the heating of a Maxwellian distribution and find that the tail particles are accelerated most strongly. In Appendix D we mention some experimental requirements which must be satisfied in order to observe stochastic acceleration.

Our numerical results indicate a transition to stochastic motion at $\varepsilon \approx 0.50$ when the propagation angle and initial particle velocity have the values used in Fig. 19. To compare this numerical result to the theoretical formula (39) we insert the values $J_{-3} = -0.17$ and $J_{-4} = 0.051$ for Bessel functions of argument $k_\perp \rho = 2.24$ and find the condition for stochastic motion to be

$$\varepsilon > 0.61 \ .$$

The agreement is as good as can be expected considering the crudeness of both the numerical measurement and the theory.

In Fig. 19 the numbers 0, 1, 2, 5, 6, 7 show the positions of a particle (with a certain z_o) after the indicated number of gyroperiods. The apparent diffusion process noted earlier seems quite rapid, and we now investigate this process more carefully. We numerically calculate the trajectories of 50 to 200 particles which have unique initial values of $v_\perp$ and v_z but initial values of $k_z z$ and ϕ arranged in a regular array (see Fig. 20). In Fig. 21 we plot, for a subset of the trajectories, the parallel velocity v_z vs. time. We first note the diffusion of v_z away from its initial value; below we study this diffusion quantitatively. Interesting features of some trajectories in Fig. 21 are periods of rapid change in v_z (large parallel acceleration) separated by periods of relatively constant v_z. These features can be understood by referring to the related Hamiltonian systems (45) and (46). If the gyroradius has an appropriate value, several of the Bessel function coefficients in (9) may have comparable magnitudes, causing the motion to resemble that of (46), at least temporarily. The periods of large parallel acceleration are thus attributed to constructive interference of the terms in (25).

To study the diffusion process quantitatively, we use the numerically calculated trajectories to compute $\langle(\Delta v_z)^2\rangle$, a quantity introduced in Section 2E. The time variation of this quantity typically has the form shown in Fig. 22. Quadratic and then linear dependences on time, as predicted by (33) and (35), are observed during the first gyroperiod or so. Thereafter, a deviation from the linear behavior, indicating either a larger or a smaller diffusion rate, generally occurs. An interpretation of this deviation which is consistent with

our numerical results is the following. The rate of diffusion of a group of particles is primarily determined by their present velocities rather than by the past history of the group (i. e., a Markovian assumption has some validity). As a group of particles diffuses, some particles reach velocities for which the diffusion rate is, say, larger than it was at the initial velocity. The diffusion rate of the whole group then appears to increase. This interpretation is indicated on Fig. 22. For long times the diffusion process ceases because the group has spread out to fill the entire stochastic region of velocity space (see Fig. 19).

Using the numerically calculated trajectories, we also compute the correlation function (23). Fig. 23 shows a typical shape for $C(\tau, t' = 0)$. In Section 2E we explained the observed shape for short τ using a linear theory (see Fig. 15). Fig. 23 extends to longer τ than Fig. 15 and reveals persistent oscillations in the correlation function. We propose two explanations for these oscillations. First, the oscillations may be an artifact of the small number of trajectories used; this possibility is demonstrated for the mapping (49) in the next section. Fig. 24 shows, however, that for parameters of interest in wave-heating, there is only a weak dependence of the measured correlation function on the number of trajectories. The second explanation is that our moderate values ($\varepsilon \lesssim 1$) of the stochasticity parameter allow long-time correlations for a significant fraction of the particle trajectories used to compute $C(\tau)$. This effect is demonstrated in the next section for the mapping (49). In addition, Fig. 25 suggests that this effect is present for the Hamiltonian (7):

increasing ε by a factor of four appears to decrease the rms level of the oscillations. The larger of the values of ε used in Fig. 25 corresponds to a wave of such large amplitude (see Section 2L) that we begin to doubt our assumption that the wave is sinusoidal.

Measurements of quantities like the correlation function thus seem somewhat problematical. One is concerned that an insufficient number of trajectories has been chosen. Elimination of the persistent oscillations requires an amplitude violating the sinusoidal assumption. On the other hand, if one wants to study these oscillations, which are a real physical effect, no theory is available with which the numerical results can be compared. In the face of these problems we have limited our study of the correlation function.

K. Correlation function of a discrete mapping

In this section we measure the dependence of a correlation function of the mapping (49) on the number of trajectories and on the size of the stochasticity parameter. We feel the results presented below support the explanations proposed in the preceding section for the behavior of the correlation function (23).

The correlation function which we measure is

$$C_i \equiv 2\langle \cos z_i \cos z_o \rangle , \tag{50}$$

where the bracket denotes the average over z_o. This quantity for the mapping (49) is analogous to (23) for the Hamiltonian (7). We iterate

(49) up to step i=24 for N=100 or 400 initial values of z:

$$z_o = 2\pi n/N \ , \ n=0, 1, 2, \ldots, N-1 \ .$$

The numerically calculated iterates are then used to compute (50). In Fig. 26 we show C_i for N=100 and a relatively large value of $\varepsilon = 0.20$. After an initial decay C_i shows persistent oscillations, just as $C(\tau)$ does in Fig. 23. Note, however, that we calculate C_i over 24 steps, each of which corresponds to one gyroperiod, while Fig. 23 extends to only about 2.4 gyroperiods. In Fig. 27 we show that an increase of the number of trajectories, N, to 400 greatly reduces the oscillations. For a quantitative measure of the reduction we compute the rms level of C_i from i=12 to 24. With N=100, $(C_i)_{rms}=0.107$, and with N=400, $(C_i)_{rms}=0.0535$. The empirical relation

$$(C_i)_{rms} \approx N^{-\frac{1}{2}}$$

is strong evidence that the persistent oscillations in Figs. 26 and 27 are caused by the finite values of N.

Next we investigate the dependence of C_i on ε, keeping N constant (=400). The results are seen by comparing Fig. 27, for which $\varepsilon=0.20$, and Fig. 28, for which $\varepsilon=0.06$. The set of trajectories used for Fig. 28 contains some nonstochastic trajectories, which cause, we believe, the persistent oscillations seen in Fig. 28.

L. Oblique electrostatic waves for acceleration of ions

In Section 2J we use, as an example, an electrostatic wave with frequency $\omega = 3.6\Omega$, propagation angle $\theta = 45^{o}$, and various amplitudes measured by $\varepsilon \equiv k_z^2 e\Phi_o/m\Omega^2$. We identify here a particular wave with these properties and show that the amplitudes used are not unreasonably large.

We concentrate on waves appropriate for heating ions, but we note that often there exists, for each ion wave, an electron wave with analogous parameters which is appropriate for heating electrons.

A plasma in a uniform magnetic field can support an obliquely propagating, electrostatic wave which we call an ion-acoustic wave. This wave is indicated in Fig. 29. The name "intermediate-frequency acoustic wave" is used in the old, but still useful review by Stringer.[98] Our terminology is based on the similarity to the ion-acoustic wave which exists in an unmagnetized plasma. In deriving the linear dispersion relation of the ion-acoustic wave in a magnetized plasma, one finds an ion response similar to the response in an unmagnetized plasma since the wave frequency is greater than the ion gyrofrequency. The electrons are strongly magnetized and move only along, not across, field lines. The electrons can, nevertheless, act to shield the potential produced by the ions as long as θ is not too close to 90^{o}. The frequency ω is thus given approximately by the unmagnetized formula

$$\omega \approx kc_s,$$

where $k^2 \equiv k_z^2 + k_\perp^2$, and the sound speed is given by $c_s^2 \equiv (T_e + 3T_i)/m_i$. Given the wave parameters $\omega = 3.6\Omega_i$ and $\theta = 45^o$ and the temperature ratio T_e/T_i, we calculate the damping rate of the wave using the formula (4.68) in Ichimaru[99] appropriate for Maxwellian distributions of electrons and ions. Just as in an unmagnetized plasma, we find a weakening of the damping as T_e/T_i increases. The damping reaches a fairly small value when T_e/T_i is increased to 16:

$$\gamma \approx -0.04\omega .$$

Such a large temperature ratio would not be required in an unmagnetized plasma to reach this damping rate. With the temperature ratio 16 chosen we can calculate the ion thermal speed, $v_{Ti} \equiv (T_i/m_i)^{\frac{1}{2}}$, to be

$$v_{Ti} \approx 0.58\Omega_i/k_z . \tag{51}$$

This speed is indicated on Fig. 19 by the hatched semicircle. The group of ions studied in Fig. 19 would thus have an initial perpendicular velocity 3.8 times the thermal speed.

We now express the wave amplitude given by $\varepsilon = 0.5$ in more familiar terms. From the fluid equations describing an ion-acoustic wave, one easily derives a relation between the potential amplitude Φ_o and the density amplitude $\delta n/n$:

$$\frac{\delta n}{n} = \frac{e\Phi_o}{m_i c_s^2} . \tag{52}$$

Using the formulas for the dielectric function D and the Debye length λ_D, we also find the expression

$$W \equiv \frac{1}{8\pi}\,\omega\,\frac{\partial D}{\partial \omega}\,\langle E^2\rangle \;=\; \frac{\Phi_o^2}{8\pi\lambda_D^2} = \frac{1}{2} n\,(e\Phi_o)^2/T_e \tag{53}$$

for the wave energy density W. Use of (51) and $T_e/T_i=16$ allows us to write $\varepsilon=0.5$ as

$$e\Phi_o \approx \frac{3}{2}\,T_i \approx \frac{1}{11}\,T_e\,. \tag{54}$$

Substitution of (54) into (52) and (53) yields

$$\delta n/n \approx \frac{1}{13}\;,\; W \approx nT_i/15\,. \tag{55}$$

The moderate numerical values in (55) appear to justify our use of the linear dispersion relation for the wave. Also, (55) gives the important result that stochasticity can occur at smaller amplitudes than nonlinear effects requiring $\delta n/n \sim 1$. For other wave parameters, however, stochasticity might not occur for any physically reasonable wave amplitude.

The low-frequency ion-acoustic wave

$$\omega \approx k_z c_s < \Omega_i$$

might also be used to heat ions. A large temperature ratio is again required to reduce the linear damping rate. This wave seems to lead to less dramatic heating of an ion distribution than the ion-acoustic wave with $\omega > \Omega_i$ which we considered above. The difference between parallel velocities in the plasma frame and in the wave frame decreases as ω decreases (see Fig. 19). For small ω the constant energy curves in the two frames are close together, implying less possibility of dramatic changes in the distribution of parallel kinetic energy (as

measured in the plasma frame).

We have considered other waves of a plasma in a uniform magnetic field but have found no wave with more favorable parameters than those given above. Lacking a definite optimization criterion, we have not performed a systematic variation of ω and θ. Values of θ close to 90^{o} are of particular interest since many waves propagate nearly perpendicular to the magnetic field; the lower hybrid wave, important in rf heating studies for tokamaks, is one example. For parameters typical of lower-hybrid-heating experiments the condition (40) for overlap of cyclotron resonances cannot be satisfied. Ion motion may be stochastic, nevertheless, because of the overlap of other resonances, as mentioned in Subsection 1C4.

M. Heating of a distribution function

In Section 2J we showed that a group of particles with given parallel and perpendicular velocities at $t=0$ may be heated by a single, oblique wave. Here we consider a Maxwellian distribution of velocities at $t=0$ and find the distortion of that distribution caused by the wave.

We use the following qualitative picture suggested by Fig. 19. An ion whose velocity satisfies (40) moves stochastically, ranging over that portion of the constant-energy semicircle defined by (40). An ion whose velocity does not satisfy (40) remains nearly fixed in velocity space. In the presence of a single, oblique wave of large amplitude the

steady-state ion distribution must therefore be constant along the stochastic portions of the constant-energy semicircles and nearly Maxwellian in the nonstochastic regions of velocity space.

This picture is implemented by a computer program which modifies an initially Maxwellian distribution to obtain the steady-state distribution. The modification is accomplished by successively considering semicircular annuli in $v_\perp v_z$-space, each of which represents particles with a small range of speeds. For each annulus the Maxwellian is integrated over the stochastic portion of the annulus to find the total number of stochastic ions in the annulus. This number is then spread over the stochastic portion of the annulus to form a distribution with a certain weighting along the constant-energy semicircle. We choose a weighting proportional to the perpendicular velocity $v_\perp$ to make the distribution uniform over the three-dimensional $(v_x v_y v_z)$ kinetic energy surface. The form of the chosen weighting determines quantitative, but not qualitative, features of the resulting distribution.

The steady-state distribution in $v_\perp v_z$-space is integrated over v_z to obtain the perpendicular distribution and over $v_\perp$ to obtain the parallel distribution. In Fig. 30 we plot these distributions on a logarithmic scale. The horizontal (velocity) axes use a quadratic scale so that a Maxwellian (indicated by $\varepsilon=0$) appears as a straight line. Results for two different values of the wave amplitude are indicated by $\varepsilon=0.25$ and 0.75. The same wave frequency and propagation angle and the same ion thermal speed are used as in the example of Section 2L.

The wave is seen to distort only the tails of the perpendicular and parallel distributions, not the bodies. The perpendicular distribution is distorted for $v_\perp \gtrsim 3v_{Ti}$ in the case $\varepsilon=0.75$. The distortion of the parallel distribution is highly asymmetric because ions tend to be accelerated to the parallel velocity of the wave frame, which is positive and much larger than the thermal speed. Although the distortions shown in Fig. 30 involve only a tiny fraction of the ions in the complete distribution, the changes in the populations of tail ions are quite dramatic.

The tiny fraction of ions which is stochastically accelerated by the wave can gain a substantial amount of energy as a result of the large velocity changes produced during stochastic acceleration. As a numerical example we consider the smaller amplitude case $\varepsilon=0.25$ for which 0.03% of the ions move stochastically. These ions increase their kinetic energy by an amount roughly equal to <u>half</u> of the energy in the wave. We thus expect the propagation characteristics of the wave to be altered significantly when stochastic acceleration occurs.

3. Analytic Description of the Diffusion Process

In Chapter 2 we introduced a simple problem illustrating the overlap of cyclotron resonances, derived and verified a stochasticity criterion, and discussed the implications of stochastic motion (wave energy is converted to plasma kinetic energy). Also, we presented results of our numerical integrations and gave explanations of many of those results. This chapter is devoted to an extremely important practical question not addressed in Chapter 2: what equations describe the rate of change of a particle distribution in the presence of a perturbation (e. g., a wave) large enough to cause stochastic motion?

We assume here, in agreement with other authors,[20,24] that the diffusion process is Markovian, and we search for an appropriate diffusion coefficient. Stochasticity tends to erase the memory of a particle's history, thus justifying, to some extent, the Markovian assumption. For our moderate values of the stochasticity parameter, ϵ, a considerable memory remains and a non-Markovian description may be necessary. Such a description was presented in Ref. 100.

A. Linear and quasilinear theories

In Section 2E we presented a linear theory which agreed well, for short times, with the results of our numerical integrations. In particular, the time-dependences of the correlation function $C(\tau)$ and the diffusion $\langle(\Delta v_z)^2\rangle$ of the parallel velocity were predicted using

the linear theory. For long times this theory cannot, however, give an adequate description if resonances overlap, since the theory does not allow for any (true) decay of correlations, which is an important feature of stochastic motion. The failure of linear theory's prediction for the correlation function is clear from (2.26) in the cases of integral values of $k_z v_{zo}/\Omega$: $C(\tau)$ is periodic with frequency Ω.

To derive a diffusion coefficient, one must assume that there exists a decay of correlations which is not present in linear theory. When the correlation time is short compared to a particle diffusion time, the limits of the τ-integrals in (2.32) can be extended to infinity. If $C(\tau, t')$ is independent of t', a diffusion coefficient

$$D = \int_0^\infty d\tau \; C(\tau) \tag{1}$$

can be found.

In quasilinear theory, one inserts in (1) the (non-decaying) correlation function $C(\tau)$ found from linear theory. This procedure gives a sensible formula for D if the wave spectrum is continuous. In our problem, however, the spectrum is discrete, and integration of the cosines in (2.26a) yields the unbroadened (δ-function) resonances in the mathematically nonsensical result

$$D = C(0) \; \Sigma_\ell \; J_\ell^2 \; (a) \; \pi \; \delta(k_z v_{zo} - \ell\Omega) \, . \tag{2}$$

Mechanisms for the decay of correlations give, effectively, a finite upper limit on the integral (1), leading to broadened resonances. When the spectrum is discrete, it is essential to take these mechanisms into

account.

B. Mechanisms for the decay of correlations

In this section we mention three mechanisms for the decay of correlations (and thus the broadening of resonances), one of which does not occur in our work and two of which do occur.

A resonance can appear broadened if the energy in the wave spectrum is increasing or decreasing at a rate γ. A particle then feels wave energy in a frequency band of half-width γ. Since we use a constant wave amplitude (i. e., a stationary wave energy spectrum) in our numerical integrations, this broadening mechanism is not present in our work.

Another resonance broadening mechanism occurs, physically, because a particle which remains near a certain resonance for only a finite time cannot determine the frequency of that resonance exactly. Work on this mechanism was begun many years ago[101] and has continued until relatively recently.[102] The standard method for treating this diffusion process gives, as we show below, insufficient broadening of the resonances and therefore cannot adequately explain our numerical results.

The standard method begins with the substitution of (2.25) into (2.23) to obtain an exact expression for $C(\tau, t')$. Approximations are made which reduce the double Bessel function sum to a single sum of the

form

$$C(\tau) = C(0)\ \mathrm{Re}\ \Sigma_\ell\ J_\ell^2(k_\perp\rho_o)[\exp\ i(k_z v_{zo} - \ell\Omega)\tau]\langle\exp(ik_z\delta z)\rangle\ , \quad (3)$$

where

$$\delta z(\tau) \equiv z(\tau) - z_o - v_{zo}\tau\ .$$

More approximations allow one to derive an equation for the diffusion coefficient:

$$D = C(0)\ \Sigma_\ell\ \ J_\ell^2(k_\perp\rho_o)\ R_\ell\ (v_{zo},\rho_o)\ . \quad (4)$$

The resonance functions R_ℓ depend on D through

$$R_\ell \equiv \int_0^\infty d\tau\ \cos\ [(k_z v_{zo} - \ell\Omega)\tau]\exp(-\tfrac{1}{3}k_z^2\ D\tau^3)\ . \quad (5)$$

The failure of the standard treatment of resonance broadening is illustrated by a numerical example. From plots like Fig. 22 we measure diffusion rates of roughly $0.05\,\Omega^3/k_z^2$. The resonance functions (5) then have full-widths (in frequency) of $\lesssim 0.5\,\Omega$, significantly narrower than the separation Ω between resonances. As a result, our attempts to calculate iteratively values $D(v_{zo})$ for the diffusion coefficient either failed to converge or gave sharp peaks near the resonances (2.11). The complete absence of such peaks in the numerically measured $D(v_{zo})$ forces us to reject (4) and (5) as a description of the diffusion process.

Evidently, some of the numerous approximations leading to (3)-(5) are poor. A serious defect of the standard treatment is the

obscuring or, possibly, the complete omission of an important mechanism for the decay of correlations (and thus the broadening of resonances). This mechanism is called mixing in Ref. 4. While only the slow (action) variables enter into the physical description of correlation decay by diffusion, for mixing the fast (angle) variables play an essential role. The mixing process is often the primary object for study in stochasticity theory (see, for example, the important Refs. 3 and 20). Mixing is rarely mentioned in the plasma physics literature, and it is customary[4] in stochasticity theory to attempt to eliminate the diffusion process. Consequently, the relation between decay of correlations by diffusion and by mixing remains obscure. Here we limit our treatment of mixing to setting up the (almost trivial) calculation of the local rate of separation of neighboring trajectories. This local rate gives information about the stochasticity only of very special systems. For more general systems a lengthy theoretical treatment of mixing is given by Chirikov,[20] but a treatment for Hamiltonian systems like ours seems not to be available. Our limited treatment may give the flavor of the mixing process but yields no information which we can compare with numerical results.

To calculate the rate of separation of two neighboring trajectories we consider the vector $\Delta \underline{Y} \equiv (\Delta z, \Delta\phi, \Delta p, \Delta\rho)$ giving the separation between two nearby points in phase space (we suppress the subscript on p_z). This vector changes its orientation and its length as the two phase points move according to the equations of motion (2.42). If the vector has infinitesimal components, the equation of motion for the vector is easily derived. We write equations (2.42) for

two different phase points $\underline{Y}_i = (z_i, \phi_i, p_i, \rho_i)$, i=1,2, subtract the corresponding pairs of equations from each other, and expand the right-hand sides in Taylor series. The result is a vector equation of the form

$$\dot{\Delta\underline{Y}} = \overleftrightarrow{A}_4(\underline{Y}) \cdot \Delta\underline{Y} , \tag{6}$$

where $\overleftrightarrow{A}_4$ is a 4x4 matrix whose elements are functions of position $\underline{Y}$ in phase space.

Since particles move on constant-energy surfaces in phase space, we are most interested in the rate of separation of trajectories lying on the same energy surface. A vector $\Delta\underline{Y}$ lying on an energy surface has components related by

$$0 = \Delta H = p\Delta p + \rho\Delta\rho + \frac{\partial V}{\partial z}\Delta z + \frac{\partial V}{\partial \phi}\Delta\phi + \frac{\partial V}{\partial \rho}\Delta\rho , \tag{7}$$

where we use the units (2.20) and

$$V \equiv \epsilon \sin (z - k_\perp \rho \sin \phi) . \tag{8}$$

Using (7) we can eliminate Δp from the right-hand sides of (6) and derive an equation of motion for $\Delta\underline{X} \equiv (\Delta z, \Delta\phi, \Delta\rho)$, the separation of two trajectories near position $\underline{X} \equiv (z, \phi, \rho)$ on the energy surface:

$$\dot{\Delta\underline{X}} = \overleftrightarrow{A}_3(\underline{X}) \cdot \Delta\underline{X} . \tag{9}$$

Using the abbreviations

$$V' \equiv \epsilon \cos (z - k_\perp \rho \sin \phi)$$

$$c \equiv \cos \phi , \quad s \equiv \sin \phi ,$$

we can write the 3x3 matrix $\overleftrightarrow{A}_3(\underline{X})$ as

$$\overleftrightarrow{A}_3 = \begin{pmatrix} -V'/p & k_\perp \rho c V'/p & k_\perp s V'/p - \rho/p \\ -k_\perp s V/\rho & k_\perp^2 cs V - k_\perp c V'/\rho & k_\perp^2 s^2 V/\rho + k_\perp s V'/\rho^2 \\ k_\perp c V & -k_\perp^2 \rho c^2 V - k_\perp s V' & -k_\perp^2 cs V \end{pmatrix} . \quad (10)$$

In (10), p is to be expressed in terms of $\underline{X}$ using (2.7).

We see that (9) has the form of three coupled, ordinary, first-order differential equations with variable coefficients. We restrict our attention to very short times for which a particle's $\underline{X}$ has changed very little. The coefficients can then be treated as constants and a general solution written:

$$\Delta\underline{X}(t) = \sum_{j=1}^{3} C_j \, \underline{\Delta}_j \, e^{\gamma_j t} . \quad (11)$$

The C_j are constants determined by the initial separation $\Delta\underline{X}(t = 0)$. The eigenvalues γ_j and eigenvectors $\underline{\Delta}_j$ are found by solving

$$[\overleftrightarrow{A}_3(\underline{X}) - \gamma\overleftrightarrow{1}] \cdot \underline{\Delta} = 0 . \quad (12)$$

The fact that $\overleftrightarrow{A}_3$ is a real matrix allows us to derive the following reality conditions for the γ_j (and also for the $\underline{\Delta}_j$): one eigenvalue is always real, while the other two are either both real or form a complex conjugate pair. From the reality conditions we can show that a real value for $\Delta\underline{X}(t = 0)$ leads to real values for $\Delta\underline{X}(t > 0)$, in spite of the complexness of the C_j, γ_j, and $\underline{\Delta}_j$ in (11).

If the initial separation $\Delta\underline{X}$ lies exactly along a real eigenvector, say $\underline{\Delta}_1$, then the separation will grow (or shrink) at the rate γ_1. However, the eigenvalues and eigenvectors depend on the position $\underline{X}$ on the energy surface for which (12) is solved. The change in $\underline{X}$ during the motion may thus lead to changes in the magnitudes and signs of the eigenvalues and in the directions of the eigenvectors. These serious complications make direct use of the local rate of separation impossible.

C. Semi-empirical model for the diffusion coefficient

In the previous section we mentioned some of the known theoretical ideas for treating decay of correlations and resonance broadening in stochastic dynamical systems. Since these theoretical ideas have not led to useful comparisons with our numerical results, we introduce here a semi-empirical model which is found to agree with those results in some respects.

Our idea is simple and physically reasonable but not derivable from any known theory. We retain the form (4) but replace the resonance function (5) with a broader function, a Lorentzian of half-width ν_ℓ:

$$R_\ell(\omega) = \int_0^\infty d\tau \cos \omega\tau \exp(-\nu_\ell \tau) = \nu_\ell(\omega^2 + \nu_\ell^2)^{-1} . \qquad (13)$$

We choose ν_ℓ to reproduce the trapping half-width calculated in Section 2D:

$$\nu_\ell = \frac{1}{2} k_z w_\ell . \tag{14}$$

Chirikov[103] suggests instead

$$\nu_\ell = (\tfrac{1}{2} k_z w_\ell)^{4/3}/\Omega^{1/3} , \tag{15}$$

which is supported by the theory in Section 2.11 of Ref. 20. Standard resonance broadening theory also leads to a half-width ν_ℓ proportional to (15), although the theories appear quite different. This result follows from (5), which gives

$$\nu_\ell = (\tfrac{1}{3} k_z^2 D)^{1/3},$$

and the estimate

$$D \approx \pi C(0) J_\ell^2/\Omega$$

following from (4) in the limit of strongly overlapping resonances. The constant factors suggested by standard resonance broadening theory yield a much smaller value for the half-width than (15). Our semi-empirical model for the diffusion coefficient is insensitive to the shape used in (13) and to the value of ν_ℓ as long as the resonance functions R_ℓ are broad enough to overlap. Consequently, our numerical comparisons, described below, do not allow us to choose between different resonance functions.

In Fig. 31 we use (4), (13), and (14) to plot the diffusion coefficient D as a function of the initial parallel velocity v_{zo}. Curve (a) uses a relatively large value of ε, curve (b) a somewhat smaller one.

We now compare the curves in Fig. 31 to values of the diffusion coefficient measured from plots like Fig. 22. The observed points and error bars in Fig. 31 are derived from the slopes of $\langle(\Delta v_z)^2\rangle$ vs. time at short times. The logic behind this comparison is, strictly speaking, not correct. Our semi-empirical model is supposed to describe a nonlinear system with stochastic motion, while the short-time slopes are not determined by stochasticity but by the linear effects discussed in Section 2E. The measured slopes give, however, a fair indication of the diffusion rate at later times when the linear theory undeniably must be replaced by a nonlinear one. Fig. 31 shows that our semi-empirical model predicts the level of and, roughly, the variation with v_{zo} of the diffusion coefficient.

D. Conclusions of Chapters 2 and 3

In Chapters 2 and 3 we have studied the motion of a charged particle in a single wave, which is propagating obliquely to a uniform magnetic field. As the wave amplitude is increased, a constant of the motion disappears, allowing the motion to become stochastic. The Chirikov criterion of overlapping resonances gives a prediction for the onset of stochasticity in good agreement with the results of numerical integration of the equations of motion.

We have numerically computed a correlation function and found evidence for its decay with time when motion is stochastic. Our results show, however, that the study of correlation functions of Hamiltonian

systems requires more careful, and costly, numerical experiments than ours.

The resemblance of stochastic motion to a diffusion process has been observed numerically. We have found no previous theory which adequately explains our observations but have introduced a semi-empirical model which gives a good description of the diffusion process.

The Hamiltonian system studied by us closely resembles many other dynamical systems. The results found by us thus may aid investigations of problems seemingly remote from particle motion in a single wave.

We have considered the possibility of using the overlap of cyclotron resonances as a mechanism for heating a particle distribution. Choice of an electrostatic wave, the ion-acoustic wave, allows parameters satisfying the requirements of our analysis. The analysis predicts rapid transfer of wave energy to ions in the tails of the perpendicular and parallel distributions. Heating of ions by this mechanism does not appear important in fusion plasmas but might be used in a small-scale laboratory experiment to observe stochastic acceleration by a single wave.

4. Overlap of Bounce Resonances Caused by the Trapped-Ion Mode

We saw in Chapters 2 and 3 how the overlap of cyclotron resonances could lead to stochastic motion in a uniform magnetic field. In a nonuniform field we would expect the results found above to be modified somewhat. Instead of studying these modifications we have chosen to investigate an entirely new phenomenon which arises when the magnetic field is nonuniform along a field line, as sketched in Fig. 32. In such a field, particles with a parallel velocity small compared to the perpendicular velocity can be trapped between magnetic mirrors and bounce along the field line about the point of minimum field magnitude. If the bounce frequency ω_b is comparable to the frequency of a wave in the plasma, the resonances

$$\omega = n\omega_b , \quad n = 1, 2, 3, \ldots$$

can be important. This chapter studies a situation in which the overlap of bounce resonances is important.

Bounce resonances occur in many different problems; in Section 4E we discuss problems which seem to us to be of interest to the fusion program. The occurrence of bounce resonances in many physical situations is expected from the discussion in Subsection 1C7: the dynamical systems studied are of a generic, rather than a special, type.

A. Choice of model and parameters

Of the many problems of interest to the fusion program we have chosen to study the motion of an ion in a large-aspect-ratio tokamak in the presence of a dissipative trapped-ion mode. That this system is described by the dynamical equations we study was not widely recognized when we began this work. A brief report of our work has already been published.[104] We were able to choose appropriate parameters by consulting the well-developed linear theory of the dissipative trapped-particle instabilities. For readers who are unfamiliar with these instabilities we include in Appendix E a discussion of the physics of the dissipative trapped-ion instability.

The parameters of the trapped-ion mode which will be important to us are its amplitude, parallel wavenumber, and frequency. We assume the amplitude Φ_o to be given by

$$e\Phi_o = 0.05\ (\Delta B/B_o)\ T_i \ , \tag{1}$$

where e is the ion charge, T_i is the ion temperature, B_o is the field at the magnetic axis, and ΔB is the modulation amplitude of the field. Note that a typical value of $\Delta B/B_o$ is one-fourth. The numerical factor 0.05 was chosen so Φ_o would be comparable to the mode amplitudes at which other[105] nonlinear processes become important and also at which trapped-particle modes have been observed[106] in experiments.

The parallel wavenumber $k_\parallel$ is given in terms of the poloidal and toroidal mode numbers m and ℓ, respectively, by

$$k_{\parallel} q R_o \equiv m - \ell q = \frac{1}{2} \quad , \tag{2}$$

where R_o is the major radius of the tokamak, and q is the safety factor on a magnetic surface near which the ion motion occurs (a precise specification of this magnetic surface will be given later). The value $\frac{1}{2}$ takes into account two properties of the trapped-ion mode. First, the modes with different values of m are coupled together strongly because trapped particles are present. For a given ℓ, several modes with adjacent values of m have appreciable amplitudes. The mode with the largest amplitude has the m which makes $|m - \ell q|$ as small as possible. Second, the radial structure[107] of a mode of given ℓ shows maximum amplitudes between the magnetic surfaces where q is rational (i. e., equal to an integer divided by ℓ). Thus, we study the motion of an ion near a surface on which $q = (m \pm \frac{1}{2})/\ell$. We believe qualitatively similar ion motion would be found for any value of $m - \ell q$ not too close to zero; this belief was verified by a few calculations with $m - \ell q = \frac{1}{4}$.

The mode frequency ω must satisfy several requirements (see Appendix E) before the mode can be unstable and grow to large amplitudes. The growth rate of the mode (due to electron collisions) is proportional to ω^2. If the plasma parameters are such that ion Landau damping (proportional to ω^4) is unimportant, then the mode with the largest possible ω will grow fastest. The mode frequency is limited by the very approximate relation $\omega < \omega_{bi}$, where the bounce frequency of a deeply trapped, thermal ion is given by

$$\omega_{bi} = (T_i \Delta B / B_o M)^{\frac{1}{2}} / q R_o \quad , \tag{3}$$

where M is the ion mass. In accordance with the approximate limit $\omega < \omega_{bi}$, we choose

$$\omega = \frac{1}{2}\omega_{bi} \quad . \tag{4}$$

Our numerical calculations of ion trajectories use only the ratios $e\Phi_o/\mu\Delta B$ and $\omega/\omega_{bi}(\mu B_o/T_i)^{\frac{1}{2}}$, where μ is the magnetic moment. The calculations thus apply to values of the amplitude and frequency other than (1) and (4), as long as those ratios are unchanged.

The electrostatic potential due to a spectrum of trapped-ion modes can be written as

$$\Phi(\Theta, \zeta, \alpha, t) = \Sigma_\ell \Phi_\ell(\Theta,\alpha) \cos(m\Theta - \ell\zeta - \omega_\ell t + \eta_\ell) \quad , \tag{5}$$

where Θ and ζ are the poloidal and toroidal angles, respectively, and α is the toroidal flux (divided by 2π) enclosed within a magnetic surface (i. e., α gives the minor radius r of a surface of circular cross section according to the approximate relation $\alpha = \frac{1}{2}B_o r^2$). The mode with toroidal mode number ℓ has a frequency ω_ℓ (assumed real in the saturated state) and phase η_ℓ. As mentioned above, m is chosen so that $|m - \ell q|$ is as small as possible. The sum over ℓ consists of modes with, in general, different linear growth rates. For simplicity in our numerical and analytical work we select from this sum the single term representing the mode with the largest linear growth rate. The α-dependence of $\Phi_\ell(\Theta,\alpha)$ leads to finite-banana-width corrections, which we neglect, to radial $\underline{E} \times \underline{B}$ drifts. The α-dependence also leads

to poloidal and toroidal $\underline{E} \times \underline{B}$ drifts, which are negligibly small compared to diamagnetic drift or thermal velocities. We thus have replaced (5) by

$$\Phi = -\Phi_o\, g(\Theta) \cos\,(m\Theta - \ell\zeta - \omega t + \eta) \quad , \tag{6}$$

where subscripts on ω and η have been dropped and we have introduced the poloidal structure factor g using

$$\Phi_\ell(\Theta) = -\Phi_o\, g(\Theta) \quad .$$

The simplest poloidal structure, and the one used for most of our work, is $g=1$. For a few calculations we have used

$$g(\Theta) = \frac{1}{2}(1 + \cos\Theta) \quad , \tag{7}$$

which models the ballooning of the mode on the outer side $(\Theta = 0)$ of the torus.

B. Transformation to action-angle variables

In studies of tokamak problems we believe significant advantages are gained by utilizing the appropriate set of action-angle variables. Once the meaning of the variables is understood, one can easily see analogies between problems in the relatively complicated tokamak configuration and in simpler configurations (e. g., a uniform or zero magnetic field). The appropriate variables for a tokamak have been used by many workers, with the most systematic formulation given by Kaufman.[108] During the course of this work a slight refinement of the

results of Ref. 108 was developed.

For the sake of completeness and to introduce the notation used here we review the ideas of Kaufman[108] in this section. We begin with Kaufman's Eq. (11) for the Hamiltonian describing guiding-center motion in quasistatic electric and magnetic fields. We assume that no quasistatic electric field is present and suppress any indication that the magnetic field might be varying slowly in time. We also take the usual large-aspect-ratio limit and find the guiding-center Hamiltonian to be

$$H_o(\Theta, \alpha, p_\zeta; \mu) = [p_\zeta + e\Psi(\alpha)/c]^2/2MR^2(\Theta,\alpha) + \mu B(\Theta,\alpha) \quad . \tag{8}$$

The magnetic moment μ appears here as a parameter which is constant in time. A more complete theory would treat $(Mc/e)\mu$ as a canonical momentum as was done in Chapter 2. In this chapter we will deal with guiding-center motion only and are thus able to reduce the number of canonical variables to four. The toroidal angle ζ does not appear in (8), since we are assuming the tokamak to be axisymmetric. The momentum p_ζ canonically conjugate to ζ is thus a constant of the unperturbed motion:

$$\dot{p}_\zeta = -\partial H_o/\partial\zeta = 0 \quad .$$

The variables Θ and α give the location of the guiding center in a plane perpendicular to $\hat{\zeta}$. These variables are chosen to be a set of Euler potentials,[109] variables in which the magnetic field is described simply and naturally. Each of the nested magnetic surfaces is labeled by α, which, physically, is the toroidal flux (divided by 2π)

enclosed by the surface. The variable Θ gives the poloidal position of the guiding center on the magnetic surface α. The toroidal field is given by

$$B_\zeta \hat{\zeta} = \nabla x \underline{A}_p , \quad \underline{A}_p = \alpha \nabla \Theta .$$

The calibration of Θ is such that, along a field line,

$$d\Theta/d\zeta = 1/q(\alpha) ,$$

with the safety factor q a function of the magnetic surface labeled by α. That these conditions can all be satisfied simultaneously was shown by Hamada[110] and discussed by Greene and Johnson[111] and Solov'ev and Shafranov.[112] The poloidal flux function Ψ is conventionally used instead of the toroidal component of the vector potential A_ζ, which determines the poloidal component of the magnetic field:

$$\Psi = -RA_\zeta , \quad \underline{B}_p = B_\Theta \hat{\Theta} = \nabla x (A_\zeta \hat{\zeta}) .$$

Ψ is a function of α with derivative

$$d\Psi/d\alpha = 1/q(\alpha) .$$

The spatial variables Θ and α are a pair of conjugate variables in Hamiltonian (8). To be precise, the momentum canonically conjugate to Θ is

$$p = e\alpha/c .$$

(For a uniform magnetic field, in Chapter 2, we found the analogous result that $m\Omega X$ is the momentum canonically conjugate to Y.) From

Hamiltonian (8) we derive the equations of motion

$$\dot{\Theta} = \frac{c}{e}\frac{\partial H_o}{\partial \alpha} = \frac{\dot{\zeta}}{q} + \frac{c}{e}\mu\frac{\partial B}{\partial \alpha} - \frac{Mc}{e}\dot{\zeta}^2 R\frac{\partial R}{\partial \alpha} \tag{9a}$$

$$\dot{\alpha} = -\frac{c}{e}\frac{\partial H_o}{\partial \Theta} = -\frac{c}{e}\mu\frac{\partial B}{\partial \Theta} + \frac{Mc}{e}\dot{\zeta}^2 R\frac{\partial R}{\partial \Theta}\,, \tag{9b}$$

where we have used

$$\dot{\zeta} = \partial H_o/\partial p_\zeta = (p_\zeta + e\Psi/c)/MR^2 \quad . \tag{10}$$

In (9) the terms proportional to $\dot{\zeta}^2$ are the curvature drift and the terms proportional to μ are the gradient drift.

We now introduce a more convenient set of variables which we denote by $(\Theta', \alpha', \zeta', p'_\zeta)$. For this purpose we use the function $\alpha_o(p_\zeta)$, defined by

$$p_\zeta + e\Psi(\alpha_o)/c = 0\,.$$

From (10) we see that, for a trapped particle, α_o is the value of α at the particle's turning point $(\dot{\zeta} = 0)$. We also note that

$$d\alpha_o/dp_\zeta = -(c/e)(d\Psi/d\alpha_o)^{-1} = -cq(\alpha_o)/e\,.$$

The generating function

$$F_2(\Theta, \zeta, \alpha', p'_\zeta) = \Theta e[\alpha' + \alpha_o(p'_\zeta)]/c + \zeta p'_\zeta$$

yields

$$\Theta' = \Theta \quad , \quad \zeta' = \zeta - q(\alpha_o)\Theta \tag{11}$$

$$\alpha' = \alpha - \alpha_o(p'_\zeta)\,, \quad p'_\zeta = p_\zeta \quad .$$

Since Θ and p_ζ are unchanged by this canonical transformation, we henceforth drop the primes on those variables.

Hamiltonian (8) can be expressed in terms of the two canonical momenta $\underline{p} = (e\alpha'/c, p_\zeta)$ and the one coordinate Θ. To obtain the simplest equations of motion and to bring out the analogies between motion in a uniform and in a nonuniform magnetic field, we express the Hamiltonian in terms of two momenta and <u>no</u> coordinates. The variables Θ and α', are replaced by action-angle variables J and ϕ.

The action variable J is given by

$$2\pi J(H_o, p_\zeta) = (e/c) \oint d\Theta\, \alpha'(\Theta, H_o, p_\zeta) \quad . \tag{12}$$

To carry out the integral in (12) explicitly, one needs to solve (8) for α'. The integral sign $\oint$ is interpreted differently for trapped and circulating particles. For a trapped particle, the variable Θ oscillates in the range $-\Theta_{TP} \leq \Theta \leq \Theta_{TP} < \pi$, where the subscript TP denotes the turning point, as the particle follows the well-known banana orbit. The integral in (12) is to be evaluated during one execution of the banana orbit. For a circulating (also known as passing, transit, or untrapped) particle, the variable Θ increases or decreases monotonically as the particle moves (in the lowest approximation) along a field line. During this motion the particle encounters successively the minima and maxima of the magnetic field. The integral in (12) is to be evaluated over <u>two</u> periods of this oscillatory motion (e. g., from one minimum of the field, past a maximum, a minimum, another maximum, and ending at a minimum). This definition of J is continuous across

the boundary between trapped and circulating particles.

The action J is closely related to the well-known longitudinal invariant $\oint v_{\|}\, ds$. In the large-aspect-ratio approximation, which we have adopted,

$$v_{\|}/R_o \approx \dot{\zeta} \approx [\Psi(\alpha) - \Psi(\alpha_o)]\, e/McR_o^2 \approx \alpha' e/McqR_o^2$$

and

$$ds \approx R_o d\zeta \approx qR_o\, d\Theta \ ,$$

so from (12)

$$2\pi J \approx M \oint v_{\|}\, ds \ .$$

Using (12) to eliminate H_o in favor of J, we write the generating function

$$F_2(\Theta, \zeta', J, \bar{p}_\zeta) = \zeta' \bar{p}_\zeta + (e/c) \int_o^\Theta d\Theta'\, \alpha'(\Theta', J, \bar{p}_\zeta) \ ,$$

where the bar on $\bar{p}_\zeta$ indicates that F_2 depends on the new (canonically transformed) momentum. The new momentum $\bar{p}_\zeta$ is in fact equal to the old momentum p_ζ, so we henceforth omit the bar. The new angle variable conjugate to J is

$$\begin{aligned} \phi = \partial F_2/\partial J &= (e/c)\int_o^\Theta d\Theta'\, \partial\alpha'/\partial J \\ &= \omega_b \int_o^\Theta d\Theta'/\dot{\Theta} = (t - t_o)\omega_b \ , \end{aligned} \tag{13}$$

where $\Theta(t_o) = 0$, and the bounce (or transit) frequency is given by

$$\omega_b(J, p_\zeta) = \partial H_o/\partial J \quad .$$

For a trapped particle, ω_b is the frequency of bouncing between magnetic mirrors. For a circulating particle, ω_b is <u>half</u> the frequency of transiting from one minimum of the magnetic field to the next. The new coordinate conjugate to p_ζ is

$$\bar{\zeta} = \partial F_2/\partial p_\zeta = \zeta' + (e/c)\int_o^\Theta d\Theta'\, \partial\alpha'/\partial p_\zeta \quad .$$

Physically, $\bar{\zeta}$ gives the value of ζ' averaged over a period of the Θ -motion. For a trapped particle, $\dot{\bar{\zeta}}$ is the (constant) drift of the banana in the toroidal direction. In Fig. 33 we illustrate the relationship between Θ and ϕ .

We show the analogies between gyromotion (Chapter 2) and bounce motion (Chapter 4) in Table I. The canonical variables we have used for a uniform and for a tokamak magnetic field are compared. Constant factors have been omitted in Table I to keep the entries simple. The intermediate variables x' and y' were not given explicitly in Chapter 2 but are shown here for comparison with ζ' and α' . The analogy between gyromotion and bounce motion is the key to understanding the relationship between classical and neoclassical transport theory.[113]

C. Guiding-center motion in absence of a wave

In Section 4F we will estimate (using the Chirikov criterion) the mode amplitude Φ_o necessary for overlap of bounce resonances.

Here we gain a better understanding of the unperturbed ($\Phi_o = 0$) motion and derive formulas we will need in Section 4F.

To make the problem analytically tractable we introduce some simplifying assumptions. We believe these assumptions do not fundamentally alter the physical mechanism (overlap of bounce resonances) which we are studying. Referring to Hamiltonian (8), we first neglect the Θ- and α-dependence of R:

$$R(\Theta,\alpha) \to R_o \quad .$$

We thus lose curvature drifts, as seen from (9). We will be most interested in particles with parallel velocity small compared to perpendicular velocity, for which curvature drifts are negligible compared to ∇B-drifts (at least in a low-β tokamak). Second, we neglect the α-dependence of B:

$$B(\Theta,\alpha) \to B(\Theta) \quad .$$

This approximation eliminates the ∇B-drift term in (9a), which is easily shown to be negligible compared to the remaining term on the right hand side of (9a) for particles with gyroradius much less than the tokamak minor radius. Finally, we ignore the shear of the magnetic field by eliminating the unwritten terms in the expansion

$$\Psi(\alpha) = \Psi(\alpha' + \alpha_o) = \Psi(\alpha_o) + \alpha' \, d\Psi/d\alpha_o + \ldots \quad .$$

With these approximations we write Hamiltonian (8) as

$$H_o(\Theta,\alpha') = (e\alpha'/cqR_o)^2/2M + \mu B(\Theta) \quad .$$

With the approximations we have used, a trapped particle executes a non-drifting banana orbit of negligible width. Hamiltonian H_o also describes the guiding-center motion of a particle near the axis of a mirror machine.

We now assume the flux surfaces have circular cross sections. This assumption, with the large-aspect-ratio approximation, guarantees that Θ is the usual poloidal angle (it gives the radian measure of a point on the flux surface, with the outer edge of the torus designated as $\Theta = 0$). We thus have

$$B(\Theta) = B_o - \Delta B \cos\Theta \quad ,$$

where B_o is the field at the magnetic axis and ΔB is the modulation amplitude of the field (we use the value of ΔB on the surface labeled by α_o). The Hamiltonian can now be written

$$H_o = (e\alpha'/cqR_o)^2/2M - \mu\Delta B \cos\Theta \quad . \tag{14}$$

The constant term μB_o has been dropped; the relation between H_o and the particles's energy E is, from here on,

$$H_o = E - \mu B_o \quad . \tag{15}$$

The shape of the magnetic field we have adopted and the symbols used to describe it are shown in Fig. 32, along with the effective potential energy levels of trapped and circulating particles.

Equation (12) for the action J can now be written as

$$2\pi J(H_o) = qR_o \oint d\Theta \, [2M(H_o + \mu\Delta B \cos\Theta)]^{\frac{1}{2}} \quad .$$

The explicit expressions for J involve κ, defined by

$$2\kappa^2 \equiv (1 + H_o/\mu\Delta B) \quad , \tag{16}$$

and $K(\kappa)$ and $E(\kappa)$, the complete elliptic integrals of the first and second kind with modulus κ:

$$J = qR_o(M\mu\Delta B)^{\frac{1}{2}} \frac{8}{\pi} \begin{cases} E(\kappa) - (1-\kappa^2)K(\kappa), & \kappa < 1 \\ \kappa E(\kappa^{-1}) & , \kappa > 1 \end{cases} . \tag{17}$$

Note that a trapped particle has $E < \mu B_M$, where $B_M \equiv B_o + \Delta B$, and thus $\kappa < 1$, while a circulating particle has $\kappa > 1$. The angle variable ϕ, which is canonically conjugate to J, is given, for $-\pi \leq \Theta \leq \pi$ and $\alpha' > 0$, by

$$\phi = \frac{\omega_b}{\omega_b(0)} \begin{cases} F(\xi,\kappa) & , \kappa < 1 \\ \kappa^{-1} F(\frac{1}{2}\Theta,\kappa^{-1}) & , \kappa > 1 , \end{cases} \tag{18}$$

where $\kappa \sin\xi = \sin\frac{1}{2}\Theta$, and $F(\xi,\kappa)$ is the incomplete elliptic integral of the first kind with amplitude ξ and modulus κ. For other ranges of Θ and α' (which is proportional to $\dot{\Theta}$) we use the definitions of ϕ indicated in Fig. 33. These definitions prevent the addition to ϕ of unwanted multiples of π when a particle crosses the separatrix. The frequency of bouncing ($\kappa < 1$) or transiting ($\kappa > 1$) is given by

$$\frac{\omega_b}{\omega_b(0)} = \frac{\pi}{2} \begin{cases} 1/K(\kappa) & , \kappa < 1 \\ \kappa/K(\kappa^{-1}), & \kappa > 1 , \end{cases} \tag{19}$$

where the bounce frequency of a deeply trapped particle ($\kappa = 0$) is

$$\omega_b(0) = (\mu\Delta B/M)^{\frac{1}{2}}/qR_o \quad . \tag{20}$$

The boundary in velocity space between the trapped and the circulating states is given by $E = \mu B_M$ or $\kappa = 1$. This boundary is referred to as the separatrix; it separates orbits of dissimilar topology in the $\Theta\alpha'$-plane. The most important fact about the separatrix is the form of ω_b near it. Fig. 34 shows both J and ω_b as a function of H_o, which is related to κ by (16); Fig. 34 uses the units given in (21). The decrease of ω_b to zero at the separatrix allows multiple, closely spaced resonances to appear near the separatrix when the mode amplitude $\Phi_o \neq 0$.

D. Hamiltonian

We can now write down the Hamiltonian which describes the guiding-center motion of an ion in a tokamak in the presence of a trapped-ion mode. With the approximations adopted above, (9a) has reduced to $\dot{\zeta} \approx q\dot{\Theta}$ which implies

$$\zeta \approx \zeta_o + q(\Theta - \Theta_o) \quad .$$

The electrostatic potential (6) due to the mode involves

$$m\Theta - \ell\zeta \approx (m - \ell q)\,\Theta + \text{const} \quad .$$

We absorb the constant term into η and write the Hamiltonian as

$$H(\Theta,\alpha',t) = H_o(\Theta,\alpha') + e\Phi(\Theta,t) \quad ,$$

with H_o given by (14) and

$$\Phi = -\Phi_o\, g(\Theta) \cos[(m - \ell q)\Theta - \omega t + \eta] \quad .$$

We choose the units of mass, length, and time such that

$$M = qR_o = \mu\Delta B = 1 \quad . \tag{21}$$

The unit of frequency is seen from (20) to be $\omega_b(0)$. Using $p = e\alpha'/c$, we write the Hamiltonian in the dimensionless form

$$H(\Theta,p,t) = \frac{1}{2}p^2 - \cos\Theta - e\Phi_o\, g(\Theta) \cos[(m - \ell q)\Theta - \omega t + \eta] \quad . \tag{22}$$

In terms of the action-angle variables the Hamiltonian is

$$H(\phi,J,t) = H_o(J) + e\Phi(\phi,J,t) \quad , \tag{23}$$

where $H_o(J)$ is the function obtained by inverting $J(H_o)$, which is possible numerically but not analytically. The perturbation has the form

$$\Phi = -\Phi_o \sum_{n=-\infty}^{\infty} U_n(J) \cos(n\phi - \omega t + \eta) \quad , \tag{24}$$

where the Fourier coefficients $U_n(J)$ are given by

$$U_n = \frac{1}{2\pi} \int_{-\pi}^{\pi} d\phi\; g(\Theta) \cos[(m - \ell q)\Theta - n\phi] \quad , \tag{25}$$

with

$$\Theta(\phi,J) = 2 \begin{cases} \sin^{-1}\{\kappa\, sn[\phi\, \omega_b(0)/\omega_b, \kappa]\} & , \kappa < 1 \\ am\,[\kappa\phi\, \omega_b(0)/\omega_b,\ \kappa^{-1}] & , \kappa > 1 \end{cases} \tag{26}$$

found by inverting (18), and $J(\kappa)$ given by (17). The notation sn refers to one of the Jacobian elliptic functions and am is the amplitude function, the inverse of the incomplete elliptic integral F. It is easiest to derive (24) and (25) by writing

$$g(\Theta) \exp [i(k\Theta + \delta)] = \Sigma_n U_n \exp [i(n\phi + \delta)]$$

and noting that

$$U_n = \frac{1}{2\pi} \int_{-\pi}^{\pi} d\phi \; g(\Theta) \exp [i(k\Theta - n\phi)]$$

is real because $g(\Theta) = g(-\Theta)$ and $\Theta(\phi) = -\Theta(-\phi)$.

The U_n can be expressed in terms of

$$V_{n,k} = \frac{1}{2\pi} \int_{-\pi}^{\pi} d\phi \cos (k\Theta - n\phi) \quad . \tag{27}$$

For the poloidal structure given by (7) and $k = m - \ell q = \frac{1}{2}$

$$U_n = \frac{1}{4} (2 V_{n,\frac{1}{2}} + V_{n,\frac{3}{2}} + V_{n,-\frac{1}{2}}) \quad .$$

E. Other problems described by the same Hamiltonian

Using the abbreviations $\varepsilon = e\Phi_o$ and $k = m - \ell q$, setting the constant η , which is unimportant for the present discussion, to zero, we write Hamiltonian (22) in the simplest case (g=1) as

$$H(\Theta,p,t) = \frac{1}{2}p^2 - \cos\Theta - \varepsilon \cos(k\Theta - \omega t) \quad . \tag{28}$$

As shown in Subsection 1C7, (28) can be written in the time-independent form

$$H(\Theta,p,\phi,I) = \frac{1}{2}p^2 + I\omega - \cos\Theta - \varepsilon\cos(k\Theta - \phi) \quad . \tag{29}$$

The Hamiltonian (28) which we are studying in this chapter occurs quite generally as an approximate Hamiltonian in dynamical systems of two or more degrees of freedom, as discussed in Subsection 1C7. In this section we mention a few problems in plasma physics described, at least approximately, by Hamiltonian (28).

In Chapter 2 we obtained in (2.13) a Hamiltonian H_L describing the motion of a particle with parallel velocity v_z (in the wave frame) near $L\Omega/k_z$. To derive H_L we assumed that, for such a particle, only one term in the complete Hamiltonian, the one varying slowest in time, was important. To determine the effect of one of the previously omitted terms (the one with $\ell = L+1$), we choose units such that

$$m = k_z = e\Phi_o J_L = 1$$

and study the Hamiltonian

$$H(\psi,p_\psi,\phi,I_L) = \frac{1}{2}p_\psi^2 + I_L\Omega + \sin\psi + \varepsilon\sin(\psi - \phi) \quad , \tag{30}$$

where $\varepsilon = J_{L+1}/J_L$. If the dependence of ε on $I_L - Lp_\psi$ (through the Bessel function argument $k_\perp\rho$) is sufficiently weak, then we can approximate (30) by (29) with k=1.

Zaslavskii and Filonenko[114] and Kaw and Kruer[115] studied the one-dimensional motion of a particle in two electrostatic waves, one of amplitude Φ_o and wavenumber k_o, the other of amplitude $\Phi < \Phi_o$ and wavenumber k. Choosing units such that

$$m = k_o = e\Phi_o = 1$$

and a reference frame moving with the large-amplitude wave, we can write the Hamiltonian for this system exactly as in (28), where $\varepsilon = \Phi/\Phi_o$. The motivation for the study in Ref. 114 was the desire to understand the conditions for validity of the quasilinear approximation. Ref. 115 studied the motion of deeply trapped particles analytically and of both deeply and barely trapped particles numerically; the numerical observations were apparently similar to ours. Stix[116] studied exactly the same system, with the hope of finding a plasma heating scheme in which energy transfered from an external source to plasma particles can be randomized even when collisions are absent.

Dobrowolny, et al.[117] considered the motion of a particle in a sinusoidally modulated magnetic field same model of a tokamak as in Section 4C) and an electrostatic wave propagating <u>parallel</u> to the magnetic field. Hamiltonian (28) describes this problem also. The values of the parameters ε and ω used by the authors of Ref. 117 were similar to our values, but the values of k (=20 and 100) were much larger. They found that under certain conditions a particle trapped at $t=0$ between magnetic mirrors could be detrapped and forced to move at the wave's phase velocity.

Rechester and Stix[37] used equations derivable from a Hamiltonian of the form (28) to study the trajectories of magnetic field lines in the presence of two tearing modes in a tokamak. The two tearing modes are peaked near rational surfaces with minor radii r_o and r_1, and Ref. 37 studies the trajectories of field lines near r_o. The perturbation parameter ε is the ratio of the tearing mode

amplitudes, measured at r_o. Ref. 37 took the dimensionless parameter $\omega >> 1$, which is apparently the appropriate limit for that problem. For our problem (particle motion in a tokamak in the presence of a trapped-ion mode), the limit $\omega < 1$ is more appropriate, as we will discuss in Section 4G.

We mention one more problem, closely related to that of Rechester and Stix,[37] but not considered explicitly in the literature, to our knowledge. The ripple of the tokamak magnetic field, caused by the discreteness of the toroidal field coils, should cause destruction of the outer contours of magnetic islands resulting from a tearing or kink mode.

F. Chirikov criterion for overlap of bounce resonances

The locations (in phase space) of the bounce resonances and the widths of the resonances follow trivially from the Hamiltonian (23) expressed in action-angle variables. From the separation between resonances and the resonance widths, we use the Chirikov criterion to derive, in this section, the condition for overlap of bounce resonances.

A particle is near the nth bounce resonance when the nth term in (24) is slowly varying in time. Since we are treating $e\Phi$ as a small perturbation of the unperturbed Hamiltonian H_o,

$$\dot{\phi} = \partial H/\partial J \approx \partial H_o/\partial J = \omega_b(J) \ .$$

The values of the action J for which bounce (or transit) resonance

occurs are thus given by

$$\omega_b(J) = \omega/n \quad . \tag{31}$$

We denote these resonant values of J by J_n and see that, since $\omega_b(J) \to 0$ as $\kappa \to 1$, there are two values of J_n for each positive integer n. The separation, $J_n - J_{n+1}$, between resonances n and $n+1$ is most conveniently expressed in terms of the resonant values of the bounce frequency:

$$\delta_n \equiv \omega_b(J_n) - \omega_b(J_{n+1}) = \omega/n(n+1) \quad . \tag{32}$$

From (32) we see that the separation between resonances decreases rapidly as n increases.

For the width of resonance n we ignore all other resonances and calculate from (23) the width of the "secondary" separatrix. This separatrix divides the ϕJ-plane into regions in which the phase $n\phi - \omega t$ is either bounded or unbounded in time. The separatrix width is calculated from (23) as follows. We introduce the new canonical variables ψ and I by means of the generating function

$$F_2(\phi, I, t) = (n\phi - \omega t)I + \phi J_n :$$

$$\psi = n\phi - \omega t$$

$$I = (J - J_n)/n$$

$$H(\psi, I) = H_o(I) - \omega I - e\Phi_o\, U_n(I) \cos\psi \quad . \tag{33}$$

We then expand H_o and U_n about $I=0$ (that is, about $J = J_n$) to obtain

$$H(\psi,I) \approx \tfrac{1}{2}(\partial^2 H_o/\partial I^2) I^2 - e\Phi_o\, U_n(I=0)\cos\psi \quad . \tag{34}$$

The motion occurs on the secondary separatrix if $H = |e\Phi_o U_n|$, with a maximum value of I given by

$$\Delta I = 2\left|e\Phi_o\, U_n/(\partial^2 H_o/\partial I^2)\right|^{\frac{1}{2}} \quad .$$

Doubling this value to obtain the full-width of resonance n and expressing the result in terms of functions of J (evaluated at J_n), we obtain

$$(\Delta J)_n = 2n\Delta I = 4\left|e\Phi_o\, U_n(J_n)/(\partial^2 H_o/\partial J_n^{\,2})\right|^{\frac{1}{2}} \quad .$$

Converting the width in action to the width in frequency by use of the function $\omega_b(J) = \partial H_o/\partial J$, we find the resonance width to be

$$\Delta_n = 4\left|e\Phi_o\, U_n(J_n)\ \partial\omega_b/\partial J_n\right|^{\frac{1}{2}} \quad . \tag{35}$$

To put (35) in a useful form we need to know the Fourier coefficients $U_n(J)$. Here we take the poloidal structure factor $g=1$, so that $U_n = V_n$, where we suppress the subscript k on $V_{n,k}$. In (27) we need $\exp(ik\Theta)$, which, for $k = m - \ell q = \frac{1}{2}$, can be put in the relatively simple form

$$\exp(ik\Theta) = \begin{cases} \mathrm{dn}\ u + i\kappa\ \mathrm{sn}\ u\ , & \kappa < 1 \\ \mathrm{cn}\ u + i\ \mathrm{sn}\ u\ , & \kappa > 1 \end{cases} ,$$

where $u = \phi 2K/\pi$ and elliptic integrals and Jacobian elliptic functions have modulus κ for $\kappa < 1$ and modulus κ^{-1} for $\kappa > 1$. Fourier series expansions of the Jacobian elliptic functions are tabulated in many references, including Abramowitz and Stegun.[118] From these

expansions we can read off the $V_n(J)$:

$$V_n(J) = \frac{\pi}{K} q^{n/2} \begin{cases} \begin{cases} (1-q^n)^{-1}, & n \text{ odd} \\ (1+q^n)^{-1}, & n \text{ even} \end{cases}, & \kappa < 1 \\ \begin{cases} 2/\kappa(1-q^{2n}), & n \text{ odd} \\ 0, & n \text{ even} \end{cases}, & \kappa > 1 \end{cases} , \tag{36}$$

where the nome q (not to be confused with the safety factor) is given by

$$q \equiv \exp(-\pi K'/K)$$

and

$$K' \equiv K(\kappa'), \quad \kappa' \equiv \begin{cases} (1-\kappa^2)^{\frac{1}{2}}, & \kappa < 1 \\ (1-\kappa^{-2})^{\frac{1}{2}}, & \kappa > 1 \end{cases} .$$

The expressions in (36) are valid for $n > 0$, which are the values of n of immediate interest to us. For $n < 0$ we note that

$$V_n = \begin{cases} \begin{cases} -V_{|n|} & \kappa < 1 \\ -q^{|n|} V_{|n|}, & \kappa > 1 \end{cases}, & n \text{ odd} \\ V_{|n|}, & n \text{ even} \end{cases} , \tag{37}$$

while for $n=0$ we have

$$V_o = \begin{cases} \pi/2K, & \kappa < 1 \\ 0, & \kappa > 1 \end{cases} . \tag{38}$$

A useful approximation for the coefficients $V_n(J)$ is easily

found in the limit $K << 1$, as is clear from Ref. 119. In this limit, (26) reduces to

$$\Theta = \Theta_{TP} \sin \phi \tag{39}$$

with

$$\Theta_{TP} \xrightarrow[K << 1]{} 2K. \tag{40}$$

Substitution of (39) into (27) and use of (2.8) yields

$$V_{n,k}[J(K)] \approx J_n(k\Theta_{TP}) , \tag{41}$$

which is further simplified by using (40). The Bessel function on the right-hand side of (41) should not be confused with the action variable J. Note that (41) is valid for all k, while (36), which carries no restriction on K, is valid only for $k = \frac{1}{2}$.

The Chirikov criterion for overlap of bounce resonances n and n+1 is given in terms of the widths Δ_n and separations δ_n by

$$\frac{1}{2}(\Delta_n + \Delta_{n+1}) > \delta_n \quad . \tag{42}$$

If the widths of resonances n and n+1 are comparable, the simpler formula

$$\Delta_n > \delta_n \tag{43}$$

may be used. When equation (42) or (43) is written out explicitly using the formulas given above, a complicated combination of elliptic integrals appears. To derive simple results which are easy to interpret we next find approximations to several of the above formulas which are

valid near the separatrix.

As $\kappa \to 1$ (either from above or below) the bounce frequency (19) becomes

$$\omega_b/\omega_b(0) \to \pi/2 \ \ln\ (4/\kappa') \ . \tag{44}$$

We differentiate (19) or (44) with respect to κ to obtain

$$\partial\omega_b/\partial J = (\partial\kappa/\partial H_o)(\partial H_o/\partial J)\partial\omega_b/\partial\kappa$$

$$\to \mp \frac{1}{M(qR_o)^2} \ \frac{1}{32\pi} \left[\frac{\omega_b}{\omega_b(0)}\right]^3 \exp\left[\pi\omega_b(0)/\omega_b\right] \ , \tag{45}$$

the minus sign applying to $\kappa < 1$, the plus to $\kappa > 1$. The nome

$$q \to \exp\left[-\pi\,\omega_b/\omega_b(0)\right] \ . \tag{46}$$

We evaluate the needed expressions, (36) and (45), at $J = J_n$ using $\omega_b = \omega_b(J_n) = \omega/n$. For (36) we choose the limit appropriate for the present problem, $\omega << \omega_b(0)$, to derive

$$q^n \to 1 - \pi\omega/\omega_b(0)$$

and thus

$$V_n(J_n) \to \begin{cases} 2/\pi n \ , & n \text{ odd} \\ \begin{cases} \omega/\omega_b(0)n, & \kappa < 1 \\ 0 & \kappa > 1 \end{cases}, & n \text{ even} \end{cases} \ .$$

To obtain the simplest possible formulas we use $V_n(J_n) = 2/\pi n$ and (43). Then the condition for overlap of resonances n and $n+1$ is

$$\left(\frac{\Delta_n}{\delta_n}\right)^2 \approx \frac{1}{\pi^2}\left(\frac{n+1}{n}\right)^2 \frac{e\Phi_o}{\mu\Delta B} \ \frac{\omega}{\omega_b(0)} \exp\left[\pi\omega_b(0)n/\omega\right] > 1 \ . \tag{47}$$

In (47) a very strong dependence on n occurs in the exponential factor, indicating overlap of all resonances with n greater than a critical n depending on Φ_o and ω. A range of particles, with values of J roughly centered about the primary separatrix ($\kappa = 1$), is expected to move stochastically. This range of J is referred to as the stochastic layer. To find the width of the layer we note the relation, which follows from (44), between the exponential factor in (47) and the distance in energy of a particle from the separatrix:

$$\exp[\pi\omega_b(0)/\omega_b(J_n)] = 32/|E - \mu B_M| \quad .$$

We choose $n=1$ in (47), anticipating our choice of Φ_o and ω, for which the $n=1$ and 2 resonances overlap. Our theoretical formula for the width of the stochastic layer is thus

$$|E - \mu B_M| < (128/\pi^2) e\Phi_o \, \omega/\omega_b(0) \quad . \tag{48}$$

We will find in the next section that (48) agrees rather well with our numerical measurements of the width of the stochastic layer. The magnitude of the right hand side of (48) will be confirmed but not necessarily the scaling with ω. If some of the approximations used above were removed, a more credible analytic result would replace (48). We expect the more accurate scaling with ω would still show the main feature revealed in (48): the width of the stochastic layer decreases with decreasing ω.

G. Discussion of numerical results

In the analytic work presented above, the magnetic moment μ played the role of a fixed parameter, which was usually not indicated explicitly in the formulas. In applying the analytic results and in choosing parameters for numerical studies appropriate to the trapped-ion mode, the dependences on μ are very important.

We wish to study the motion of a representative sample of ions distributed throughout velocity space. Since we are considering guiding-center motion, the gyrophase is irrelevant and the location of an ion in velocity space is given by two variables. For the first of these variables we will always take the magnetic moment μ. For given μ the second variable specifies the depth of trapping in the effective potential energy well (the last term in (14)) produced by the modulated magnetic field. Of the possible choices for the second variable we have already used J, κ, $H_o/\mu\Delta B$, and $E - \mu B_M$. Other variables used in the literature are E, $\Theta_{TP} \equiv \cos^{-1}(1 - 2\kappa^2)$, and $\lambda \equiv \mu/E = (B_m + 2\kappa^2\Delta B)^{-1}$, where $B_m \equiv B_o - \Delta B$.

We have used the values of μ given in the first column of Table II. For each μ we calculate trajectories of ions with several different values of $J(t=0)$. The equations of motion which we integrate numerically are derived from (22):

$$\dot{\Theta} = p \tag{49a}$$

$$\dot{p} = -\sin\Theta - e\Phi_o\,[g(\Theta)\,(m - \ell q)\sin\chi - g'(\Theta)\cos\chi], \tag{49b}$$

where $\chi \equiv (m - \ell q)\Theta - \omega t + \eta$. The numerical integration scheme is very similar to the one described in Section 2G. The trajectory information,

$\Theta(t)$ and $p(t)$, found by integrating (49) is converted to $\phi(t)$ and $J(t)$ using the formulas (14), (16)-(19). To display the trajectories in two dimensions we use the surface of section method described in Section 2I. For the present problem we use the information $\phi(t)$ and $J(t)$ to plot a point in the ϕJ-plane whenever ωt is a multiple of 2π.

The relative size of the term in (22) representing the trapped-ion mode is given by $e\Phi_o/\mu\Delta B$, the ratio of the potential energy due to the mode to the effective potential energy due to the modulated magnetic field. This ratio is shown in the second column of Table II for a mode amplitude given by (1). The ratio increases as μ decreases, indicating a stronger perturbation of the trajectories of low-energy ions than of high-energy ones. In our numerical calculations we choose units such that (21) holds, so the dimensionless value of the mode frequency ω is $\omega/\omega_b(0)$, which we show in the third column of Table II for the choice of frequency given by (4).

We show in Figs. 35 and 36 the increasingly perturbed trajectories as μ decreases. The parameter values are those given in the last three lines of Table II. The moderate mode amplitude (1) is seen to lead to trajectories unlike the unperturbed trajectories, which would be straight, horizontal lines. The prominent islands represent the fundamental (n=1) resonance $\omega_b = \omega$; the islands below the separatrix $(J = 8/\pi)$ show the bounce resonance of trapped particles, and the islands above the separatrix the transit resonance of circulating particles. In each of the figures we show one stochastic

trajectory; it is represented by the scattered points which do not lie on any smooth curve.

Motion becomes stochastic when an invariant ceases to exist (more precisely, the invariant changes character from isolating[120] to non-isolating). Surface of section plots allow us to map out the regions of phase space in which the invariant exists.

As seen in Figs. 35 and 36, the analytic form of the invariant, when it exists, is not simply J. In some regions of phase space (e. g., $J < 2$ in Fig. 35a) the invariant is approximately J, but near the $n=1$ resonances the invariant curves are topologically different from straight, horizontal lines, indicating a different analytic form for the invariant. The method of Taylor and Laing (Section 2D) could be used to find one of the many possible analytic forms. Note that an invariant can still exist in the presence of a single resonant perturbation, but multiple resonances which overlap prevent existence of an invariant. The bounce resonances discussed in Section 4F cause disappearance of the invariant in the vicinity of the separatrix.

We obtain from the surface of section plots a measure of the velocity space region in which stochastic effects are strong as follows. Near the separatrix most trajectories (excluding those within the islands) are stochastic, while away from the separatrix most are not stochastic. We find a rough boundary between the stochastic and nonstochastic regions by searching for the nonstochastic trajectories "closest" to the separatrix. With a planimeter we measure the area bounded by the horizontal line $(J = 8/\pi)$ representing the separatrix and

the "closest" trajectory below it and by the vertical lines at $\phi = 0$ and 2π. This area gives a measure of the width (in action) of the part of the stochastic layer inside the separatrix. A similar measurement involving the "closest" trajectory above the separatrix yields the width of the stochastic layer outside the separatrix. We repeat the measurements for the five values of μ given in the first column of Table II and plot the widths on Fig. 37, interpolating between our ten measurements with two heavy curves.

In Fig. 37 we also show by dashed lines the locations of the ions satisfying $\omega = \omega_b \equiv \omega_b(J, \mu)$ and thus the locations of the prominent islands in Figs. 35 and 36. The nonstochastic regions within these islands have not been indicated in Fig. 37.

The contour lines in Fig. 37 show the distribution of ions in velocity space. A Maxwellian distribution is used, and the appropriate Jacobian factor is included so the number of ions in a unit area of Fig. 37 is proportional to the value (designated below by N) shown by the contour lines. The explicit formula used to calculate the contour lines is

$$N = \left(\frac{y}{x+1}\right)^{\frac{1}{2}} \exp\left\{-[1 + (\Delta B/B_o)x]y + 1\right\}, \tag{50}$$

where the velocity space variables are denoted by

$$x = H_o/\mu\Delta B, \quad y = \mu B_o/T_i \quad .$$

The exponential factor in (50) is seen from (15) to be $\exp(-E/T_i + 1)$. The pre-exponential factor is derived from the factor j in

$$d^3v = \pi \, dv_{\parallel} \, d(v_{\perp}^2) = j \, dx \, dy \, ,$$

where $v_{\parallel}$ and $v_{\perp}$ are measured at $\Theta = 0$. Suppressing unimportant constant factors we have

$$v_{\perp}^2 \propto y$$

$$v_{\parallel}^2 = 2E/M - v_{\perp}^2 = 2(H_o + \mu\Delta B)/M \propto (x + 1)y$$

and

$$j \propto \left(\frac{\partial v_{\parallel}}{\partial x}\right)_y \propto \left(\frac{y}{x + 1}\right)^{\frac{1}{2}}.$$

For Fig. 37 we chose $B_o/\Delta B = 4$.

We have compared the measurements of the widths of the stochastic layer inside and outside the separatrix to the theoretical prediction (48). Agreement ($\pm 40\%$) is found when the layer is relatively narrow; for parameters giving very wide layers, as in Fig. 36, (48) becomes inaccurate due to the assumption $\kappa \to 1$ used to derive it.

The agreement between the measurements and (48) is equally good for both the inside and outside parts of the stochastic layer. This result is surprising, at first, because the Fourier coefficients (36), which appear in the resonance widths (35), have different forms inside ($\kappa < 1$) than outside ($\kappa > 1$) the separatrix. It is therefore possible to derive different widths for the inside and outside parts. In the limit $\omega >> \omega_b(0)$, Rechester and Stix[37] noted that the resonances outside are twice as far apart (since resonances with even n are effectively absent) as the resonances inside, and the widths outside are $2^{\frac{1}{2}}$ times greater than inside. These facts lead to the conclusion that the part of the layer outside the separatrix should be only <u>half</u> as wide

as the inside part. This conclusion does not follow in the limit $\omega << \omega_b(0)$ which is more appropriate to our problem involving the trapped-ion mode. In our limit, doubts arise about the applicability of the theoretical approach used to calculate the widths of the parts of the layer, as discussed below. We are thus unable to explain theoretically the relation between the inside and outside widths which we observe numerically.

The perturbation levels $e\Phi_o/\mu\Delta B$ which we use in the numerical calculations are large enough to raise doubts about the validity of the perturbation scheme used theoretically. In particular, the widths Δ_n can easily become extremely large due to the factor $\partial\omega_b/\partial J_n$ in (35), causing the overlap criterion (42) to lose its sense. Also, when (42) is extremely well satisfied for n=1, the width of the stochastic layer cannot be found from (42), because the width is determined by resonances other than (31). A new theoretical problem, in which the unperturbed motion is determined not by the modulated magnetic field but by the n=1 resonance, would have to be considered. The close agreement between the crude theoretical calculation in Section 4F and the numerical results shown in Fig. 37 is thus somewhat surprising. Either the agreement is fortuitous, which we think unlikely, or the theory has a broader range of validity than one would expect at first.

We saw in Figs. 35 and 36 that an initial condition lying within the stochastic layer leads to a trajectory which visits most parts of the layer. To find the rate with which a typical ion moves from one side of the layer to the other, we calculate an ensemble of trajectories

and plot the action J vs. time in Fig. 38. Each ensemble consists of 100 trajectories with values of $\phi(t = 0)$ and $\eta(t = 0)$ (see (24)) distributed over the interval $[0, 2\pi)$ in a regular 10x10 array; each trajectory has the same initial value of the variable J and the same value of the parameter μ. The chosen set of initial phases represents an ensemble of ions distributed uniformly in toroidal angle (through η) and in bounce phase ϕ (position along a banana orbit). A subset of the trajectories in two such ensembles is shown in Fig. 38. One ensemble has $J(t=0) \gtrsim 1$, which lies outside the stochastic layer; these trajectories show no tendency to depart far from their initial value of J, and, in fact, have a gross periodicity with frequency $\omega_b(J) - \omega$. The other ensemble has $J(t=0)$ lying within the stochastic layer; these trajectories are not periodic and tend to spread out to fill the layer. The rate of spreading is quite rapid; a significant amount of spreading occurs in the first wave period (up to $\omega_b(0)t = 4\pi$) and the ensemble has essentially filled the layer in roughly four wave periods. The implications for the trapped-ion mode of this rapid motion within the stochastic layer will be discussed in Section 4I.

In Fig. 39 we contrast, in a different way, the spreading tendency of an ensemble within the stochastic layer to the lack of spreading of an ensemble outside the layer. Here we plot, for the same ensembles as in Fig. 38, the value of $(\Delta J)^2$ averaged over the ensemble, where $\Delta J \equiv J(t) - J(t=0)$. Plots like Fig. 39 allow us to measure the rate of spreading of an ensemble of stochastic trajectories. Zaslavskii and Filonenko[114] attempted to calculate this diffusion rate, but their result is smaller by a factor of about ten than the rate

suggested by Fig. 39. The cause of the large dip in $\langle(\Delta J)^2\rangle$ near $\omega_b(0)t = 40$ is not known at this time. A possible cause is the presence in the ensemble of trajectories lying in or near nonstochastic regions.

H. Other closely related work

In the preceding sections we have shown that a single trapped-ion mode can cause stochastic ion motion, which results in transitions between the trapped and circulating states and irreversible changes in an initial distribution function. Our nonlinear, collisionless detrapping mechanism differs from mechanisms considered by earlier authors.[121,122] In this section we clarify those differences. Then we discuss work[119] which mentioned some of the physical ideas which are important in our work. We briefly describe previous numerical calculations[123,124] in which stochastic particle motion in a tokamak was observed. Finally, we call attention to the proposal[125] that the enhanced electron heat transport in tokamaks could be explained using the large radial excursions of some electrons in the presence of certain trapped-particle modes. We do not mention here several other nonlinear processes which may be important for the trapped-ion mode; these processes are discussed in the comprehensive review article by Tang.[105]

Jablon[121] studied a nonlinear, collisionless mechanism for mode damping which relies on the mode's perpendicular electric field to

cause detrapping of particles. Errors and questionable assumptions in Ref. 121 led to incorrect conclusions. Ehst[122] corrected some of the errors and concluded that Jablon's mechanism could be neglected in comparison to his own nonlinear, collisional mechanism. A followup on Ehst's work is desirable to assess fully the importance of Jablon's mechanism.

Jablon's mechanism can be explained physically as follows. The mode's electric field has a component lying within a magnetic surface and perpendicular to a field line. This component causes a radial $\underline{E} \times \underline{B}$ drift. During half of a mode period a trapped particle's banana center drifts inward, to radii r for which the effective potential energy well $\mu B(\theta)$ is shallower. The value of μB_M may decrease to less than the particle's energy E, implying a transition to the circulating state. An outward drift of a circulating particle can similarly cause a trapping transition. After a particle is detrapped, it moves along a field line to a region where the mode's phase is different (because $k_{||} \neq 0$), and there it is retrapped. Successive transitions between the trapped and circulating states lead to diffusion of particles along a field line. This diffusion tends to eliminate the density perturbation caused by the mode and could cause saturation of the instability. Jablon augmented this single-mode picture of the detrapping by assuming a spectrum of many modes was present; without such turbulence Jablon's mechanism is probably inoperative.

Jablon's mechanism requires a nonzero $k_{||}$ in order that diffusion along a field line be able to move particles from the crest of

the mode to the trough. Jablon did not consider the forces on particles due to the mode's parallel electric field. Our work shows that the parallel electric field can have a very strong effect on particle motion.

Ehst[122] considered a saturation mechanism involving parallel forces on the particles but requiring collisions. He noted that, in linear theory, detrapping occurs because of collisional changes of the magnetic moment μ, the energy E remaining approximately constant. He then showed that a finite-amplitude trapped-ion mode, acting together with collisions, could cause changes in E, which could also lead to detrapping. His quantitative study of this mechanism concluded that it could cause saturation only at an unreasonably large mode amplitude. Ehst did not recognize that a single mode, without any collisions at all, could cause detrapping.

Dobrowolny, et al.[119] studied the quasilinear diffusion in parallel kinetic energy H_o of trapped particles. The wave spectrum consisted of many waves, either sound waves or drift waves. The authors of Ref. 119 pointed out that a trapped particle moving in an electrostatic wave with $k_{||} \neq 0$ feels fluctuating potentials at all harmonics of its bounce frequency. Quasilinear diffusion thus occurs whenever the wave spectrum contains energy at multiples of the bounce frequency of typical particles. Ref. 119 considered drift waves with parallel phase velocities between the ion and electron thermal speeds:

$$v_{Ti} < \omega/k_{||} < v_{Te} .$$

For these waves diffusion of ions was found not to occur. We have shown that stochastic ion motion (sometimes resembling diffusion) can occur for the trapped-ion mode, which has a much lower frequency. Also, we have emphasized that stochastic motion can occur even for a single wave.

Coppi and Taroni[123,124] numerically integrated equations of motion similar to our (49) in a study of particle orbits in the presence of certain trapped-particle modes in tokamak. Differences in the equations and parameters used in Refs. 123 and 124 and by us prevent a straightforward comparison of the numerical results obtained in the two studies. Nevertheless, it is clear that Coppi and Taroni observed stochastic particle motion (identifiable by successive detrapping and trapping transitions) caused by a single mode. They gave only numerical results on stochastic motion; we have given a theory, based on the overlap of bounce resonances, which allows us to predict the conditions under which stochastic motion occurs.

Coppi and Pozzoli[125] used the results of Ref. 123 which found that "quasi-banana" orbits execute large radial radial excursions. These orbits show large oscillations in J but no transitions to the circulating state; the orbits are therefore probably not stochastic. The large radial excursions were proposed in Ref. 125 as an explanation for the enhanced electron heat transport observed in tokamaks. A pseudoclassical diffusion coefficient was derived.

I. Effects of stochastic motion on the mode

One of the goals of this study is to assess the importance of overlap of bounce resonances as a mechanism for saturation of the trapped-ion instability. In this section we describe our progress towards this goal, giving the qualitative results we have obtained. Quantitative results require further numerical work.

To understand the effects of stochastic motion on the mode we must know how stochastic ions move in the action space of J and p_ζ. Our discussion of the physics of the trapped-ion mode in Appendix E makes clear the importance of changes in p_ζ (i. e., radial excursions of the banana center). In our treatment of ion Landau damping in Section 5 of the appendix we use (52), derived below under the assumption that only one of the resonances $\omega = n\omega_b$ is important. This assumption is not valid when motion is stochastic, and we must determine the radial excursions by numerical integration of the equations of motion. We add an equation for $\dot{p}_\zeta$ to the equations (49) which we integrated in Section 4G. We use the variables (11) to express the potential (6) as

$$\Phi = -\Phi_o\, g(\Theta) \cos\left[(m - \ell q)\Theta - \ell\zeta' - \omega t + \eta\right].$$

The Hamiltonian equation of motion for $\dot{p}_\zeta$ is then

$$\dot{p}_\zeta = -\partial H/\partial\zeta' = -e\,\partial\Phi/\partial\zeta' .$$

We neglect the radial (p_ζ) dependence of H_o, which eliminates Jablon's mechanism and possibly other effects. We also assume that the radial variation of Φ is slow enough that the p_ζ-dependence of Φ is negligible. Then

$$\dot{\zeta}' = \partial H/\partial p_\zeta = 0 ,$$

and we can set $\zeta'=0$. The equations we integrate are thus (49) and

$$\dot{p}_\zeta = e\Phi_o g(\Theta)\ell \sin\chi . \tag{51}$$

Since p_ζ does not appear in (49), inclusion of (51) changes none of the results reported in Section 4G.

If only the nth term in the sum (24) is important and $g=1$, it is easy to show using (22)-(24) and (51) that a relation exists between changes of J and p_ζ:

$$\dot{p}_\zeta = -(\ell/n)\dot{J} . \tag{52}$$

To integrate (51) numerically we must choose values for ℓ and $p_\zeta(t=0)$. From the results of Ref. 126 we take $\ell=5$, imagining that $m=10$ and $q=1.9$ so (2) is satisfied. To determine appropriate values for p_ζ we use $q(\alpha) = \text{const}$ to derive a relation between p_ζ and the position r of the banana center:

$$-p_\zeta = \frac{e\Psi}{c} = \frac{e\alpha}{cq} = \frac{1}{2} M\Omega r^2/q . \tag{53}$$

The ion gyrofrequency is represented by Ω. Using the values $r/R_o = \Delta B/B_o = \frac{1}{4}$ and $q=1.9$ and our choice of units (21), we find

$$-p_\zeta = [\Omega/\omega_b(0)]/220 . \tag{54}$$

For typical tokamak parameters[126]

$$T_i = 3 \text{ keV}, \; B_o = 50 \text{ kG}, \; R_o = 132 \text{ cm} ,$$

we find the ion gyroradius $\rho_i \equiv (T_i/M)^{\frac{1}{2}}/\Omega \approx 1.5\,\text{mm}$ and

$$\frac{\Omega}{\omega_{bi}} = \frac{R_o}{\rho_i}\, q \left(\frac{B_o}{\Delta B}\right)^{\frac{1}{2}} \approx 3300 . \tag{55}$$

For a thermal ion ($\mu B_o = T_i$) we thus find from (54) and (55)

$$-p_\zeta \approx 15 .$$

Equation (53) tells us the relation between changes in p_ζ and in r:

$$\Delta r = -\Delta p_\zeta\, (q/M\Omega r) .$$

Using the same parameter values as in the preceding paragraph, we find

$$\Delta r/r \approx -\Delta p_\zeta/30 .$$

With typical values determined, we proceed to the numerical integration of (49) and (51). In Fig. 40 we show two trajectories in Jp_ζ-space. The motion represented in (a) is determined to be <u>not</u> stochastic by a glance at the surface of section plot in ϕJ-space. The motion in (b) <u>is</u> stochastic, which is clear from the three transitions between the trapped and circulating states during the integration time of five waveperiods. (Recall that the separatrix at $J \approx 2.55$ is the boundary between trapped and circulating ions.) Both trajectories in Fig. 40 lie roughly along the diagonal line determined by (52) with n=1. Other trajectories which we have integrated also

show this characteristic, even though the trajectories differ markedly in their fine details.

Our numerical results thus indicate ion motion along lines with slope

$$dp_\zeta/dJ = -\ell \,, \tag{56}$$

one of which is shown by the triple-headed arrow in Fig. 44. The irregular oscillatory motion along these lines has a rate which is a fair fraction of the wave frequency ω. This rate can easily be much greater than the rate of collisional diffusion in Jp_ζ-space. (Note that collisional diffusion from $J=0$ to $J \approx 2.55$ occurs at the rate $\nu_{ef,i}$, which is much less than ω.) Collisional diffusion, which attempts to maintain a local Maxwellian distribution, cannot counteract the tendency of mode-induced diffusion to flatten the distribution along the lines with slope (56). In the presence of a finite-amplitude trapped-ion mode we therefore expect distortion of the distribution function f_o in the manner sketched in Fig. 41. For clarity the distortion has been kept relatively mild. The large excursions in J which are evident in Fig. 40 would lead to a distribution distorted in a much broader band about the separatrix.

The distortion of f_o implies nonlinear shifts in the frequency and growth rate of the trapped-ion mode. As discussed in Appendix E, the mode's frequency is determined by $\underline{E} \times \underline{B}$ convection of trapped ions (and also, strictly speaking, barely circulating ions). In the presence of a finite-amplitude mode, $\underline{E} \times \underline{B}$ convection of barely trapped and

barely circulating ions contributes little to the density perturbation because the slope of f_o in the relevant direction is greatly reduced. A nonlinear shift to a lower frequency results, analogous to the reduction of ω below ω^* because of the failure of circulating ions to $\underline{E} \times \underline{B}$ convect.

The nonlinear reduction of ω leads to a decrease of the electron collisional growth rate (proportional to ω^2) and therefore has a stabilizing influence on the mode.

A further stabilizing effect is an increase in the rate of transitions between the trapped and circulating states. In a finite-amplitude mode the usual collisional rate of pitch-angle diffusion is enhanced by mode-induced diffusion. The enhancement is greatest in the stochastic layer. The larger detrapping rate leads to a more rapid exchange of energy between the mode and the ions according to the mechanism described in Section 3 of Appendix E.

The nonlinear modifications to the Landau damping process are probably destabilizing because of the reduction of the slope of f_o. (Note that a large enough temperature gradient leads to growth instead of damping; the nonlinear modifications are then stabilizing.) We recall however that ions with different values of the magnetic moment μ contribute to Landau damping (observe the dashed lines in Fig. 37 which show the locations of the resonant ions). Deeply trapped ions give the largest contribution[127] to Landau damping by the bounce resonance $\omega = \omega_b$, but distortions of the distribution function f_o are small near $J=0$ where the deeply trapped ions are located. Our study

therefore indicates that nonlinear modifications to Landau damping are small. It is desirable, however, to extend the present work with both qualitative and quantitative studies.

J. Conclusions of Chapter 4

In Chapter 4 we have studied a possible saturation mechanism for the dissipative trapped-ion instability. Numerical integration of the equations of motion in a single trapped-ion mode shows that ions move stochastically in a layer surrounding the trapped-circulating boundary. The width of this stochastic layer increases with the mode amplitude Φ_o and with the mode frequency ω. For relevant parameters the width of the layer is quite large; for $\omega = \frac{1}{2}\omega_{bi}$ a substantial fraction of the ions moves stochastically in a mode of amplitude given by $e\Phi_o = 0.05\,\epsilon T_i$. A theory, based on the overlap of bounce resonances, predicts a width for the stochastic layer in agreement with the numerical results.

Our plots display the strikingly large excursions in longitudinal action J and in radius r which can occur whether motion is stochastic or not.

We have made a qualitative study of the effects of stochastic motion on the nonlinear stabilization of the trapped-ion mode. In the stochastic layer the motion resembles a diffusion process with a high rate compared to collisional diffusion. A distortion of the distribution function in this layer leads to a nonlinear reduction of the mode frequency and stabilizing modifications to the electron

collisional growth rate and the ion collisional damping rate found in linear theory.

Because of its generic nature the dynamical system studied in Chapter 4 occurs in a large number of other problems. Our methods and results are therefore of interest to researchers outside of the tokamak area.

Appendix A. Equations for transition between oblique and perpendicular propagation

In terms of the variables defined and discussed in Section 2B, we write the Hamiltonian

$$H(z, p_z, \phi, p_\phi, t) = H_o(p_z, p_\phi) + e\Phi_o \sin(k_z z - k_\perp \rho \sin\phi - \omega t) \qquad (1)$$

to describe a particle in a uniform magnetic field and an electrostatic wave propagating at an arbitrary angle to the field. In (1) we use variables z and p_z giving the position and the parallel momentum in the reference frame in which the center of mass of the plasma is at rest; the origin of z is chosen as in Section 2C.

For oblique propagation ($k_z \neq 0$), we note that since z and t appear in (1) only in the combination $k_z z - \omega t$, we can use the generating function

$$F_2(z, p_\psi, t) = (k_z z - \omega t) p_\psi$$

to transform to new variables ψ and p_ψ:

$$\psi = k_z z - \omega t, \qquad p_\psi = p_z/k_z$$

$$K(\psi, p_\psi, \phi, p_\phi) = H + \partial F_2/\partial t$$

$$= k_z^2 p_\psi^2/2m - p_\psi \omega + p_\phi \Omega + e\phi_o \sin(\psi - k_\perp \rho \sin\phi). \qquad (2)$$

We make the mathematical transformation generated by

$$F_2(\psi, p_\psi') = \psi(p_\psi' + m\omega/k_z^2)$$

to the wave frame momentum $p_\psi' = p_\psi - m\omega/k_z^2 = (p_z - m\omega/k_z)/k_z$.

The transformed Hamiltonian is equivalent to (2.7).

For perpendicular propagation ($k_z = 0$), (1) is independent of z, and the parallel momentum p_z is a constant of the motion. Dropping the constant parallel kinetic energy from (1) and converting to a time-independent system of two degrees of freedom (see Subsection 1C7), we find an expression for the Hamiltonian which is identical to (2) with k_z set to zero. Hamiltonian (2) can thus be used to investigate both the cases of oblique and of perpendicular propagation.

We expand (2) in a series of Bessel functions. If the wave amplitude is small enough, all terms in this series, except possibly one, can be considered rapidly varying in time. Retaining only the term varying slowest, we approximate (2) by

$$K_L = k_z^2 p_\psi^2/2m - p_\psi\omega + p_\phi\Omega + e\Phi_o J_{-L}(k_\perp\rho)\sin(\psi + L\phi) .$$

We use

$$F_2(\psi, \phi, p_\eta, P_\phi') = (\psi + L\phi)p_\eta + \phi p_\phi'$$

to transform to new variables $\eta, \phi', p_\eta, p_\phi'$:

$$\eta = \psi + L\phi, \qquad \phi' = \phi$$

$$p_\eta = p_\psi \ , \quad p_\phi' = p_\phi - Lp_\eta$$

$$K_L(\eta, p_\eta; p_\phi') = k_z^2 p_\eta^2/2m - p_\eta(\omega - L\Omega) + p_\phi'\Omega + e\Phi_o J_{-L}(k_\perp\rho)\sin\eta . \quad (3)$$

The gyroradius is now given by

$$\rho = [2(p_\phi' + Lp_\eta)/m\Omega]^{\frac{1}{2}} .$$

Note that p_ϕ' is an invariant in (3). Our approximation has thus reduced the motion to one degree of freedom.

Fixed points of the motion are found by solving

$$\begin{cases} 0 = \dot{\eta} = \dfrac{k_z^2 p_\eta}{m} - (\omega - L\Omega) + e\Phi_o \sin\eta \dfrac{d}{dp_\eta} J_{-L}(k_\perp \rho) & (4a) \\ 0 = \dot{p}_\eta = -e\Phi_o J_{-L}(k_\perp \rho) \cos\eta \,. & (4b) \end{cases}$$

Several families of fixed points may exist. Family 1 is important when k_z is large and the last term in (4a) is negligible:

$$\eta = \pm \tfrac{1}{2}\pi, \; p_\eta \approx m(\omega - L\Omega)/k_z^2 .$$

These fixed points give the locations of the cyclotron resonances studied in Chapter 2. The resonant values of p_η become very large as k_z becomes small, and very few (if any) particles are able to interact strongly with the cyclotron resonances. Another set of resonances may exist near the fixed points of Family 2; when the first term of (4a) is negligible, these fixed points are given by

$$\eta = \pm \tfrac{1}{2}\pi, \; p_\eta \text{ from } e\Phi_o \frac{d}{dp_\eta} J_L(k_\perp \rho) = \pm (\omega - L\Omega) \,.$$

When these fixed points exist, they can be shown to be stable. They have been considered by Aamodt and Bodner,[41] Timofeev,[16] and Fukuyama, et al.[40] The same authors mention the corresponding unstable fixed points, which are given by

$$\begin{cases} \eta = \sin^{-1}\left[(\omega - L\Omega)/e\Phi_o \dfrac{d}{dp_\eta} J_L(k_\perp \rho)\right] \\ p_\eta \text{ from } J_L(k_\perp \rho) = 0 \,. \end{cases}$$

Other families of fixed points arise when two terms of the Bessel function series are retained. These families have been observed by Fukuyama, et al.[40] and by Karney,[128] who have begun the theoretical study of these families.

The transition between Families 1 and 2 is determined by the ratio of the first and last terms in (4a), which we denote by R:

$$R = \left| \frac{k_z}{k_\perp} \frac{m v_z v_\perp}{e\Phi_o} \frac{1}{LJ_L'} \right| .$$

The ratio R is large for the parameters used in Section 2L, justifying our neglect of the last term in (4a). For parameters appropriate to studies of lower hybrid heating, R may be small, justifying neglect of the first term in (4a). Even if the first term is not negligible, however, Karney[129] notes that it may cause only small changes in the locations of fixed points.

Appendix B. Stochastic acceleration by an electromagnetic wave

Stochastic acceleration by an electrostatic wave is treated in detail in this thesis. Here we discuss the possibility that an electromagnetic wave could cause stochastic acceleration.

The motion of a charged particle in a uniform magnetic field plus a perturbing electromagnetic wave can be described by Hamiltonian (2.4) with the perturbation given by

$$V = \frac{1}{2} e \left(\Phi - \frac{1}{c} \underline{v} \cdot \underline{A}\right) \exp\left[i(k_z z + k_\perp y)\right] + \text{c.c.} \ .$$

Here Φ and $\underline{A}$ are the complex amplitudes of the wave's scalar and vector potentials. As in Section 2C we use wave frame variables. Expressing the velocity $\underline{v}$ in terms of the canonical variables introduced in Section 2B yields

$$\underline{v} \cdot \underline{A} = p_z A_z/m - v_\perp (A_x \sin\phi + A_y \cos\phi) \ ,$$

where $v_\perp = (2p_\phi \Omega/m)^{\frac{1}{2}}$. We introduce

$$A_\pm \equiv A_x \pm i A_y$$

and write

$$A_x \sin\phi + A_y \cos\phi = (A_+ e^{i\phi} - A_- e^{-i\phi})/2i \ .$$

Use of (2.8) then allows us to write

$$V(z, \phi, p_z, p_\phi) = \frac{1}{2} e \Sigma_\ell \Phi_\ell \exp[i(k_z z - \ell\Phi)] + \text{c.c.},$$

where the complex amplitude

$$\Phi_\ell = (\Phi - p_z A_z/mc)J_\ell + (v_\perp/c)(A_+ J_{\ell+1} + A_- J_{\ell-1}) \qquad (1)$$

plays the same role for an electromagnetic wave that $\Phi_o J_\ell$ played for an electrostatic wave. An electromagnetic wave can thus trap a particle with parallel velocity near any of the resonant velocities given by (2.11). The trapping widths are found from (2.14) by replacing $\Phi_o J_\ell$ with Φ_ℓ. If Φ_ℓ is large enough the wave can cause stochastic acceleration.

As an example of a particular electromagnetic wave we consider a high-frequency Alfvén wave. By this name we refer to a wave on the same branch as the magnetosonic (compressional Alfvén) and whistler waves but with a frequency a few times the ion gyrofrequency. The dispersion diagram in Fig. 29 shows the location of the high-frequency Alfvén wave. When the propagation angle $\theta = 0°$(i. e., $k_\perp$=0), this wave is right-hand-circularly-polarized, and (1) reduces to

$$\Phi_\ell = (v_\perp/c)A_- J_{\ell-1}(k_\perp \rho) . \qquad (2)$$

When the wave propagation is oblique (k_z, $k_\perp \neq 0$), (2) is still a good approximation for certain combinations of wave frequency ω and angle θ. When (2) is valid, the condition of overlapping cyclotron resonances appears difficult to satisfy. Using the same values of $k_\perp \rho$ and $k_z v_z/\Omega$ (which determines ℓ) as in Fig. 19, we find the Bessel function $J_{\ell-1}$ to be smaller than J_ℓ by a factor of about three. A high-frequency Alfvén wave with amplitude given by

$$(v_\perp/c)\ |k_z^2\ eA_-/m_i\Omega_i^2| = 1.5 \qquad (3)$$

could thus be expected to cause ion heating similar to that caused by the ion-acoustic wave of Section 2L which has

$$k_z^2 e\Phi_o/m_i\Omega_i^2 = 0.5 \ .$$

To check whether (3) is a reasonable wave amplitude we use $k_z = k_\perp$ and calculate

$$\delta B_z/B_o \approx k_z|A_-|/B_o = 1.5\ \Omega_i/k_z v_\perp \ . \tag{4}$$

For the linear cyclotron-harmonic damping of the wave to be weak we use the crude condition that the ion thermal speed satisfy

$$v_{Ti} \lesssim 0.5\ \Omega_i/k_z ; \tag{5}$$

this condition means the distribution function "fits" between the resonant parallel velocities $\ell\Omega_i/k_z$ (compare (2.51)). Combining (4) and (5), we find that ions with $v_\perp \approx 4v_{Ti}$ are stochastically accelerated if

$$\delta B_z/B_o \gtrsim 0.75 \ . \tag{6}$$

A high-frequency Alfvén wave with amplitude (6) would not obey the requirements of our analysis that the wave be sinusoidal and satisfy the linear relations for the frequency and polarization. On the basis of this example we conclude that an electromagnetic wave of reasonable amplitude is less likely to cause stochastic acceleration by overlap of cyclotron resonances than is an electrostatic wave. It is clear, however, that many choices of parameters were made in arriving at (6), and the possibility of strong stochastic effects due to an

electromagnetic wave cannot be ruled out.

Appendix C. Stochastic acceleration by a nonsinusoidal wave

The problems treated in detail in this thesis involve stochastic motion caused by a sinusoidal wave. We note here that such motion can occur as well for a nonsinusoidal wave. Stochasticity might appear at a lower value of the wave amplitude in the nonsinusoidal case.

We consider a plane electrostatic wave for which the potential is an arbitrary periodic function of the phase $\underline{k} \cdot \underline{x} - \omega t$. As in Section 2C we eliminate the time dependence by using wave frame variables and write the perturbation as

$$V = e \Sigma_n \Phi_n \sin (n \underline{k} \cdot \underline{x} + \delta_n) ,$$

which replaces (2.5). The operations performed in Section 2C allow us to write the equation

$$V(z, \phi, p_\phi) = e \Sigma_n \Phi_n \sin (nk_z z - nk_\perp \rho \sin \phi + \delta_n) ,$$

which replaces (2.6). Use of (2.8) now yields

$$V = e \Sigma_n \Phi_n \Sigma_\ell J_\ell(nk_\perp \rho) \sin (nk_z z - \ell\phi + \delta_n) . \qquad (1)$$

Equation (1) has essentially the same form as (1.20). As noted in our discussion of (1.25), (1) shows the existence of resonant velocities

$$v_z = (\ell/n)\Omega/k_z$$

distributed along the real number line as the rational numbers are distributed. The complications implied by this distribution have deterred us from study of nonsinusoidal waves. One might expect,

however, that a nonsinusoidal wave would lead more easily to stochastic motion than a sinusoidal one because of the presence of the large number of additional resonances of finite width (proportional to $\Phi_n^{\frac{1}{2}}$).

Appendix D. Experimental requirements for observing stochastic acceleration

Stochastic acceleration of ions by a single ion-acoustic wave was seen in Sections 2L and 2M to lead to the heating of a Maxwellian distribution. We believe a fairly simple laboratory experiment could observe these effects. When stochasticity occurs one should see a change in propagation characteristics of a launched, obliquely propagating wave, and one might observe a high-energy tail in the parallel distribution. Some care must be taken experimentally in launching an ion-acoustic wave in order to avoid effects mentioned in Refs. 130 and 131. Assuming that the desired wave can be launched, we give here the experimental requirements suggested by our theoretical work.

To observe ion tail-heating by an ion-acoustic wave, the following requirements must be met.

1. The wave frequency $\omega(\approx k c_s)$ should be a few times the ion gyrofrequency Ω_i, but not too close to a multiple of Ω_i to avoid cyclotron-harmonic damping.
2. The propagation angle θ with respect to the magnetostatic field $\underline{B}$ should be in the vicinity of 45°.
3. The temperature ratio T_e/T_i should be high enough that the wave damping is small, but there must be ions with gyroradii comparable to the perpendicular wavelength $(k_\perp \rho_i \gtrsim 1)$.
4. The ion collision frequency ν_i must be less than about $0.1\Omega_i$ so the collisionless theory is applicable.

5. The distance L_x in the $\underline{k} \times \underline{B}$ direction over which the wave amplitude is uniform should satisfy $k_z L_x \gtrsim \omega/\Omega_i$. Otherwise, ions $\underline{E} \times \underline{B}$ -drift out of the wave before significant acceleration occurs.
6. The density amplitude must be as large as $\delta n/n \sim 0.1$.

To observe electron tail-heating by a Langmuir wave, the analogous requirements are the following.

1. $\omega (\approx \omega_{pe})$ a few times Ω_e, but not too close to a multiple of Ω_e.
2. $\theta \sim 45^o$.
3. The Debye length λ_D should be small enough $(k\lambda_D \lesssim 0.25)$ that the wave damping is weak, but electrons with gyroradii such that $k_\perp \rho_e \gtrsim 1$ must exist.
4. $\nu_e \lesssim 0.1\ \Omega_e$.
5. $k_z L_x \gtrsim \omega/\Omega_e$.
6. $\delta n_e/n_e \sim 0.1$.

Appendix E. Physics of the dissipative trapped-ion instability

In this appendix we give a physical discussion of the dissipative trapped-ion instability, which leads to the large amplitude mode considered in Chapter 4. Our discussion should serve as a useful introduction to the instability for readers unfamiliar with it. Also, a detailed understanding of the physics of the instability aids us in assessing the effects of the stochastic ion motion on the nonlinear development of the instability. Our discussion draws heavily on ideas expressed by Ehst.[122]

1. Introduction

The dissipative trapped-ion instability is expected to occur in tokamaks which are hot enough that a typical trapped ion can bounce between magnetic mirrors (execute a banana orbit) before Coulomb collisions detrap it. This condition is expressed as

$$\omega_{bi} > \nu_{ef,i} ,$$

where the typical bounce frequency ω_{bi} is defined in (4.3) and $\nu_{ef,i}$ is an effective collision frequency for ions.

Several other conditions are generally assumed in the simplest derivations of the dissipative trapped-ion instability. The mode frequency ω must lie between the effective collision frequencies for ions and electrons:

$$\nu_{ef,i} < \omega < \nu_{ef,e} . \qquad (1)$$

A typical trapped ion must bounce in less than a wave period:

$$\omega < \omega_{bi} \ . \tag{2}$$

A typical circulating ion must travel farther than a parallel wavelength during a wave period:

$$\omega < k_{\|} v_{Ti} \ , \tag{3}$$

where $k_{\|}$ is defined in (4.2) and $v_{Ti} \equiv (T_i/m_i)^{\frac{1}{2}}$ is the ion thermal speed. One chooses $k_{\|}$ to reflect the tendency of the mode to minimize variations of the perturbed potential along a field line.

When these conditions are satisfied, the simplest theories lead to the dispersion relation

$$\omega = \frac{1}{2}\varepsilon^{\frac{1}{2}}\omega^* + i(\mathrm{Re}\ \omega)^2/\nu_{ef,e} - i(\nu_{ef,i} + \nu_{LD}) \ . \tag{4}$$

In (4) ε is the inverse aspect ratio of the magnetic surface to which the radially local theory refers. Also appearing in (4) are the ion Landau damping rate ν_{LD} and the so-called diamagnetic drift frequency,

$$\omega^* = k_\perp \frac{T_e c}{eB} \frac{1}{n}\frac{dn}{dr} \ ,$$

expressed here in terms of the derivative of the density n with respect to minor radius r.

In the sections below we discuss the physics of the instability and gain some understanding of the conditions assumed in deriving dispersion relation (4).

2. $\underline{E} \times \underline{B}$ convection of trapped particles

For certain "drift" waves the main effect of the density gradient is to allow $\underline{E} \times \underline{B}$ drifts in the wave's electric field to change the density of some particle species. In a hot tokamak this type of drift wave is called a dissipative trapped-ion mode and the species undergoing this $\underline{E} \times \underline{B}$ convection are the trapped particles, both electrons and ions.

The simplest pictures[132] showing density changes caused by $\underline{E} \times \underline{B}$ convection are complicated somewhat in the tokamak geometry. In Fig. 42 we draw an "unrolled" magnetic surface with ζ, the toroidal angle, on the horizontal axis, and with Θ, the poloidal angle, on the vertical axis. At the left we indicate the variation of the magnetic field with Θ. With the short-dash line we show a field line on the magnetic surface; the safety factor is assumed to be $q=\frac{7}{3}$. The line with an arrow at each end represents the banana orbit of a deeply trapped particle. At the right we show that the density gradient is out of the page.

We assume an electrostatic wave is present with the solid lines in Fig. 42 showing the crests (electric potential a maximum) and the long-dash lines showing the troughs (potential a minimum). The direction of the wave's electric field and the direction of the $\underline{E} \times \underline{B}$ convection are shown. The density gradient together with $\underline{E} \times \underline{B}$ convection causes the density of both ions and electrons to be increasing or decreasing as shown.

The defeat of $\underline{E} \times \underline{B}$ convection for any species has a profound effect on the mode. The failure of circulating particles to $\underline{E} \times \underline{B}$ convect, as discussed below in Section 4, causes the mode frequency to drop below the usual drift wave frequency ω^*. If $\underline{E} \times \underline{B}$ convection of trapped electrons were not defeated by collisions, as discussed in Section 3, the perturbations in the charge density due to electrons and ions would cancel and the mode would not exist. If $k_\parallel$ were not as small as possible, some trapped ions would cross crests and troughs of the wave during their bounce motion. This would tend to average the $\underline{E} \times \underline{B}$ drifts of these ions which would then contribute little to the charge density perturbation. A lower mode frequency would result which would lead in turn to a lower growth rate (see (4)).

Condition (2) on the mode frequency simplifies the theoretical work but is not necessary for existence of an instability. With (2) one can often ignore the details of the ion banana orbits and treat the motion of banana centers, the bounce-averaged locations of the guiding centers. Where (2) is not satisfied (i. e., for large $k_\perp$) the trapped-ion instability is replaced by the dissipative trapped-electron instability.

3. Collisions of trapped particles

We next consider the effects of collisions. First, we show that collisions allow the existence of the mode. Second, we describe the mechanism for instability (due to electron collisions) and the analogous process of ion collisional damping.

Study of Fig. 42 reveals an important fact about $\underline{E} \times \underline{B}$ convection: it produces a density perturbation in phase with the potential perturbation. In Fig. 43 we illustrate the potential perturbation $\tilde{\Phi}$ and, with solid lines, the density perturbations $\tilde{n}_{ts}$ of trapped particles (s=i,e) in the absence of collisions ($\nu_{ef,s}=0$).

The density perturbations $\tilde{n}_{ts}$ are modified by collisions which change trapped particles to circulating ones and vice versa. After a detrapping collision a particle moves along a field line, changing its relation to the wave phase. A detrapping collision followed by a trapping collision thus has the effect of producing a random change in the wave phase of a trapped particle. The rate of detrapping collisions is greatest where the density of trapped particles is greatest ($\tilde{n}_{ts} > 0$). The rate of trapping collisions is proportional to the density of circulating particles, which is relatively insensitive to $\tilde{n}_{ts}$ if the number of circulating particles exceeds the number of trapped ones (large-aspect-ratio approximation). The net rate of increase of trapped particles due to collisions is thus a maximum where $\tilde{n}_{ts}$ is a minimum, as shown by the arrows in Fig. 43.

Competition between $\underline{E} \times \underline{B}$ convection and collisions leads to the density perturbations $\tilde{n}_{ts}$ shown by dashed lines in Fig. 43. For the ions, $\nu_{ef,i} < \omega$ so collisions are weak compared to $\underline{E} \times \underline{B}$ convection, and $\tilde{n}_{ti}$ is only slightly altered by collisions. For the electrons, $\nu_{ef,e} > \omega$, so collisions are strong compared to $\underline{E} \times \underline{B}$ convection, and $\tilde{n}_{te}$ is greatly reduced by collisions. The charge density perturbation $\tilde{\rho}_t \equiv e(\tilde{n}_{ti} - \tilde{n}_{te})$, shown at the bottom of Fig. 43, is thus positive

where $\tilde{n}_{ti}$ is positive, and causes the potential perturbation assumed at the outset.

Since $\tilde{n}_{ts}$ changes due to two processes with different phases relative to $\tilde{\Phi}$, $\tilde{n}_{ts}$ suffers a phase shift δ_s due to collisions, as shown in Fig. 43. These phase shifts are often cited as the cause of collisional damping and growth, but we give a more direct explanation below.

Collisions cause a net exchange of energy between the wave and a particle species. To show this, we consider the effects of pitch-angle collisions, which can detrap or trap a particle but do not change its (total) energy. The net effect of detrapping and trapping collisions is to allow movement of particles from regions of positive potential, where $\tilde{n}_{ts}$ is enhanced by $\underline{E} \times \underline{B}$ convection, to regions of average (zero) potential. Ions move down a potential energy gradient, gaining kinetic energy and causing the mode to damp due to ion collisions. Electrons move up a potential energy gradient, losing kinetic energy and causing the mode to grow due to electron collisions.

4. Shielding by circulating particles

Condition (3), which is necessary to prevent excessive ion Landau damping (see Section 5), also defeats the $\underline{E} \times \underline{B}$ convection process for circulating particles. A typical circulating particle sees such a rapid variation in the direction of the mode's electric field that its radial drifts are insignificant. Consequently, the main effect

of the circulating particles is to provide Debye shielding of the charge density produced by the trapped particles. Condition (3) guarantees that circulating particles can move fast enough to keep up with the changing potential of the mode. Debye shielding causes a reduction of the trapped-particle charge density $\tilde{\rho}_t$, and thus of the mode frequency, by a factor $k^2\lambda_D^2(<<1)$, where λ_D is an appropriately averaged Debye length for the circulating ions and electrons.

5. Ion Landau damping

Ions which are well into the circulating region of velocity space $(v_\parallel \gtrsim v_\perp)$ are affected little by the modulations of the magnetic field, and the analysis of Landau damping by these ions follows the analysis for a uniform magnetic field. To prevent strong damping of the trapped-ion mode the parallel distribution function must have a small slope at $\omega/k_\parallel$. Condition (3) is thus an approximate requirement for the damping to be weak.

A mode with a given m and ℓ cannot satisfy condition (3) near the rational surface $q = m/\ell$ because $k_\parallel \to 0$ (see (4.2)). In a naive theory of the radial structure of the mode, we might therefore expect to find a depressed mode amplitude near rational surfaces. These expectations hold up to some extent in a more complete theory, as shown by Gladd and Ross.[107]

The reader may wish to postpone study of the following paragraphs until he has reached Section 4I.

Ions with moderate parallel velocities ($v_{\|} \sim \epsilon^{\frac{1}{2}} v_{\perp}$) are best treated using the action-angle variables introduced in Section 4B. These variables allow us, in Section 4F, to write the Hamiltonian (4.34) describing motion near a resonance $\omega = n\omega_b$ in exactly the same form as the Hamiltonian describing motion near the resonance $\omega = kv$ in an unmagnetized plasma. The physical description of ion Landau damping of the trapped-ion mode by bounce and transit resonances is then analogous to the description of the simple unmagnetized case given by Chen.[132] Before giving the description analogous to Chen's, we show how the radial ($\underline{E} \times \underline{B}$) excursions, which are not present in the simple unmagnetized problem, have an important effect on the trapped-ion mode problem.

A trapped-ion mode affects ion motion in a tokamak by simultaneously changing the longitudinal action J (through the parallel electric field) and the radial position r (through the perpendicular electric field). If the ion motion is dominated by a single one of the resonances $\omega = n\omega_b$, the motion occurs on a straight line (see (4.52)) in the action space shown in Fig. 44. One such straight line (with arrowheads) is illustrated in the figure. It is easy to show that the Landau damping rate is proportional to the slope of the distribution function f_o along this straight line. In Fig. 44 we have sketched contours of a locally Maxwellian distribution. Since the straight line is neither horizontal nor vertical, the damping rate depends on both $\partial f_o/\partial J$ and $\partial f_o/\partial r$, in general. In the large-aspect-ratio limit, $\partial f_o/\partial r$ gives the dominant contribution to the damping rate.

The triple-headed arrow in Fig. 44 shows the excursion in action space of an ion in the presence of a trapped-ion mode of small amplitude. During the excursion the ion's energy changes (through changes of the action J). Ions moving towards B are gaining energy, those moving towards A are losing energy. Damping of the mode occurs because more ions are gaining energy than are losing it.

Textbook treatments of Landau damping generally consider the damping of a wave present in the plasma at t=0. To show the relevance of Landau damping to tokamak plasmas we must go beyond such treatments and consider the effect of Coulomb collisions. Collisions cause diffusion in velocity space. In the action space of Fig. 44, including collisions would cause ion trajectories to diffuse in both J and r (velocity-space diffusion changes the positions r of the banana centers of our guiding-center ions just as collisions can change the guiding centers of gyrating ions). Collisions cause arrival of ions into the region of the resonance $\omega = n\omega_b(J)$ at a certain rate. After arrival at A an ion begins to move towards B, gaining energy and contributing to damping of the mode. Ions which arrive at B and begin moving towards A contribute to wave growth, but the greater number of ions at A than at B causes the net effect to be damping.

REFERENCES

1. T. M. O'Neil, "Collisionless damping of nonlinear plasma oscillations," Phys. Fluids 8, 2255 (1965).
2. A good list of references is given by J. Canosa, "Frequency shift of a nonlinear plasma wave and its initial damping," Phys. Fluids 19, 1952 (1976).
3. G. Benettin, L. Galgani, and J. Strelcyn, "Kolmogorov entropy and numerical experiments," Phys. Rev. A 14, 2338 (1976).
4. G. M. Zaslavskii and B. V. Chirikov, "Stochastic instability of non-linear oscillations," Usp. Fiz. Nauk 105, 3 (1971) [Sov. Phys.-Usp. 14, 549 (1972)].
5. J. A. Tataronis and F. W. Crawford, "Cyclotron harmonic wave propagation and instabilities," J. Plasma Phys. 4, 231 and 249 (1970).
6. I. B. Bernstein, "Waves in a plasma in a magnetic field," Phys. Rev. 109, 10 (1958).
7. B. B. Kadomtsev and O. P. Pogutse, "Trapped particles in toroidal magnetic systems," Nucl. Fusion 11, 67 (1971).
8. M. Kruskal, "Asymptotic theory of Hamiltonian and other systems with all solutions nearly periodic," J. Math. Phys. 3, 806 (1962).
9. A. Garren, R. J. Riddell, L. Smith, G. Bing, L. R. Henrick, T. G. Northrop, and J. E. Roberts, "Individual particle motion and the effect of scattering in an axially symmetric magnetic field," in Proceedings of the Second United Nations International

Conference on the Peaceful Uses of Atomic Energy (United Nations, Geneva, 1958), vol. 31, p. 65.

10. R. H. Cohen, G. Rowlands, and J. H. Foote, "Nonadiabaticity in mirror machines," UCRL-78889 (Dec. 1976).

11. V. I. Arnold, "On the behaviour of the adiabatic invariant with a slow periodic variation of the Hamiltonian," Dokl. Akad. Nauk SSSR 142, 758 (1962) [Sov. Math.-Doklady 3, 136 (1962)].

12. B. V. Chirikov, "Resonance processes in magnetic traps," At. Energ. 6, 630 (1959) [Sov. J. At. Energy 6, 464 (1959) or J. Nucl. Energy C (Plasma Phys.) 1, 253 (1960)].

13. S. N. Rodionov, "Experimental test of the behavior of charged particles in an adiabatic trap," At. Energ. 6, 623 (1959) [Sov. J. At. Energy 6, 459 (1959) or J. Nucl. Energy C (Plasma Phys.) 1, 247 (1960)].

14. M. N. Rosenbluth, "Superadiabaticity in mirror machines," Phys. Rev. Lett. 29, 408 (1972).

15. R. E. Aamodt and J. A. Byers, "Particle motion in magnetic mirrors with high-frequency electric field fluctuations," Phys. Rev. Lett. 29, 1305 (1972).

16. A. V. Timofeev, "Confinement of charged particles in adiabatic traps in the presence of monochromatic cyclotron oscillations," Nucl. Fusion 14, 165 (1974).

17. F. Jaeger, A. J. Lichtenberg, and M. A. Lieberman, "Theory of electron cyclotron resonance heating--I. Short time and adiabatic effects," Plasma Phys. 14, 1073 (1972).

18. M. A. Lieberman and A. J. Lichtenberg, "Theory of electron

cyclotron resonance heating--II. Long time and stochastic effects," Plasma Phys. 15, 125 (1973).

19. A. J. Lichtenberg and H. L. Berk, "Adiabaticity limits to radio-frequency-augmented magnetic-mirror confinement," Nucl. Fusion 15, 999 (1975).

20. B. V. Chirikov, Research Concerning the Theory of Non-linear Resonance and Stochasticity, (CERN Trans. 71-40, Geneva, 1971).

21. V. G. Ponomarenko, L. Ya. Trainin, V. I. Yurchenko, and A. N. Yasnetskii, "Experimental investigation of the motion of individual charged particles in a mirror device," Zh. Eksp. Teor. Fiz. 55, 3 (1968) [Sov. Phys.-JETP 28, 1 (1969)].

22. V. F. Aleksin, V. N. Pyatov, V. P. Sebko, and V. I. Tyupa, "Effect of a longitudinal current on the magnetic configuration in a stellarator," Zh. Tekh. Fiz. 45, 536 (1975) [Sov. Phys.-Tech. Phys. 20, 335 (1975)] and "Resonant effects in a stellarator with a longitudinal current in the plasma," Fiz. Plazmy 2, 219 (1976) [Sov. J. Plasma Phys. 2, 120 (1976)].

23. M. N. Rosenbluth, R. Z. Sagdeev, J. B. Taylor, and G. M. Zaslavskii, "Destruction of magnetic surfaces by magnetic field irregularities," Nucl. Fusion 6, 297 (1966).

24. N. N. Filonenko, R. Z. Sagdeev, and G. M. Zaslavskii, "Destruction of magnetic surfaces by magnetic field irregularities: Part II," Nucl. Fusion 7, 253 (1967).

25. B. S. Akshanov, N. A. Manzyuk, V. I. Muratov, V. N. Pyatov, V. P. Sebko, and V. I. Tyupa, "Possible interpretation of the maximum plasma pressure in a stellarator," Zh. Eksp. Teor. Fiz.

Pis'ma Red. 21, 212 (1975) [JETP Lett. 21, 94 (1975)].

26. R. P. Freis, C. W. Hartman, F. M. Hamzeh, and A. J. Lichtenberg, "Magnetic-island formation and destruction in a levitron," Nucl. Fusion 13, 533 (1973).

27. F. M. Hamzeh, "Magnetic-surface destruction in toroidal systems," Nucl. Fusion 14, 523 (1974).

28. S. L. Davis, R. J. Hawryluk, and J. A. Schmidt, "Observation of magnetic islands in the FM-1 spherator," Phys. Fluids 19, 1805 (1976).

29. M. N. Rosenbluth, R. Y. Dagazian, and P. H. Rutherford, "Nonlinear properties of the internal m=1 kink instability in the cylindrical tokamak," Phys. Fluids 16, 1894 (1973).

30. B. Coppi, R. Galvão, R. Pellat, M. Rosenbluth, and P. H. Rutherford, "Resistive internal kink modes," MATT-1271 (July 1976).

31. J. F. Drake and Y. C. Lee, "Kinetic theory of tearing instabilities," Phys. Fluids 20, 1341 (1977).

32. J. M. Finn, "The destruction of magnetic surfaces in tokamaks by current perturbations," Nucl. Fusion 15, 845 (1975).

33. J. C. Hosea, C. Bobeldijk, and D. J. Grove, "Stability experiments on the ST tokamak," in Plasma Physics and Controlled Nuclear Fusion Research (International Atomic Energy Agency, Vienna, 1971), vol. II, p. 425; and I. H. Hutchinson, "Magnetic probe investigation of the disruptive instability in tokamak LT-3," Phys. Rev. Lett. 37, 338 (1976).

34. T. H. Stix, "Magnetic braiding in a toroidal plasma," Phys. Rev.

Lett. 30, 833 (1973).

35. T. H. Stix, "On current penetration and plasma disruption," Phys. Rev. Lett. 36, 521 (1976).

36. J. M. Finn, "The coupling of tearing modes in tokamaks," PPPL-1322 (Jan. 1977).

37. A. B. Rechester and T. H. Stix, "Magnetic braiding due to weak asymmetry," Phys. Rev. Lett. 36, 587 (1976).

38. F. Karger, H. Wobig, S. Corti, J. Gernhardt, O. Klüber, G. Lisitano, K. McCormick, D. Meisel, and S. Sesnic, "Influence of resonant helical fields on tokamak discharges," in Plasma Physics and Controlled Nuclear Fusion Research (International Atomic Energy Agency, Vienna, 1975), vol. I, p. 207.

39. C. F. F. Karney and A. Bers, Plasma Research Report 76/7, Research Laboratory of Electronics, Massachusetts Institute of Technology (Jan. 1976), and "Stochastic ion heating by a perpendicularly propagating electrostatic wave," Phys. Rev. Lett. 39, 550 (1977).

40. A. Fukuyama, H. Momota, R. Itatani, and T. Takizuka, "Stochastic acceleration by an electrostatic wave near ion cyclotron harmonics," Phys. Rev. Lett. 38, 701 (1977).

41. R. E. Aamodt and S. E. Bodner, "Nonlinear dynamics of a single harmonic loss-cone flute mode," Phys. Fluids 12, 1471 (1969); R. E. Aamodt, "Particle motion in the presence of three-dimensional finite amplitude harmonic cyclotron waves," Phys. Fluids 13, 2341 (1970).

42. D. J. Tetreault, "Renormalization of the wave particle resonance

in turbulent plasma," Ph.D. Thesis, Massachusetts Institute of Technology, 1976 (unpublished).

43. M. Hénon and C. Heiles, "The applicability of the third integral of motion: some numerical experiments," Astron. J. 69, 73 (1964).

44. G. H. Lunsford and J. Ford, "On the stability of periodic orbits for nonlinear oscillator systems in regions exhibiting stochastic behavior," J. Math. Phys. 13, 700 (1972).

45. H. Goldstein, Classical Mechanics (Addison-Wesley, Reading, Mass., 1965).

46. B. Barbanis, "On the isolating character of the 'third' integral in a resonance case," Astron. J. 71, 415 (1966).

47. G. Contopoulos and M. Moutsoulas, "Resonance cases and small divisors in a third integral of motion. II," Astron. J. 70, 817 (1965).

48. G. Contopoulos, "Resonance phenomena and the non-applicability of the 'third' integral," Bull. Astron. 2, 223 (1967) and "Orbits in highly perturbed dynamical systems. III. Nonperiodic orbits," Astron. J. 76, 147 (1971).

49. G. Contopoulos, "A third integral of motion in a galaxy," Z. Astrophys. 49, 273 (1960).

50. F. C. Gustavson, "On constructing formal integrals of a Hamiltonian system near an equilibrium point," Astron. J. 71, 670 (1966).

51. G. Contopoulos, "On the existence of a third integral of motion," Astron. J. 68, 1 (1963).

52. D. A. Dunnett, E. W. Laing, and J. B. Taylor, "Invariants in the motion of a charged particle in a spatially modulated magnetic field," J. Math. Phys. 9, 1819 (1968).

53. H. Poincaré, New Methods of Celestial Mechanics (Washington, National Aeronautics and Space Administration, 1967), vol. 3, p. 176.

54. K. C. Mo, "Theoretical prediction for the onset of widespread instability in conservative nonlinear oscillator systems," Physica 57, 445 (1972).

55. K. S. J. Nordholm and S. A. Rice, "Quantum ergodicity and vibrational relaxation in isolated molecules," J. Chem. Phys. 61, 203 and 768 (1974).

56. M. Hénon, "Exploration numérique du problème restreint," Ann. Astrophys. (Paris) 28, 499 and 992 (1965), Bull. Astron. (Paris) 1, fasc. 1, 57 (1966) and fasc. 2, 49 (1966).

57. M. Hénon, "Numerical exploration of the restricted problem," Astron. Astrophys. 1, 223 (1969) and 9, 24 (1970).

58. M. Hénon, "Stability of periodic orbits in the restricted problem," in Periodic Orbits, Stability and Resonances (Reidel, Dordrecht, Holland, 1969), ed. G. E. O. Giacaglia, p. 349.

59. A. J. Dragt and J. M. Finn, "Insolubility of trapped particle motion in a magnetic dipole field," J. Geophys. Res. 81, 2327 (1976).

60. M. Braun, "Particle motion in a magnetic field," J. Differential Equations 8, 294 (1970).

61. D. L. Hitzl, "The swinging spring ...," Astron. Astrophys. 40,

147 and 41, 187 (1975) and Cel. Mech. 12, 359 (1975).

62. K. B. Dysthe and O. T. Gudmestad, "On resonance and stability of conservative systems," J. Math. Phys. 16, 56 (1975).

63. M. G. Olsson, "Why does a mass on a spring misbehave?" Am. J. Phys. 44, 1211 (1976).

64. C. Froeschlé and J.-P. Scheidecker, "Stochasticity of dynamical systems with increasing number of degrees of freedom," Phys. Rev. A12, 2137 (1975).

65. I. E. Farquhar, "Ergodicity and related topics," in Irreversibility in the Many-Body Problem, ed. J. Biel and J. Rae (Plenum, New York, 1972), p. 29.

66. J. L. Lebowitz, "Ergodic theory and statistical mechanics," in Transport Phenomena, ed. G. Kirczenow and J. Marro (Springer-Verlag, New York, 1974) [Lecture Notes in Physics, vol. 31], p. 202.

67. J. L. Lebowitz and O. Penrose, "Modern ergodic theory," Physics Today 26, 23 (Feb. 1973).

68. L. Galgani and A. Scotti, "Recent progress in classical nonlinear dynamics," Riv. Nuovo Cim. 2, 189 (1972).

69. J. Ford, "Stochastic behavior in nonlinear oscillator systems," in Lectures in Statistical Physics, ed. W. C. Schieve (Springer-Verlag, New York, 1974) [Lecture Notes in Physics, vol. 28], p. 204.

70. J. Ford, "The transition from analytic dynamics to statistical mechanics," Adv. Chem. Phys. 24, 155 (1973).

71. J. Ford, "The statistical mechanics of classical analytic

dynamics," in Fundamental Problems in Statistical Mechanics, ed. E. D. G. Cohen (North-Holland, Amsterdam, 1975), p. 21

72. G. H. Walker and J. Ford, "Amplitude instability and ergodic behavior for conservative nonlinear oscillator systems," Phys. Rev. 188, 416 (1969).

73. R. M. May, "Biological populations with nonoverlapping generations: stable points, stable cycles, and chaos," Science 186, 645 (1974).

74. F. C. Hoppensteadt and J. M. Hyman, "Periodic solutions of a logistic difference equation," SIAM J. Appl. Math. 32, 73 (1977).

75. R. M. May, "Simple mathematical models with very complicated dynamics," Nature (Lond.) 261, 459 (1976).

76. A. Cox, "Lengths of geomagnetic polarity intervals," J. Geophys. Res. 73, 3247 (1968).

77. T. Rikitake, "Oscillations of a system of disk dynamos," Proc. Camb. Philos. Soc. 54, 89 (1958).

78. A. E. Cook and P. H. Roberts, "The Rikitake two-disc dynamo system," Proc. Camb. Philos. Soc. 68, 547 (1970).

79. L. D. Landau and E. M. Lifshitz, Fluid Mechanics (Addison-Wesley, Reading, Mass., 1959).

80. D. Ruelle and F. Takens, "On the nature of turbulence," Comm. Math. Phys. 20, 167 (1971) and 23, 343 (1971).

81. J. P. Gollub and H. L. Swinney, "Onset of turbulence in a rotating fluid," Phys. Rev. Lett. 35, 927 (1975).

82. J. B. McLaughlin and P. C. Martin, "Transition to turbulence in a statically stressed fluid system," Phys. Rev. A 12, 186 (1975).

83. E. N. Lorenz, "Deterministic nonperiodic flow," J. Atmosph. Sciences 20, 130 (1963).

84. M. Hénon, "A two-dimensional mapping with a strange attractor," Comm. Math. Phys. 50, 69 (1976).

85. G. R. Smith and A. N. Kaufman, "Stochastic acceleration by a single wave in a magnetic field," Phys. Rev. Lett. 34, 1613 (1975).

86. G. R. Smith and A. N. Kaufman, "Diffusion due to a single wave in a magnetized plasma," in Plasma Physics, ed. H. Wilhelmsson (Plenum, New York, 1977), p. 475.

87. P. J. Palmadesso, "Resonance, particle trapping, and Landau damping in finite amplitude obliquely propagating waves," Phys. Fluids 15, 2006 (1972).

88. M. L. Woolley, "The motion of a charged particle interacting with a plane electromagnetic wave propagating at an arbitrary angle to a uniform magnetic field," Plasma Phys. 13, 1141 (1971).

89. T. H. Stix, "Fast-wave heating of a two-component plasma," Nucl. Fusion 15, 737 (1975).

90. A. B. Kitsenko, I. M. Pankratov, and K. N. Stepanov, "The nonlinear phase of monochromatic-oscillation excitation by a charged-particle beam in a plasma located in a magnetic field," Zh. Eksp. Teor. Fiz. 66, 166 (1974) [Sov. Phys.-JETP 39, 77 (1974)].

91. A. H. Nayfeh, Perturbation Methods (Wiley, New York, 1973).

92. J. B. Taylor and E. W. Laing, "Invariant for a particle interacting with an electrostatic wave in a magnetic field," Phys.

Rev. Lett. 35, 1306 (1975).

93. I. S. Gradshteyn and I. M. Ryzhik, Tables of Integrals, Series, and Products (Academic, New York, 1965).

94. C. Risk, "A guide to frequently used differential equation solvers," UCID-3703 (Jan. 1975).

95. C. Froeschlé, "A numerical study of the stochasticity of dynamical systems with two degrees of freedom," Astron. and Astrophys. 9, 15 (1970).

96. J. M. Greene, "Two-dimensional measure-preserving mappings," J. Math. Phys. 9, 760 (1968).

97. M. A. Lieberman and A. J. Lichtenberg, "Stochastic and adiabatic behavior of particles accelerated by periodic forces," Phys. Rev. A 5, 1852 (1972).

98. T. E. Stringer, "Low-frequency waves in an unbounded plasma," Plasma Phys. 5, 89 (1963).

99. S. Ichimaru, Basic Principles of Plasma Physics (Benjamin, Reading, Mass., 1973).

100. J. A. Krommes and G. R. Smith, "Renormalization for stochastic equations," Bull. Am. Phys. Soc. 21, 1152 (1976).

101. T. H. Dupree, "A perturbation theory for strong plasma turbulence," Phys. Fluids 9, 1773 (1966).

102. P. Rolland, "The importance of trapping in strong plasma turbulence," J. Plasma Phys. 15, 57 (1976).

103. B. V. Chirikov, private communication.

104. G. R. Smith, "Overlap of bounce resonances and the motion of ions in a trapped-ion mode," Phys. Rev. Lett. 38, 970 (1977).

105. W. M. Tang, "Microstability theory in tokamaks: a review," PPPL-1354 (June 1977), to be published in Nucl. Fusion.

106. P. Deschamps, R. Gravier, C. Renaud, and A. Samain, "Observation of drift instability due to particle trapping in a corrugated geometry," Phys. Rev. Lett. 31, 1457 (1973); S. C. Prager, A. K. Sen, and T. C. Marshall, "Dissipative trapped-electron instability in cylindrical geometry," Phys. Rev. Lett. 33, 692 (1974) and S. C. Prager, T. C. Marshall, and A. K. Sen, "Dissipative trapped electron instability in a linear machine," Plasma Phys. 17, 785 (1975).

107. N. T. Gladd and D. W. Ross, "Trapped ion instability in plasmas with magnetic shear," Phys. Fluids 16, 1706 (1973).

108. A. N. Kaufman, "Quasilinear diffusion of an axisymmetric toroidal plasma," Phys. Fluids 15, 1063 (1972).

109. Many references on Euler potentials are given by D. P. Stern, "Representation of magnetic fields in space," Reviews of Geophysics and Space Physics 14, 199 (1976).

110. S. Hamada, "Hydromagnetic equilibria and their proper coordinates," Nucl. Fusion 2, 23 (1962).

111. J. M. Greene and J. L. Johnson, "Stability criterion for arbitrary hydromagnetic equilibria," Phys. Fluids 5, 510 (1962).

112. L. S. Solov'ev and V. D. Shafranov, "Plasma confinement in closed magnetic systems," Reviews of Plasma Physics (Consultants Bureau, New York, 1970), 5, 1.

113. F. L. Hinton and R. D. Hazeltine, "Theory of plasma transport in toroidal confinement systems," Rev. Mod. Phys. 48, 239 (1976).

114. G. M. Zaslavskii and N. N. Filonenko, "Stochastic instability of trapped particles and conditions of applicability of the quasi-linear approximation," Zh. Eksp. Teor. Fiz. 54, 1590 (1968) [Sov. Phys.-JETP 27, 851 (1968)].

115. P. K. Kaw and W. L. Kruer, "Particle orbits in two waves of arbitrary amplitude," Phys. Fluids 14, 190 (1971).

116. T. H. Stix, "Aspects of stochastic heating," in Third Symposium on Plasma Heating in Toroidal Devices, Varenna, Italy, 1976 (to be published by Editrice Compositori, Bologna, 1977).

117. M. Dobrowolny, A. Orefice, and R. Pozzoli, "Interaction of particles trapped in a magnetic field with coherent electrostatic waves," Plasma Phys. 16, 479 (1974).

118. M. Abramowitz and I. A. Stegun, Handbook of Mathematical Functions (National Bureau of Standards, Washington, D. C., 1967).

119. M. Dobrowolny, A. Orefice, and R. Pozzoli, "Trapped-particle scattering by electrostatic turbulence in toroidal plasmas," Nucl. Fusion 13, 485 (1973).

120. R. Balescu, Equilibrium and Nonequilibrium Statistical Mechanics (Wiley, New York, 1975), appendix.

121. C. J. Jablon, "Nonlinear saturation of the collisional trapped-particle instability," Phys. Rev. Lett. 28, 880 (1972).

122. D. A. Ehst, "Nonlinear saturation of the dissipative trapped ion instability," Ph.D. Thesis, Massachusetts Institute of Technology, 1976 (unpublished).

123. B. Coppi and A. Taroni, "Quasi-trapped particle orbits due to

toroidal plasma modes," Plasma Phys. 16, 161 (1974).

124. B. Coppi and A. Taroni, "Scattering of toroidal orbits by standing even modes," Plasma Phys. 17, 951 (1975).

125. B. Coppi and R. Pozzoli, "Three electron populations model for current carrying plasmas," Plasma Phys. 16, 223 (1974).

126. W. M. Tang, "Effect of toroidal gradient drifts on the dissipative trapped-ion instability," Phys. Fluids 17, 1249 (1974).

127. W. M. Tang, "Effect of ellipticity on the collisional trapped-particle instability," Nucl. Fusion 13, 883 (1973).

128. C. F. F. Karney, "Stochastic heating of ions in a tokamak by rf power," Ph.D. Thesis, Massachusetts Institute of Technology, 1977 (unpublished).

129. C. F. F. Karney, private communication.

130. T. Christensen and N. Hershkowitz, "Near field diffraction pattern of ion acoustic waves," Phys. Fluids 20, 840 (1977).

131. T. Chen and L. Schott, "Excitation of ion acoustic waves with probes," Phys. Fluids 20, 844 (1977).

132. F. F. Chen, Introduction to Plasma Physics (Plenum, New York, 1974).

List of First Authors Referenced

Woolley	88
Zaslavskii	4,114

TABLE I. Analogies between gyromotion and bounce motion.

magnetic field	uniform	tokamak
old variables	$x,\ p_x$ $y,\ p_y$	$\zeta,\ p_\zeta$ $\alpha,\ \Theta$
intermediate variables:		
center of oscillation	$\begin{cases} x' = x + p_y = X \\ p_x = -Y \end{cases}$	$\begin{cases} \zeta' = \zeta - q(p_\zeta)\Theta \\ p_\zeta \end{cases}$
motion about center	$\begin{cases} y' = y + p_x = -\rho \sin\phi \\ p_y = -\rho \cos\phi \end{cases}$	$\begin{cases} \alpha' = \alpha - \alpha_o(p_\zeta) \\ \Theta \end{cases}$
new variables:		
center of oscillation	guiding center $X,\ Y$	banana center $\phi,\ J$
motion about center	gyromotion $\phi,\ \mu$	bounce motion $\bar{\zeta},\ p_\zeta$
frequency of oscillation	Ω	ω_b

TABLE II. Parameter values used for numerical studies.

$\frac{\mu B_o}{T_i}$	$\frac{e\Phi_o}{\mu\Delta B} = 0.05\ \frac{T_i}{\mu B_o}$	$\frac{\omega}{\omega_b(0)} = \frac{1}{2}\left(\frac{T_i}{\mu B_o}\right)^{\frac{1}{2}}$
4.0	0.0125	0.25
2.0	0.025	0.353
1.0	0.05	0.5
0.5	0.1	0.707
0.25	0.2	1.0

FIGURE CAPTIONS

1. The magnetic moment μ vs. time, showing jumps and rapid oscillations. The arrows indicate the times of passage through the points of minimum magnetic field. Courtesy of R. H. Cohen, Lawrence Livermore Laboratory.
2. (a) Magnetic surfaces in a tokamak shown in a poloidal cross section when no current perturbations are present (the axisymmetric, Ohmic heating current is the only current present). The surfaces are labeled by the value of the safety factor q. The axis of symmetry of the tokamak, if shown, would be a vertical line some distance to the left of the largest circle. (b) The same surfaces when current perturbations are present. The perturbations are near the minor radii where $q=2$ (mode numbers $m=2$ and $n=1$) and where $q=3$ ($m=3$ and $n=1$).
3. (a) Equipotential lines of the Hénon-Heiles potential, (1.7c). (b) Equipotential lines of the Barbanis potential, (1.14).
4. Two arrangements of masses and springs, whose motion is described by the Hénon-Heiles Hamiltonian (1.7) if the springs have a cubicly anharmonic potential energy.
5. Surface of section plots (from Ref. 43) for the Hénon-Heiles system, (1.7), showing disappearance of a constant of the motion as the energy E is raised.
6. Surface of section plots (from Ref. 58) for the equal-mass restricted three-body problem showing disappearance of a constant of the motion as the Jacobi constant C is lowered.

7. Behavior of the logistic difference equation (1.27) for various values of the growth rate r (from Ref. 73).
8. Observations of geomagnetic polarity intervals (from Ref. 76). Hatched periods are those in which the polarity was the same as at present.
9. Schematic picture (from Ref. 78) of the Rikitake two-disk dynamo.
10. Typical time evolution of the current I_1, which is proportional to X_1, for the Rikitake dynamo (from Ref. 78).
11. Results of an experiment on fluid motion between cylinders (from Ref. 81).
12. Structure of the strange attractor of the mapping (1.30) (from Ref. 84). The resolution increases clockwise, starting at the upper left.
13. Specification of the particle position (x, y) in terms of the canonical variables used in the text.
14. Contour plot of (2.22) for the parameters $k_\perp \rho_E \equiv k_\perp (2E/m)^{1/2}/\Omega = 1.48$, $\varepsilon = 0.1$, and $\theta \equiv \tan^{-1}(k_\perp/k_z) = 45°$. The definition of ε is given in (2.21b).
15. The correlation function $C(\tau)$, normalized to unity at $\tau=0$, computed analytically from (2.26) (solid curve) and from (2.30) (dashed curve) and from numerically calculated trajectories (dotted curve). The wave amplitude is given by $\varepsilon=0.75$ and the propagation angle by $\theta = 45^o$. The initial speed is $v = 5\Omega/k_z$, and the initial parallel velocity is $v_z = 0$.
16. The diffusion $\langle(\Delta v_z)^2\rangle$ in parallel velocity, computed analytically from (2.26) and (2.32) (solid curve) and from

numerically calculated trajectories (dotted curve). The parameters are the same as in Fig. 15.

17. Surface of section plot illustrating three non-overlapping resonances. The initial conditions, indicated by X's, were chosen to yield trajectories very close to the three separatrices. The points representing the trajectories have been connected with hand-drawn curves. The wave amplitude is given by $\varepsilon=0.025$, the other parameters are the same as in Fig. 14.

18. Surface of section plot showing a divided phase space. The parameters are the same as in Fig. 14.

19. Surface of section plots contrasting the motion in velocity space in the presence of a small- or of a large-amplitude wave. The wave has frequency $\omega = 3.6\Omega$ and propagation angle $\theta = 45^{o}$. Trajectories of a group of ten particles are represented. At $t=0$ this group has values of $k_z z = N\pi/5$, $N=0, 1, 2, \ldots, 9$, but has unique values of $\phi(=\pi)$, $v_\perp$ and v_z. The chosen value of the perpendicular velocity is given by $k_z v_\perp/\Omega = k_\perp \rho = 2.24$ and of the parallel velocity by $k_z v_z/\Omega = -3.6$. The hatched semicircle shows the extent of the thermal ions considered in the wave-heating example of Sections 2L and 2M.

20. Array of 100 initial values of $k_z z$ and ϕ used to approximate numerically the average defined by (2.24).

21. Particle trajectories, represented by plotting the parallel velocity vs. time. The same parameters are used here as in Fig. 15. The initial speed and parallel velocity are the same for all trajectories, but the initial phases $k_z z$ and ϕ differ.

22. The mean square deviation in parallel velocity vs. time. The parameters are the same as in Fig. 14.

23. The correlation function (2.23) for $t'=0$, normalized to unity at $\tau=0$, illustrating persistent oscillations. The parameters are the same as in Fig. 15. The array of 200 initial values is similar to Fig. 20, except that 20 values of $k_z z$ and 10 values of ϕ are used. The range $\pi \leq \phi < 2\pi$ used here gives identical results to those obtained using a set of 20 initial values of ϕ in the range $0 \leq \phi < 2\pi$ because of a symmetry which exists for $v_z=0$. For comparison with other figures the number of initial values is thus, effectively, 400.

24. The normalized correlation function (2.23) for $t'=0$, comparing measurements obtained using 400 (effectively) and 100 initial values of $k_z z$ and ϕ. The solid curve is the one already shown in Fig. 23. The dashed curve was obtained using the array of 100 initial values shown in Fig. 20.

25. The normalized correlation function (2.23) for $t'=0$, comparing measurements for two values of the stochasticity parameter ε. The solid curve here is the same as the dashed curve in Fig. 24. The value $\varepsilon=3$ is used for the dashed curve.

26. Correlation function (2.50) for the mapping (2.49), illustrating persistent oscillations. The parameters used are $p_o=0$, $\varepsilon=0.20$, and $N=100$.

27. Correlation function (2.50), illustrating reduction of the oscillations when N is increased to 400, other parameters remaining the same as in Fig. 26.

28. Correlation function (2.50), illustrating oscillations attributed to nonstochastic trajectories. Parameters are identical to Fig. 27 except $\varepsilon=0.06$.

29. Dispersion diagram (ω vs. k) for a plasma in a uniform magnetic field, showing the high-frequency Alfvén wave (Appendix B) and the ion-acoustic wave (Sections 2L and 2M). Adapted from a figure in Ref. 98.

30. The perpendicular ($f_\perp$) and parallel ($f_\parallel$) distribution functions in the presence of a finite-amplitude, obliquely propagating, electrostatic wave. The distortions to Maxwellian distributions ($\varepsilon=0$) are shown for two wave amplitudes, $\varepsilon=0.25$ and 0.75.

31. Agreement between our semi-empirical model for the diffusion coefficient $D(v_z)$ and values of D measured from plots like Fig. 22. As v_z is varied, the gyroradius is also varied to keep the speed v constant. The propagation angle $\theta = 45^o$. (a) $k_z v/\Omega=5$, $\varepsilon=1$. (b) $k_z v/\Omega=6$, $\varepsilon=0.75$.

32. The variation of the magnetic field B with distance s along a field line or with poloidal angle Θ. A sinusoidal modulation of amplitude ΔB is added to an average field B_o. The horizontal lines show the energy levels of trapped and circulating particles in the effective potential energy well $\mu B(\Theta)$. The physical interpretation of H_o is indicated at right.

33. Relationship between the variables Θ and ϕ, showing continuity of the definition across the separatrix, which separates the closed curves (trapped particles) from the open curves (circulating particles). The action J increases outwards from

the O-points ($\dot{\Theta} = 0$, $\Theta = 0$ and 2π).

34. The action J and the bounce (or transit) frequency ω_b as a function of H_o.

35. Surface of section plots showing ion trajectories in the ϕJ-plane. The parameter values are given in the lines of Table II: (a) line 3, (b) line 4. All figures take the poloidal structure factor g=1. Comparison of (a) and (b) illustrates the stronger effect of a mode with given amplitude on a lower-energy ion. Note, especially, the larger stochastic region in (b) than in (a).

36. Surface of section plot continuing the sequence of Fig. 35a,b. The parameter values are given in line 5 of Table II.

37. The extent in velocity space of the stochastic region (between the heavy curves) for a trapped-ion mode with parameters (4.1,2,4). The dashed lines show the locations of the resonant ($\omega = \omega_b$) ions. The contours show the density per unit area (on the figure) of ions in a Maxwellian distribution.

38. Trajectories of ions chosen from two ensembles with different initial values of the action J. The lower set of trajectories lies outside the stochastic layer, the upper set lies within it. The values of the mode amplitude Φ_o and the frequency ω are given in line 3 of Table II.

39. The diffusion $\langle(\Delta J)^2\rangle$ of the action J vs. time, calculated from the ensembles of trajectories used in Fig. 38.

40. Trajectories of ions in the action space introduced in Appendix E (see Fig. 44). The initial conditions are shown by the X's

marked 0. The numbered pluses indicate the locations at intervals of the wave period. The parameters are taken from line 4 of Table II. The initial angles are $\Theta=0$ and $\eta=0$. The initial values of H_o are (a) 0.44, and (b) 0.92 .

41. Distortion of the unperturbed distribution function f_o in the presence of a finite-amplitude trapped-ion mode.

42. An "unrolled" magnetic surface, illustrating density changes due to $\underline{E} \times \underline{B}$ convection in a trapped-ion mode.

43. Perturbations in potential ($\tilde{\Phi}$), in densities of trapped ions ($\tilde{n}_{ti}$) and trapped electrons ($\tilde{n}_{te}$), and in charge density ($\tilde{\rho}_t$) caused by a trapped-ion mode. The dashed curves show the modifications to the density perturbations in the presence of collisions.

44. The action space used for a tokamak to represent guiding-center motion and distribution functions. The longitudinal action J appears on the vertical axis. The horizontal axis is (minus) the canonical angular momentum p_ζ, which determines the average radial position r of the guiding center (i. e., for a trapped particle, r is the banana center). The dashed line is the separatrix. Contour lines are shown for a local Maxwellian distribution f_o with density decreasing with increasing r but with a constant temperature. The triple-headed arrow shows both the direction of guiding-center motion in the presence of a trapped-ion mode and the line along which the slope of f_o is measured (in a calculation of the Landau damping rate).

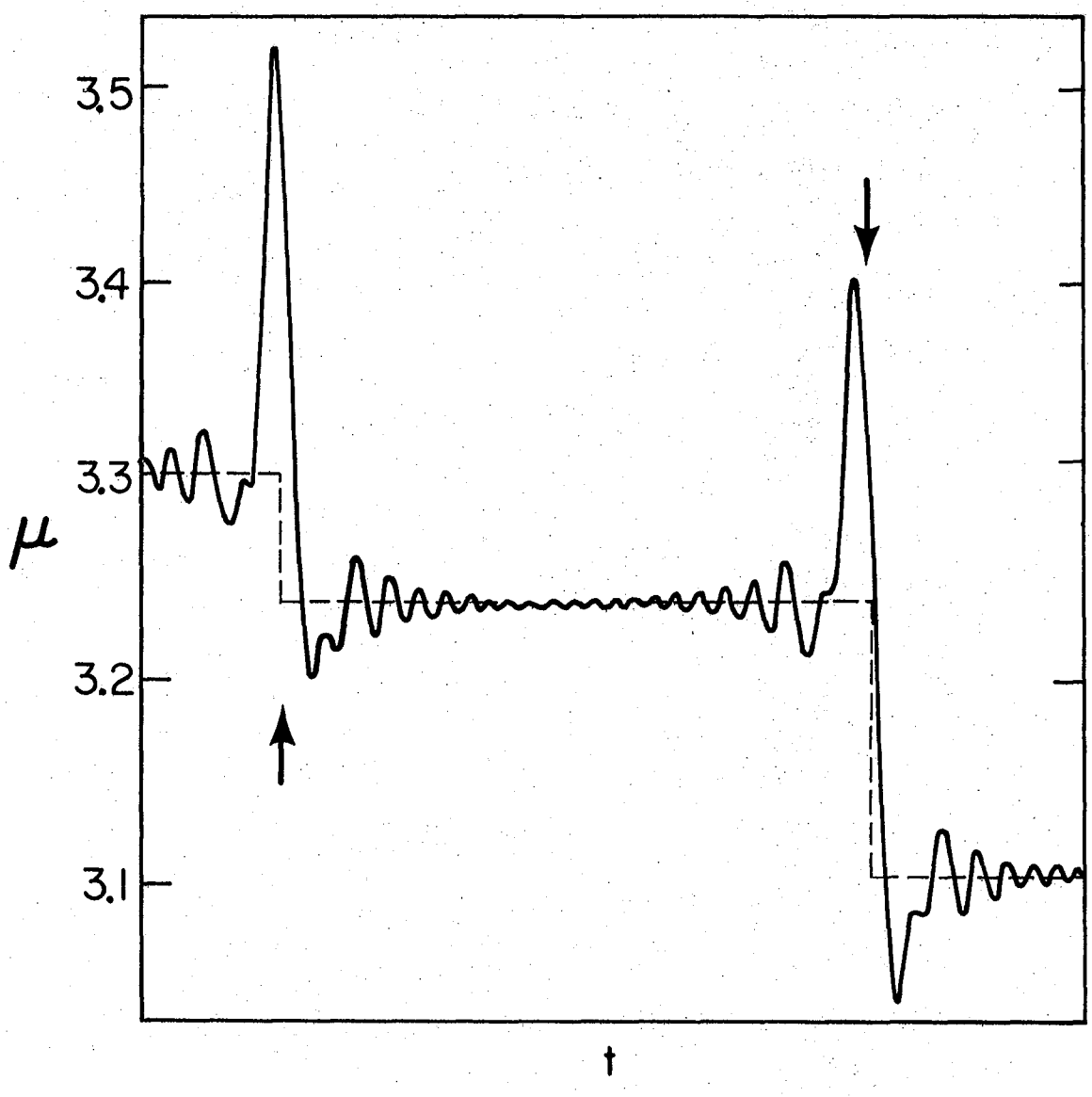

XBL 773-612

Fig. 1

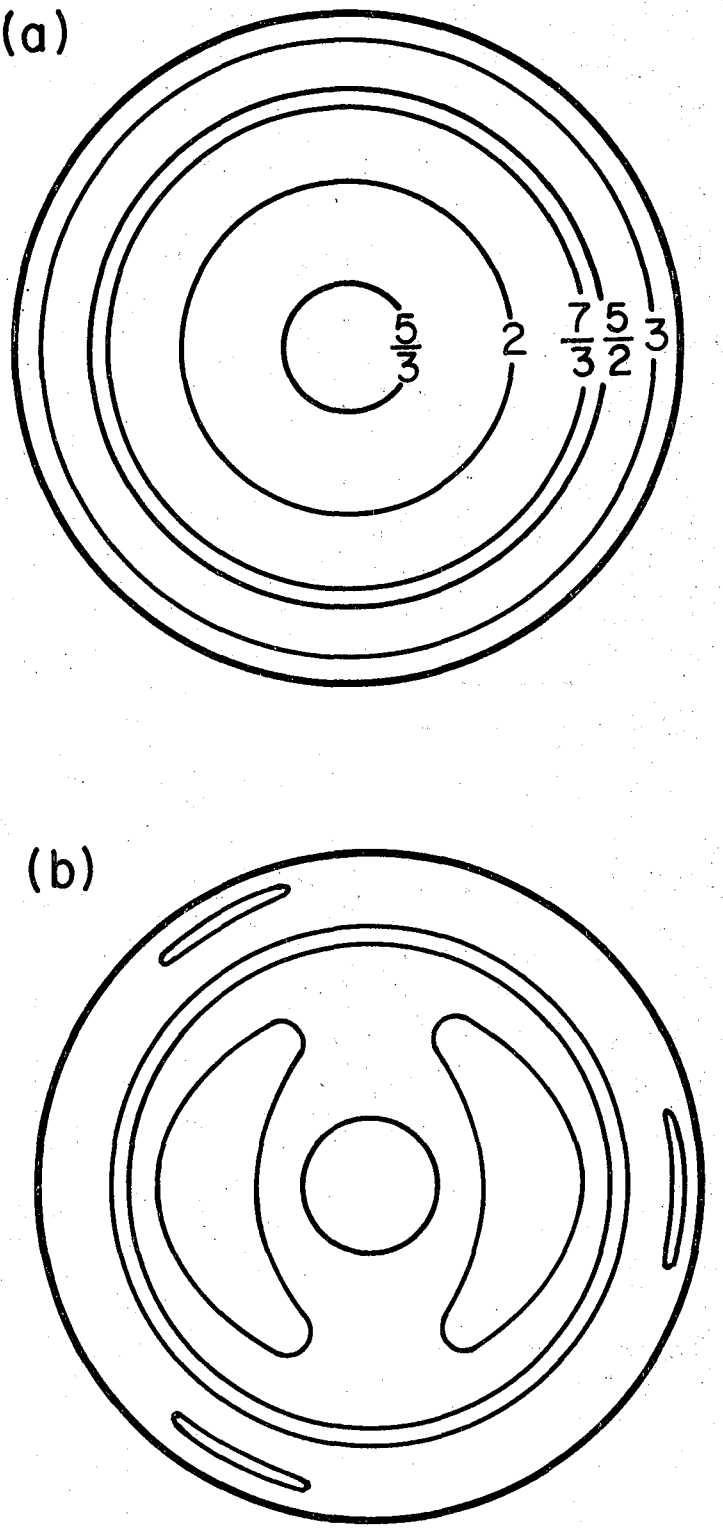

XBL775-3413

Fig. 2

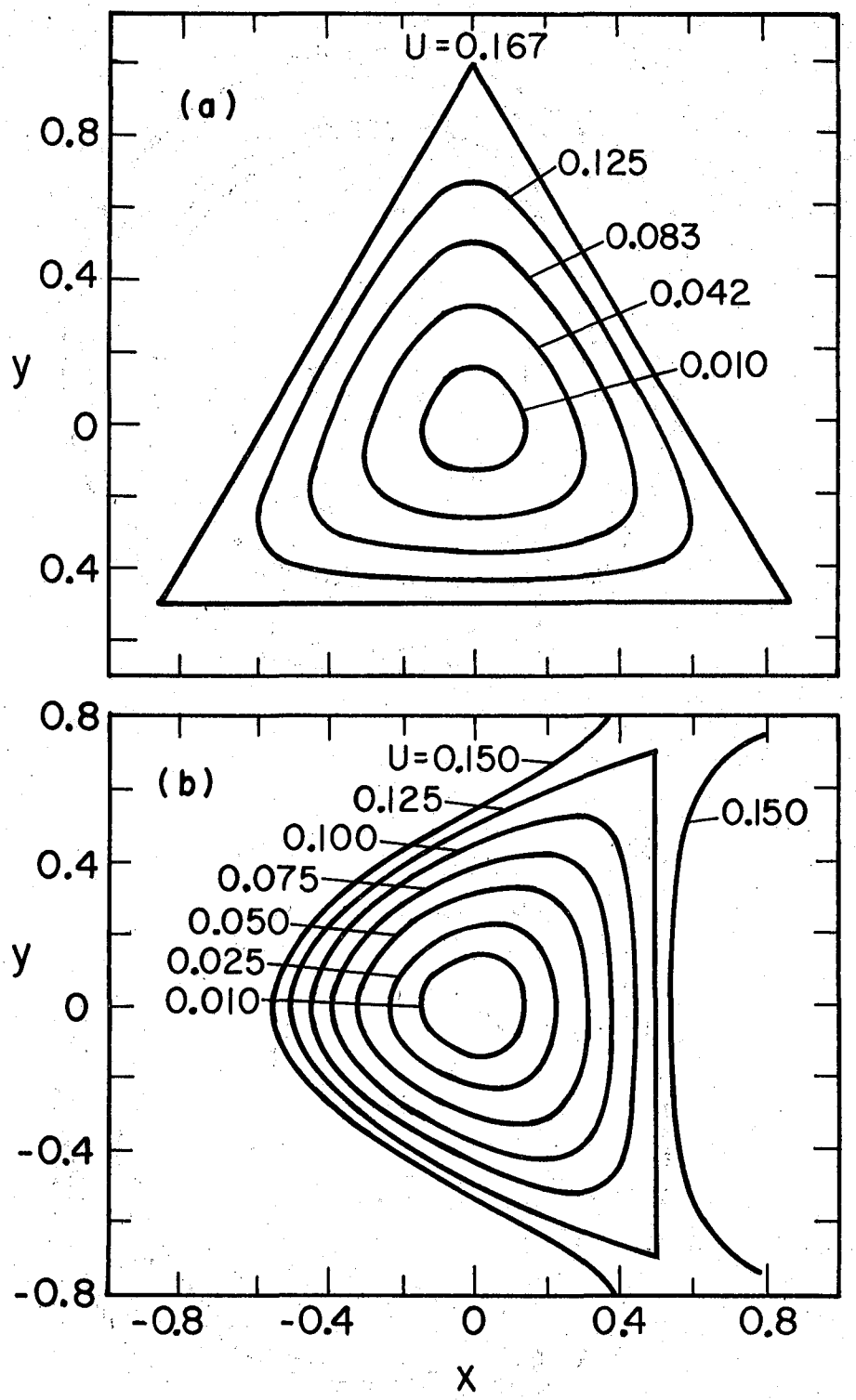

XBL775-3412

Fig. 3

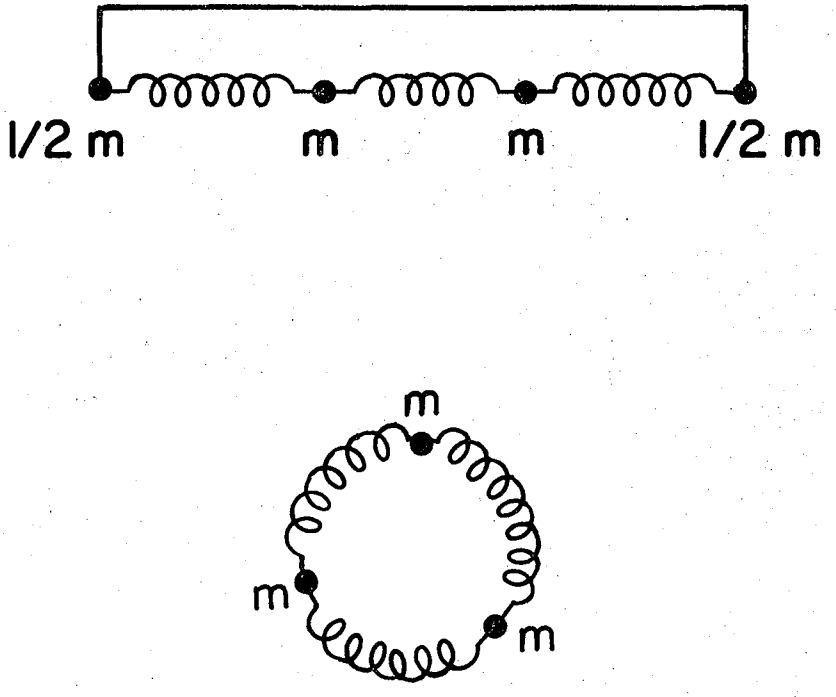

XBL773-609

Fig. 4

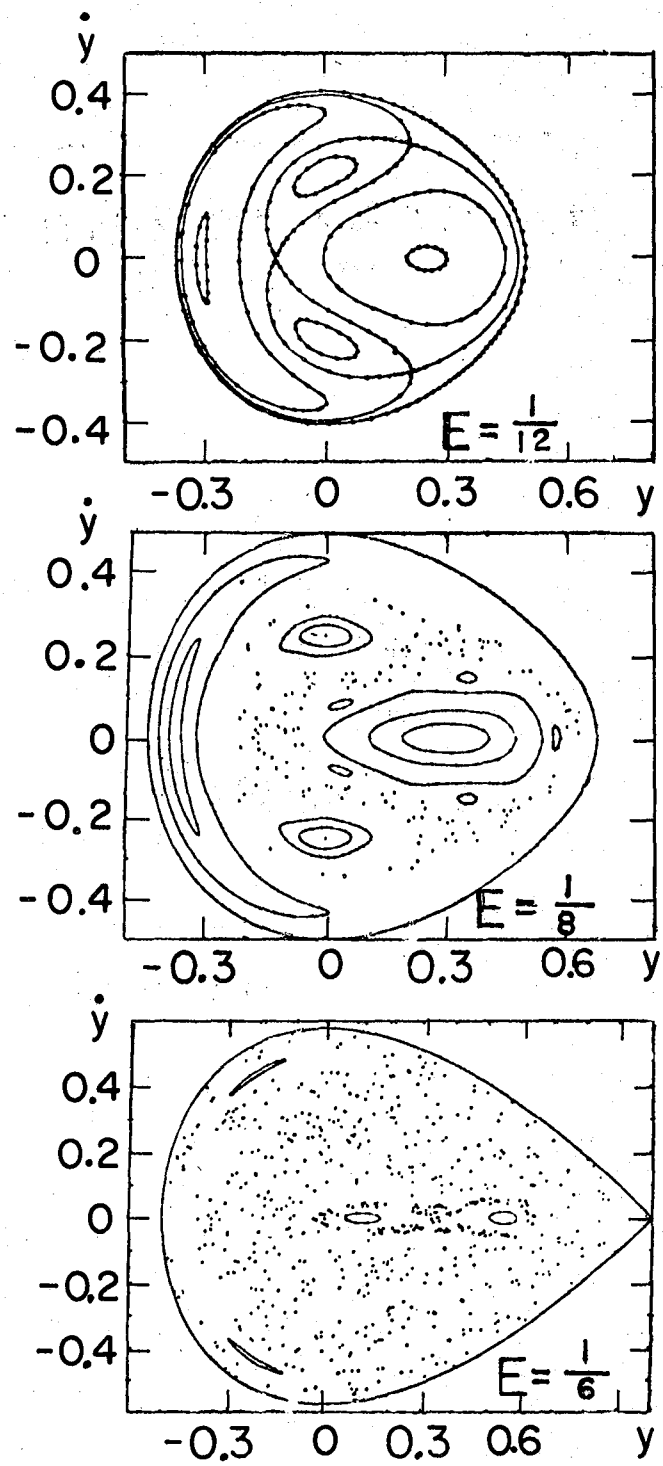

XBL773-614

Fig. 5

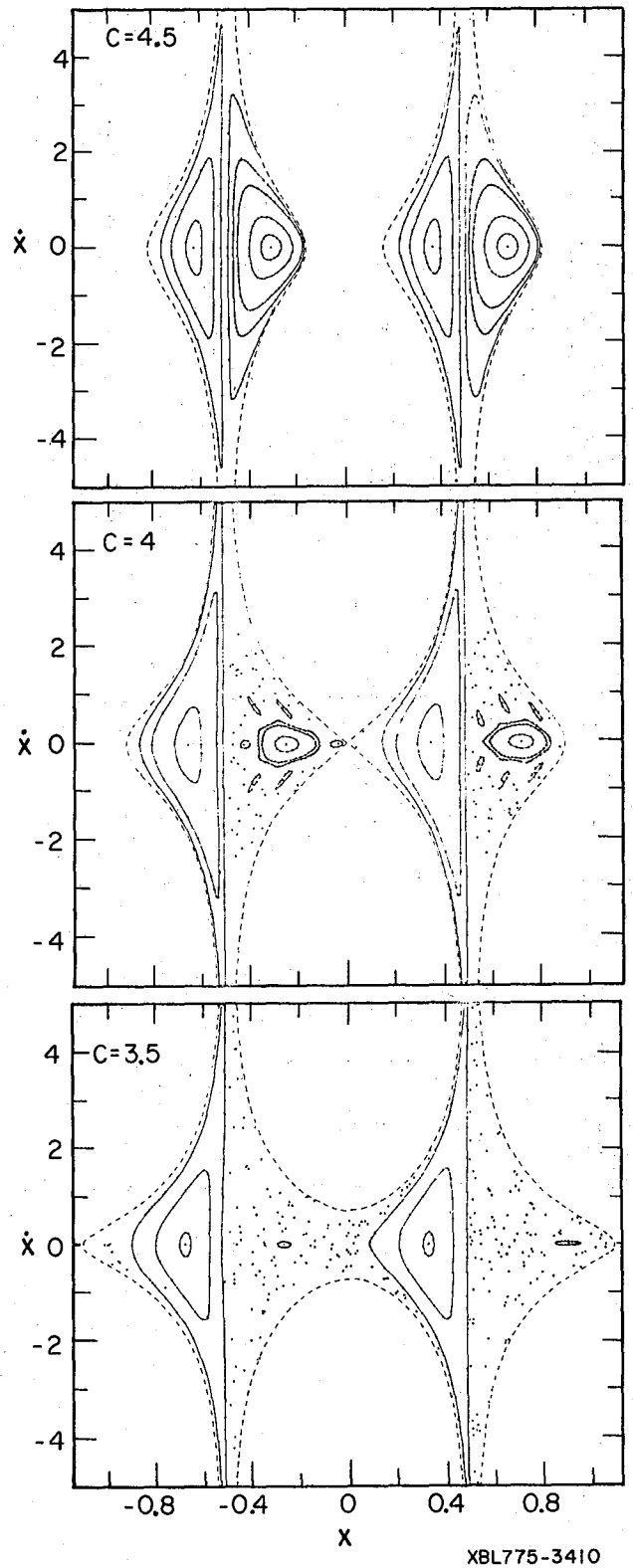

Fig. 6

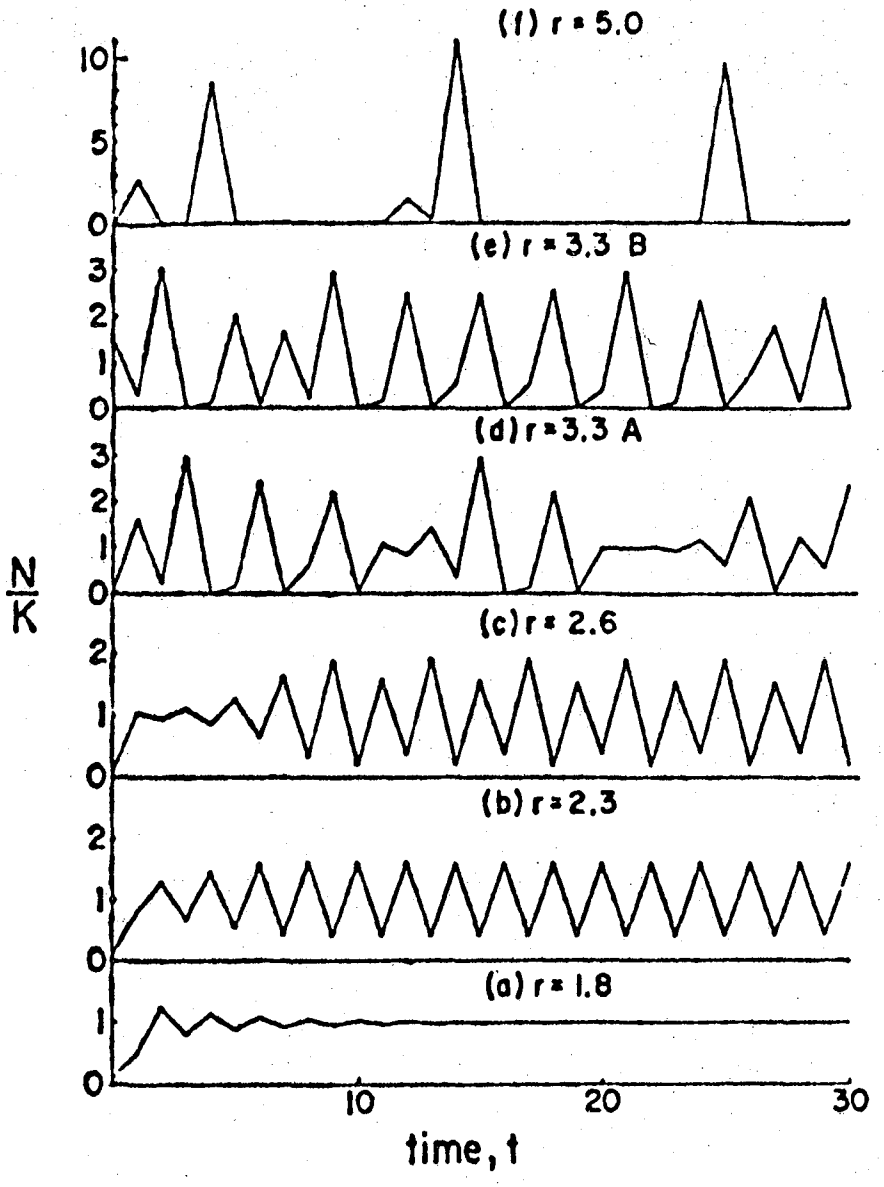

XBL 772-7803

Fig. 7

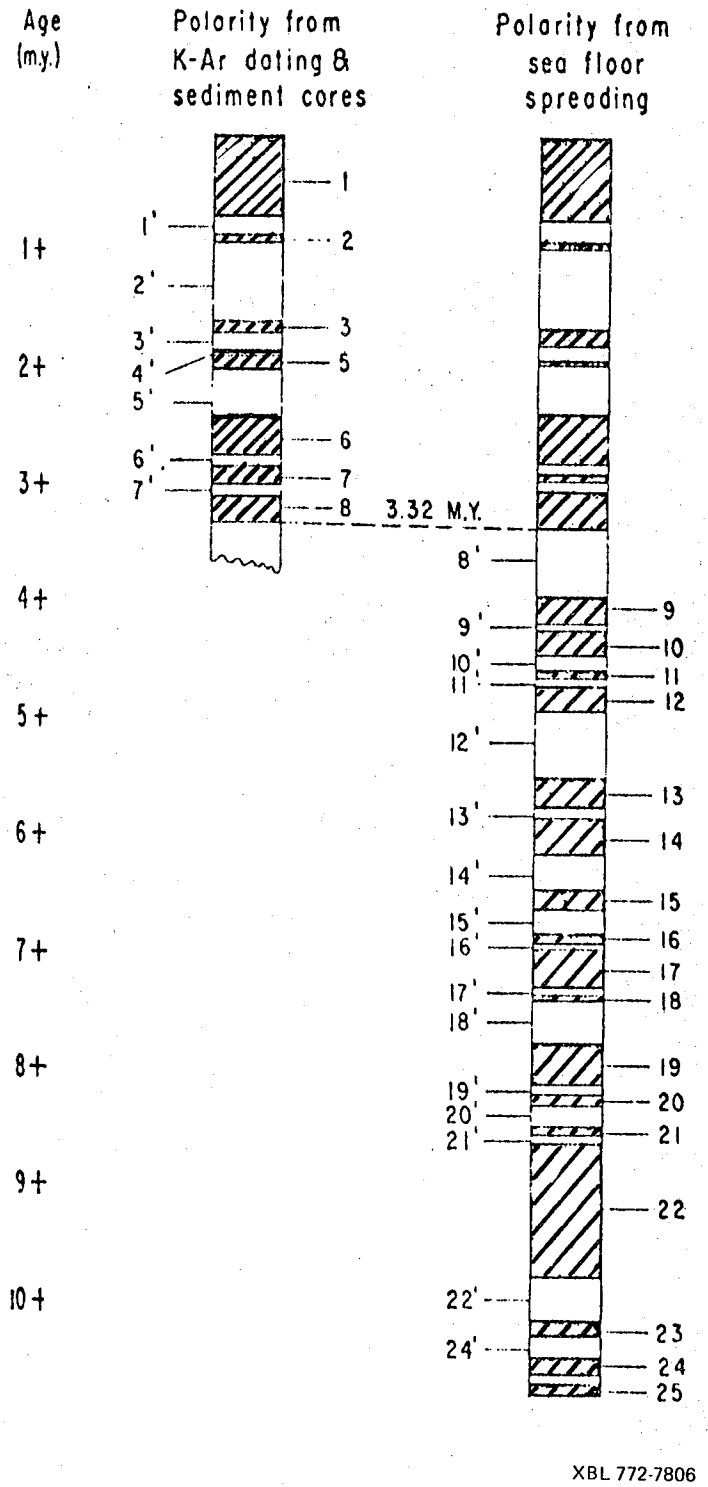
Age
(m.y.)
Polarity from
K-Ar dating &
sediment cores
Polarity from
sea floor
spreading
1+
2+
3+
4+
5+
6+
7+
8+
9+
10+
3.32 M.Y.
XBL 772-7806

Fig. 8

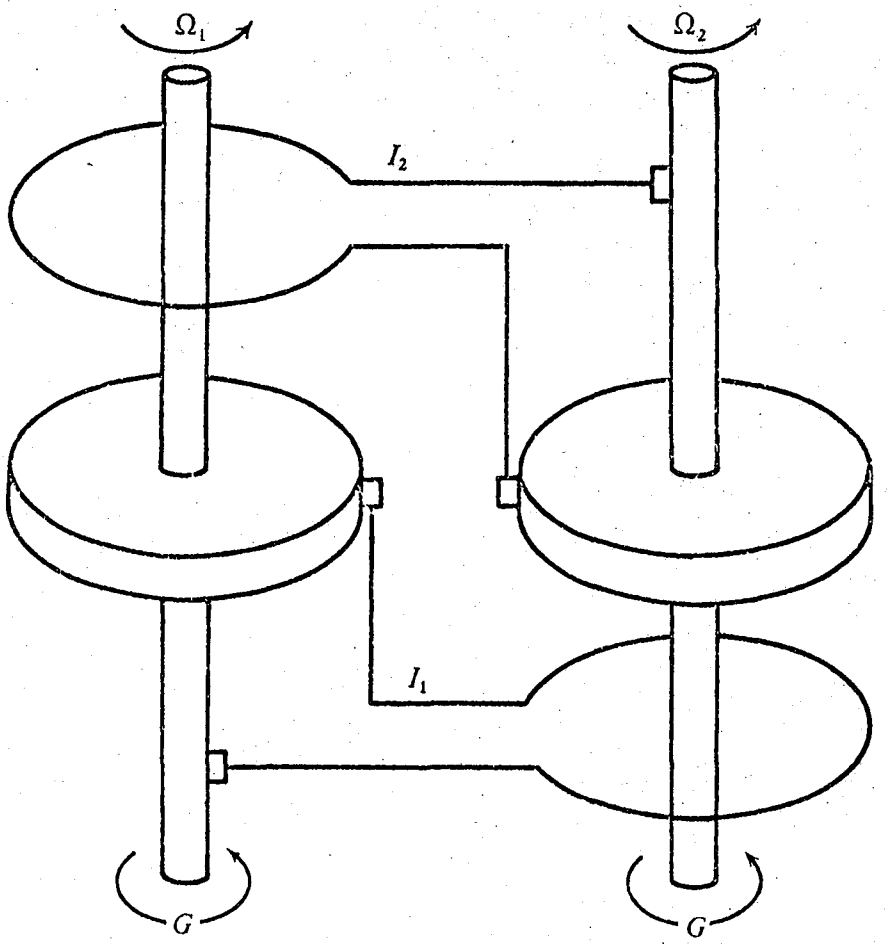

XBL 772-7804

Fig. 9

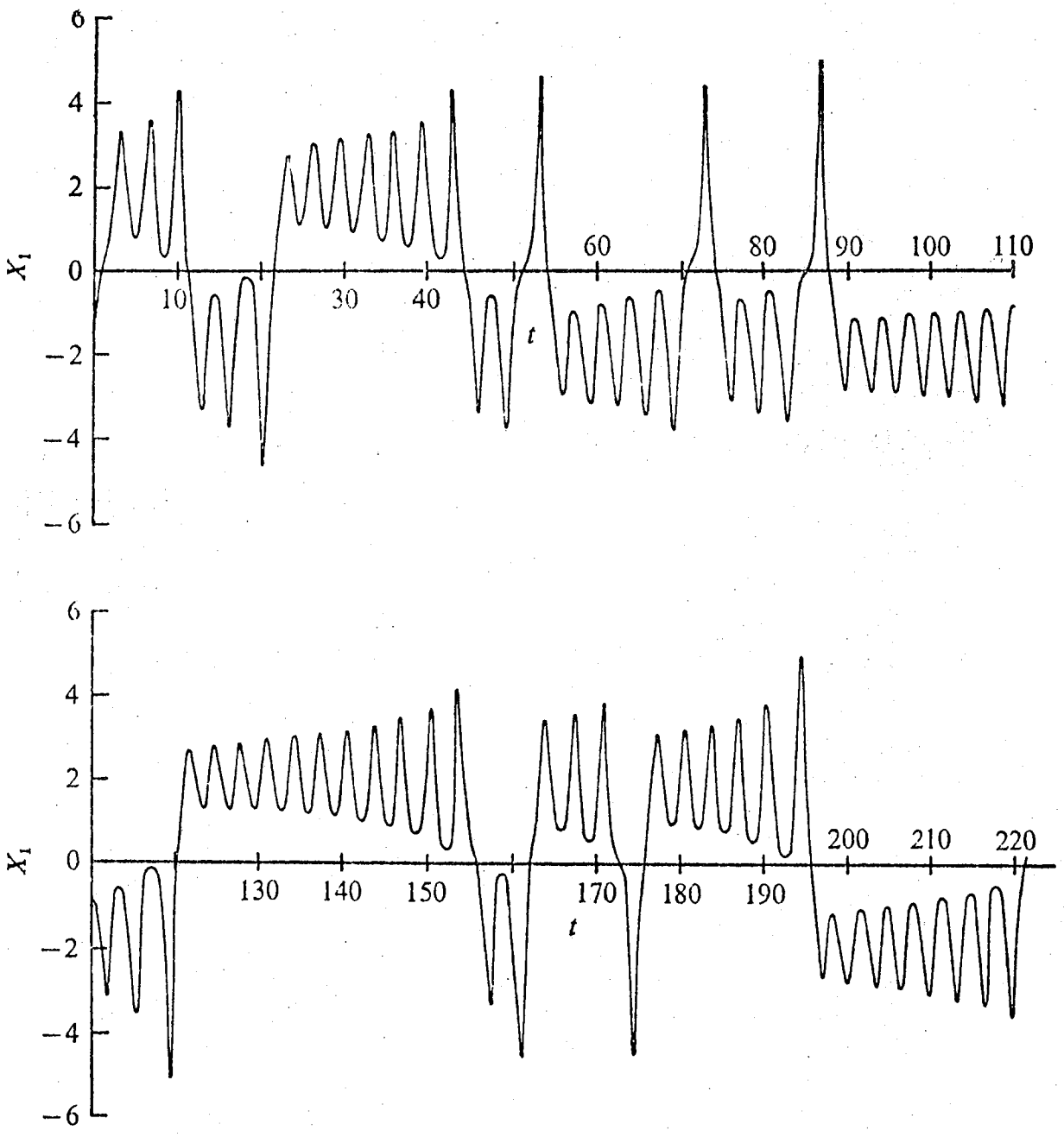
6
4
2
0
−2
−4
−6
X_1
10
30
40
60
80
90
100
110
t
6
4
2
0
−2
−4
−6
X_1
130
140
150
170
180
190
200
210
220
t
XBL 772-7805

Fig. 10

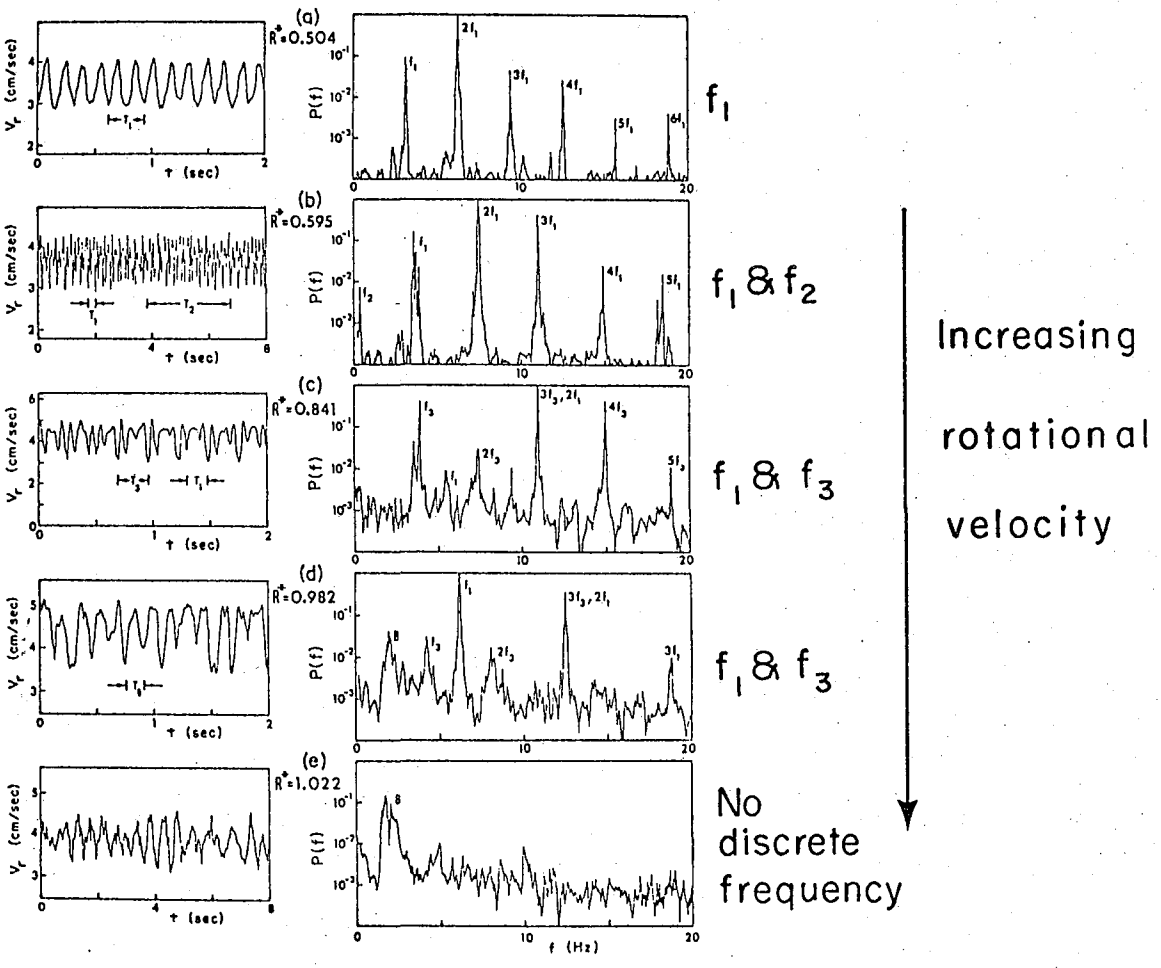

XBL773-615

Fig. 11

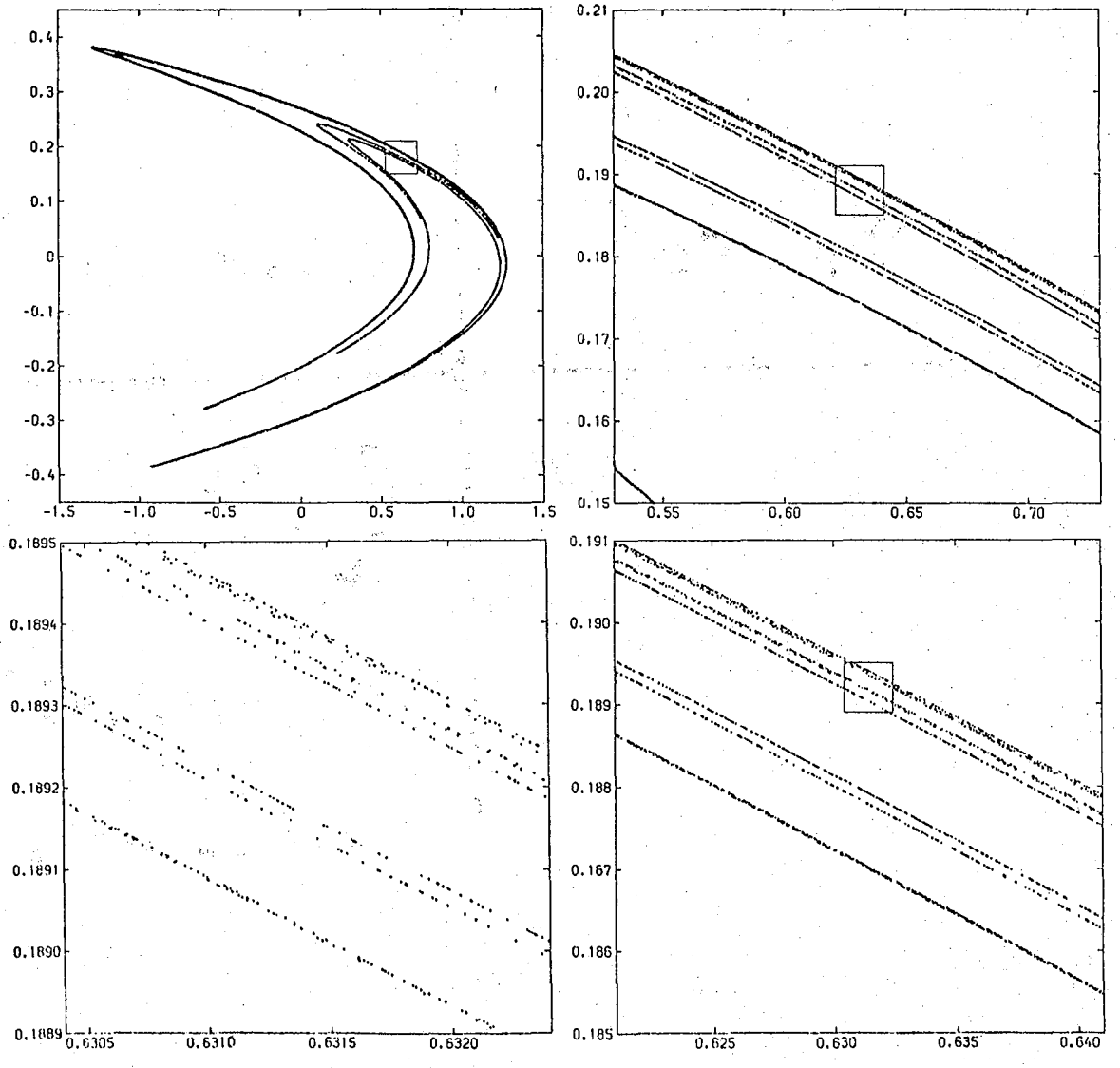

XBL 772-7807

Fig. 12

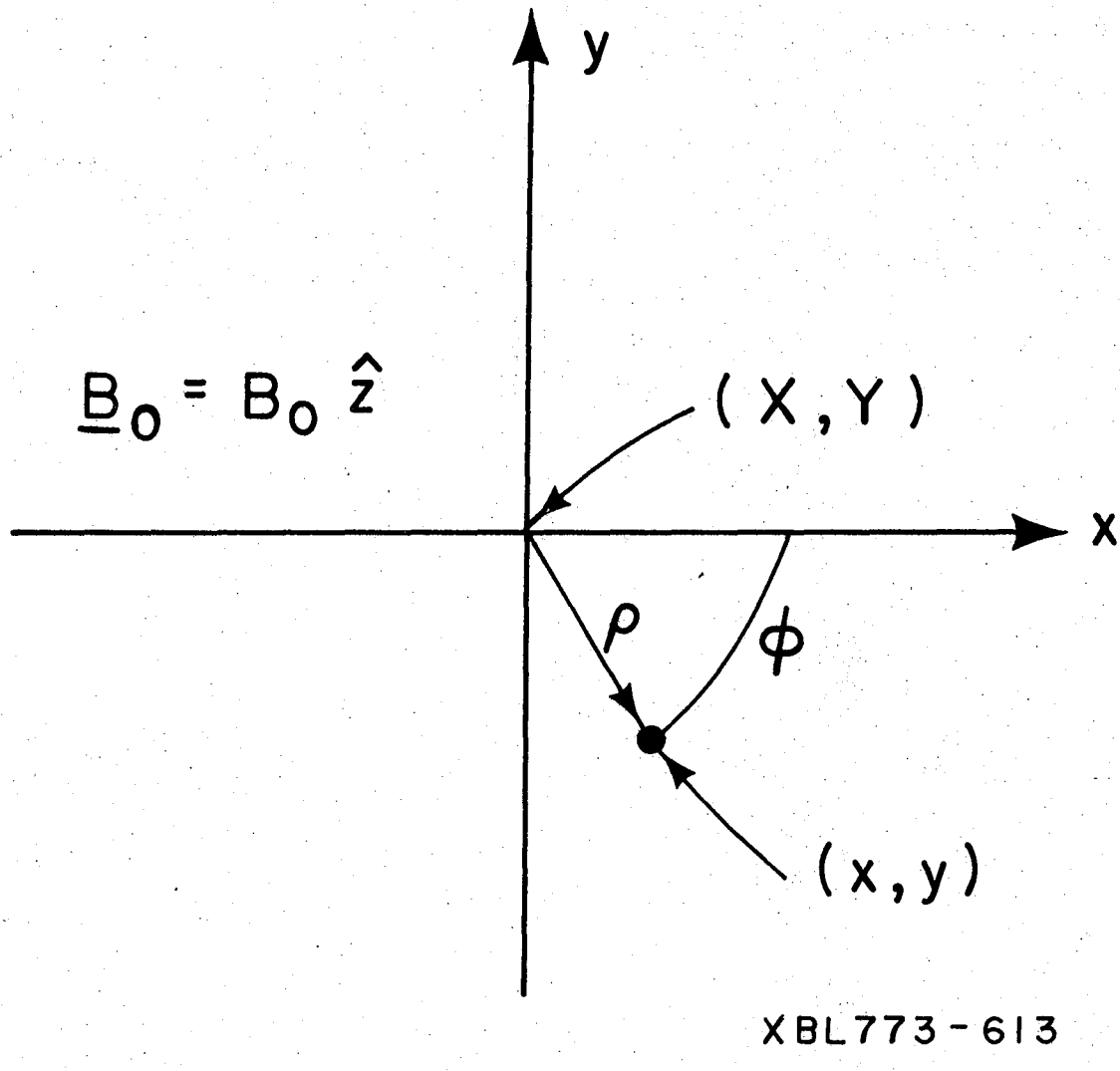

Fig. 13

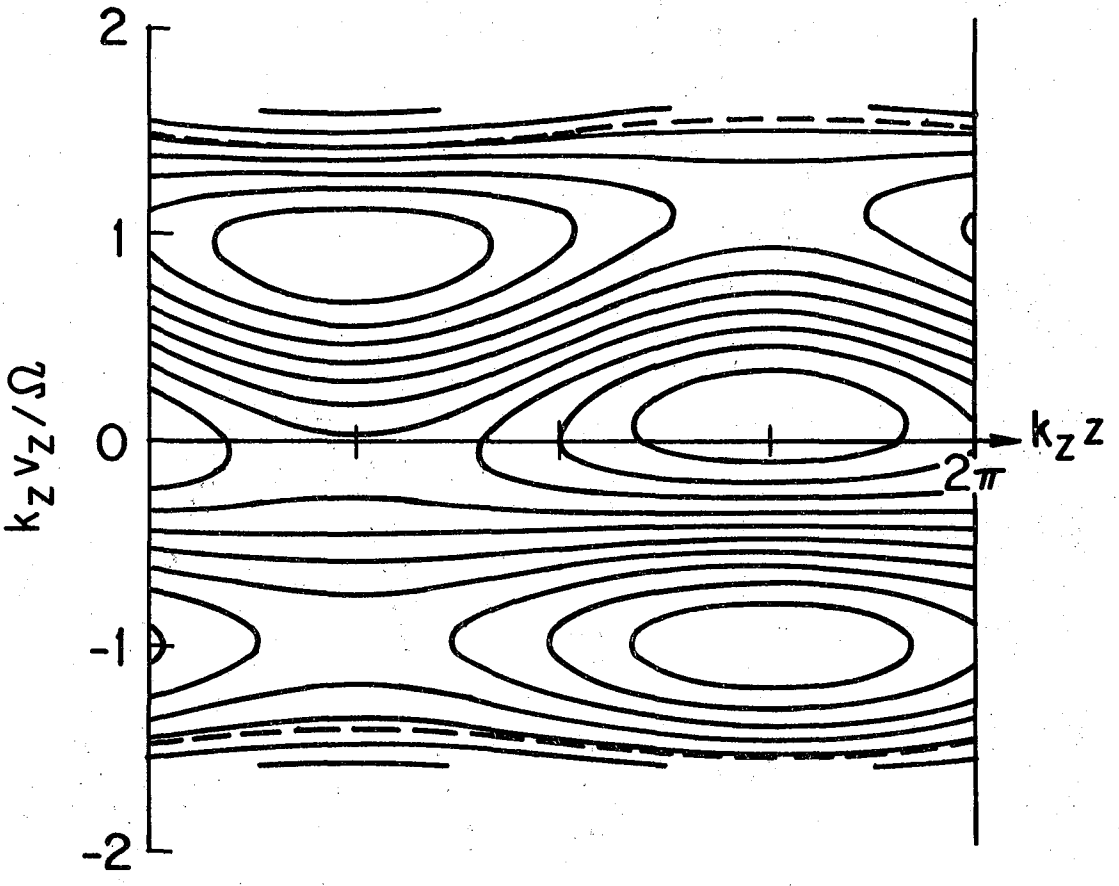

XBL775-3411

Fig. 14

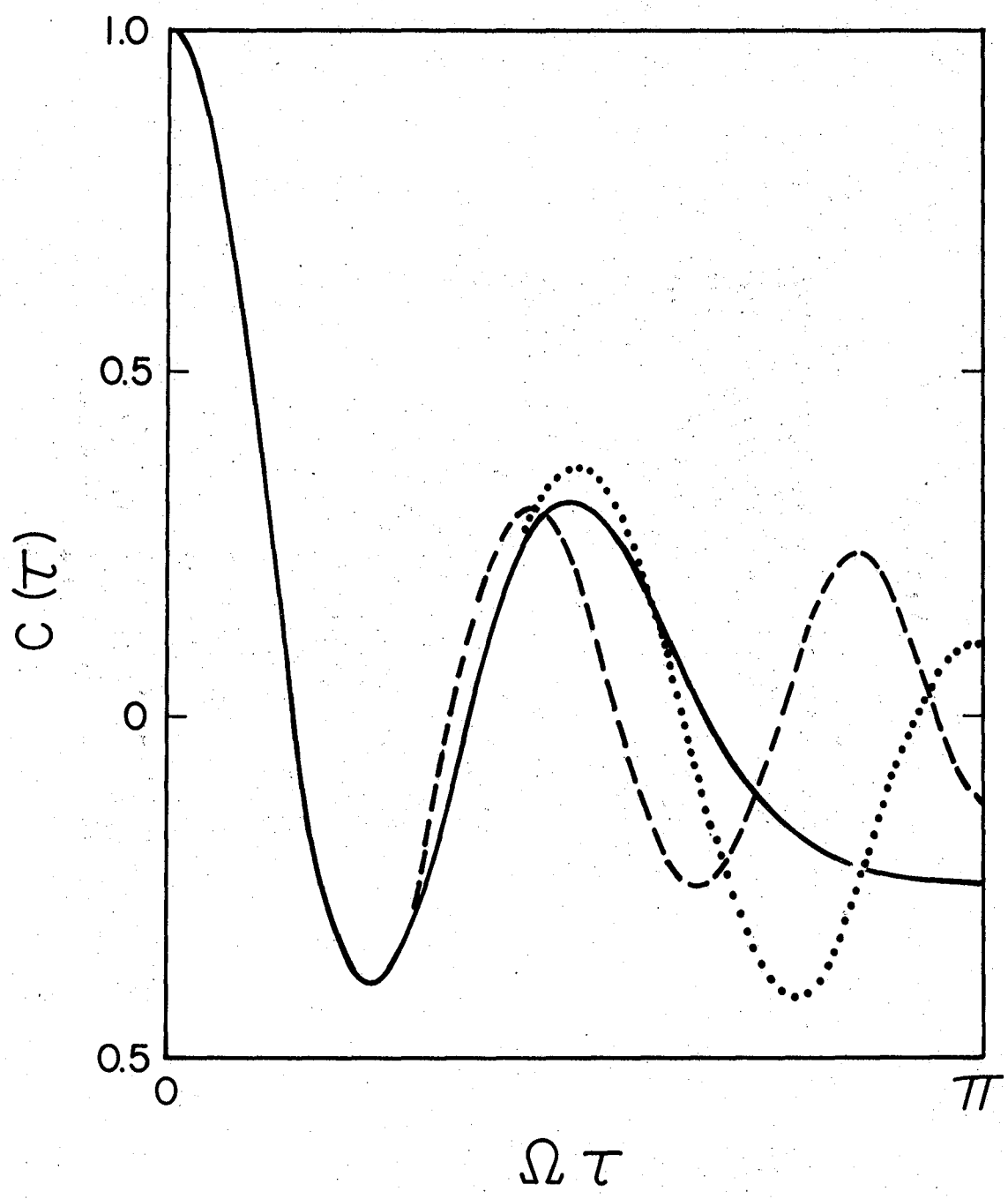

XBL 777-1379

Fig. 15

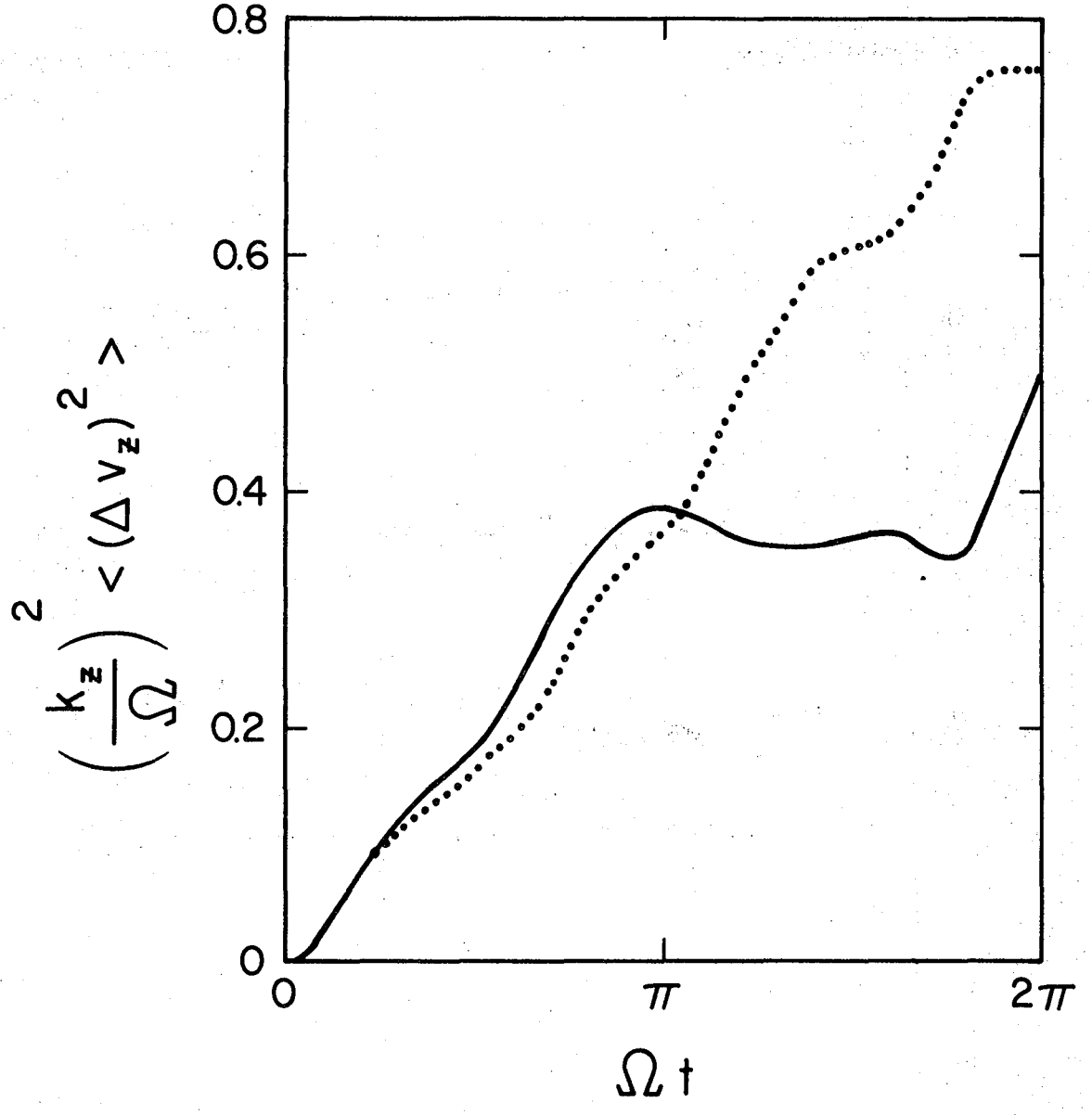

XBL 777-1378

Fig. 16

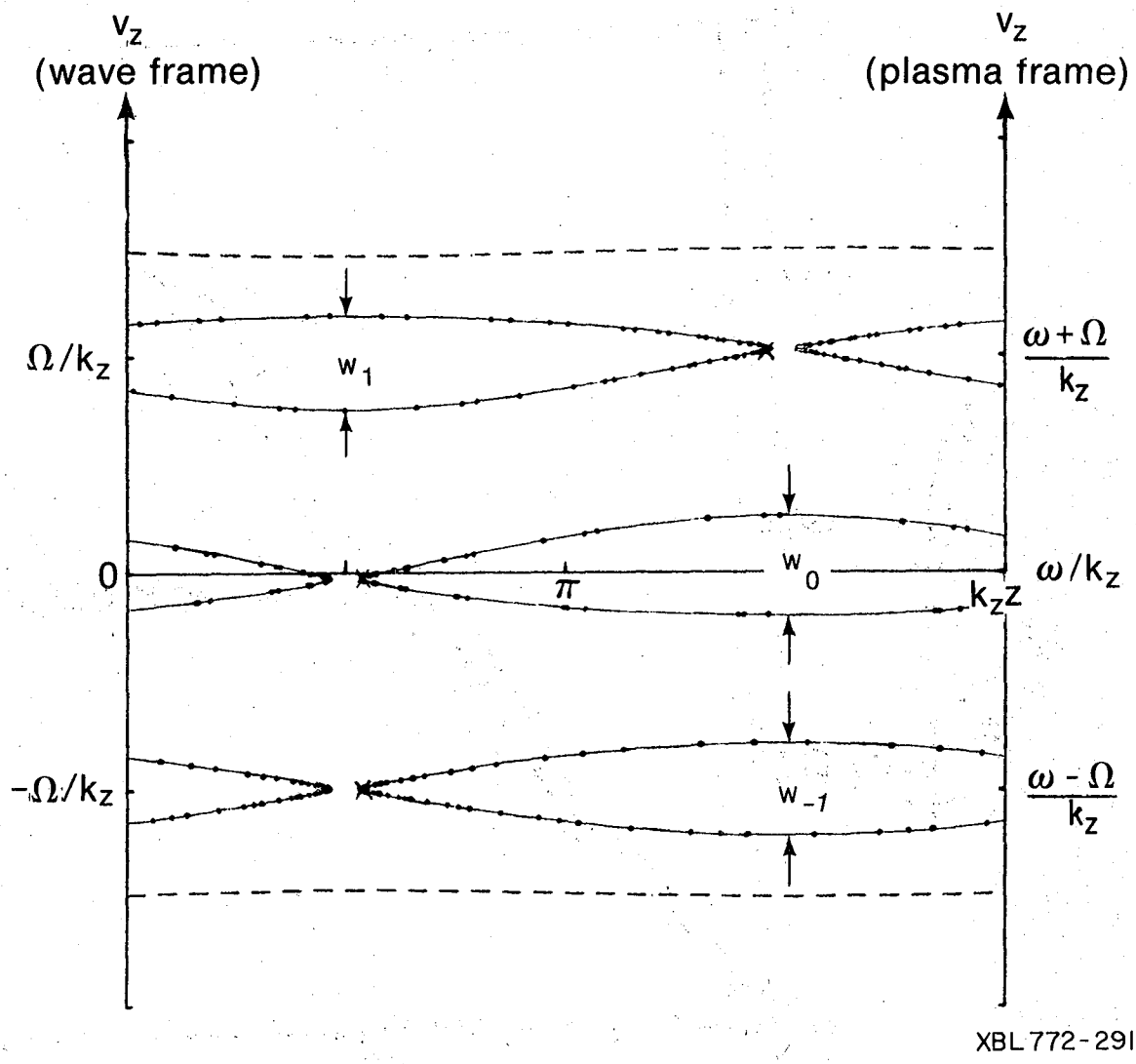
v_z
(wave frame)
v_z
(plasma frame)
Ω/k_z
w_1
$\frac{\omega+\Omega}{k_z}$
0
w_0
π
$k_z z$
ω/k_z
$-\Omega/k_z$
w_{-1}
$\frac{\omega-\Omega}{k_z}$
XBL 772-291

Fig. 17

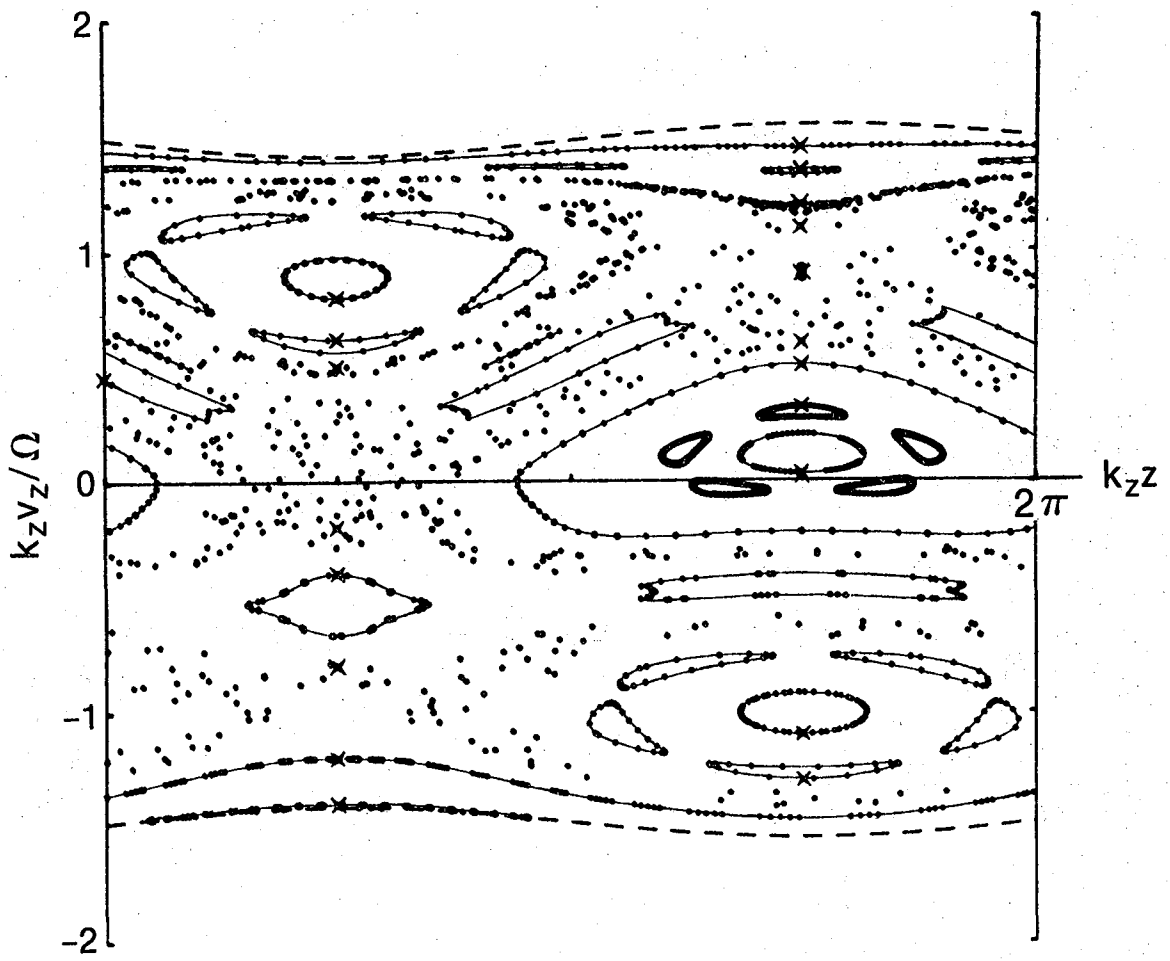

XBL 772-290

Fig. 18

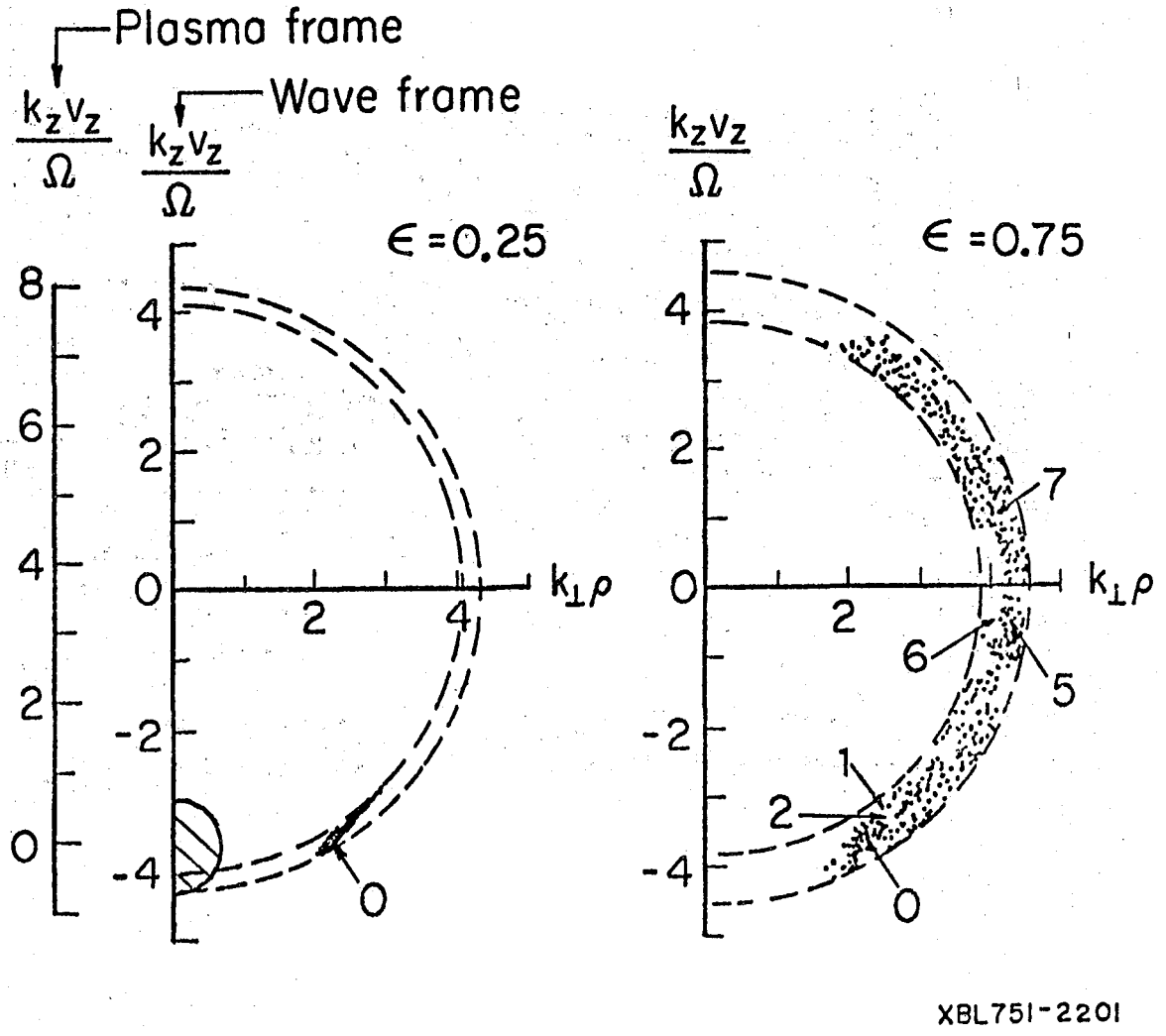
Plasma frame
Wave frame
$\frac{k_z v_z}{\Omega}$
$\frac{k_z v_z}{\Omega}$
$\epsilon = 0.25$
$\epsilon = 0.75$
$k_\perp \rho$
$k_\perp \rho$
8
6
4
2
0
-2
-4
0
2
4
7
6
5
1
2
0
XBL751-2201

Fig. 19

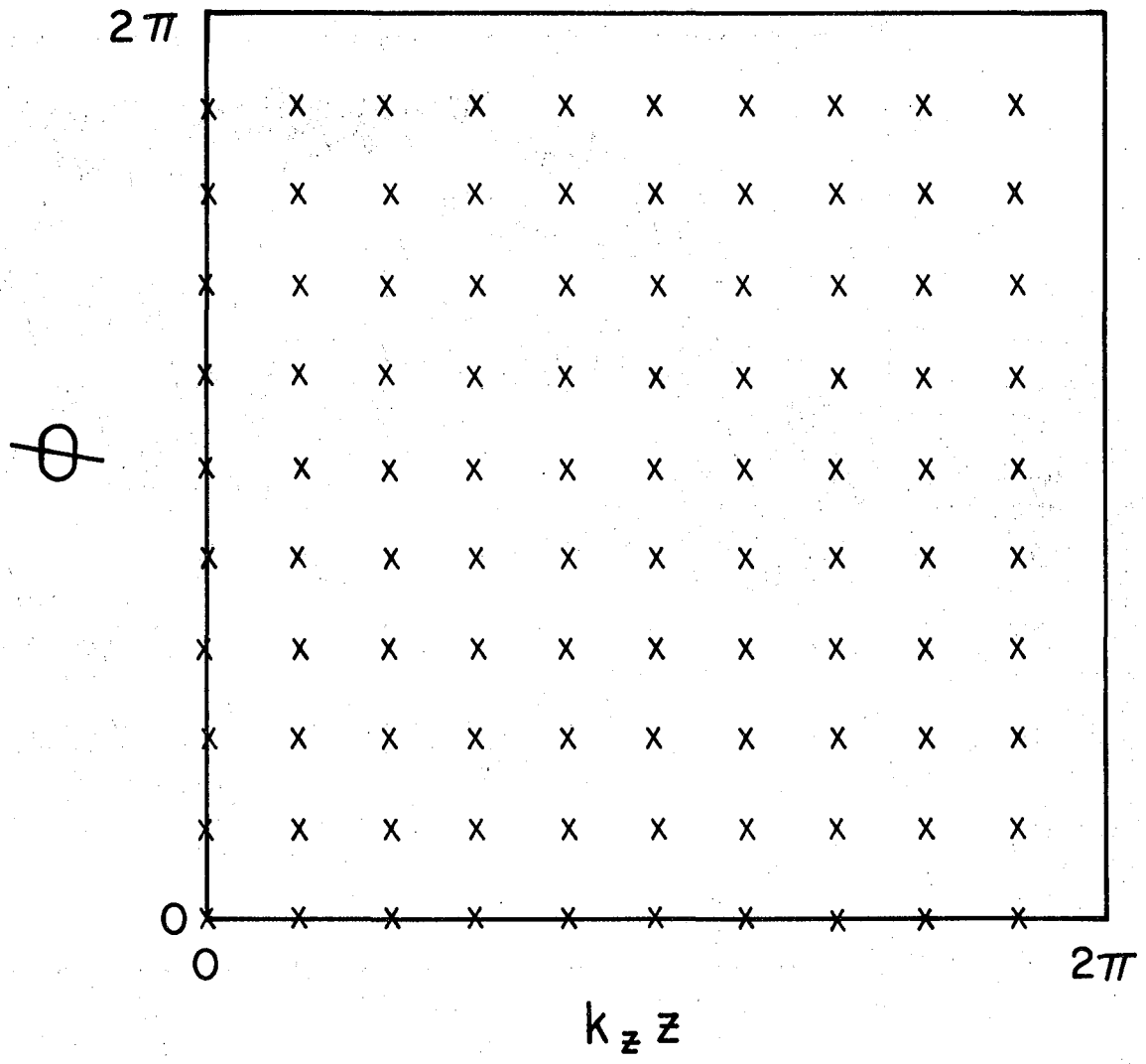

XBL 777-1377

Fig. 20

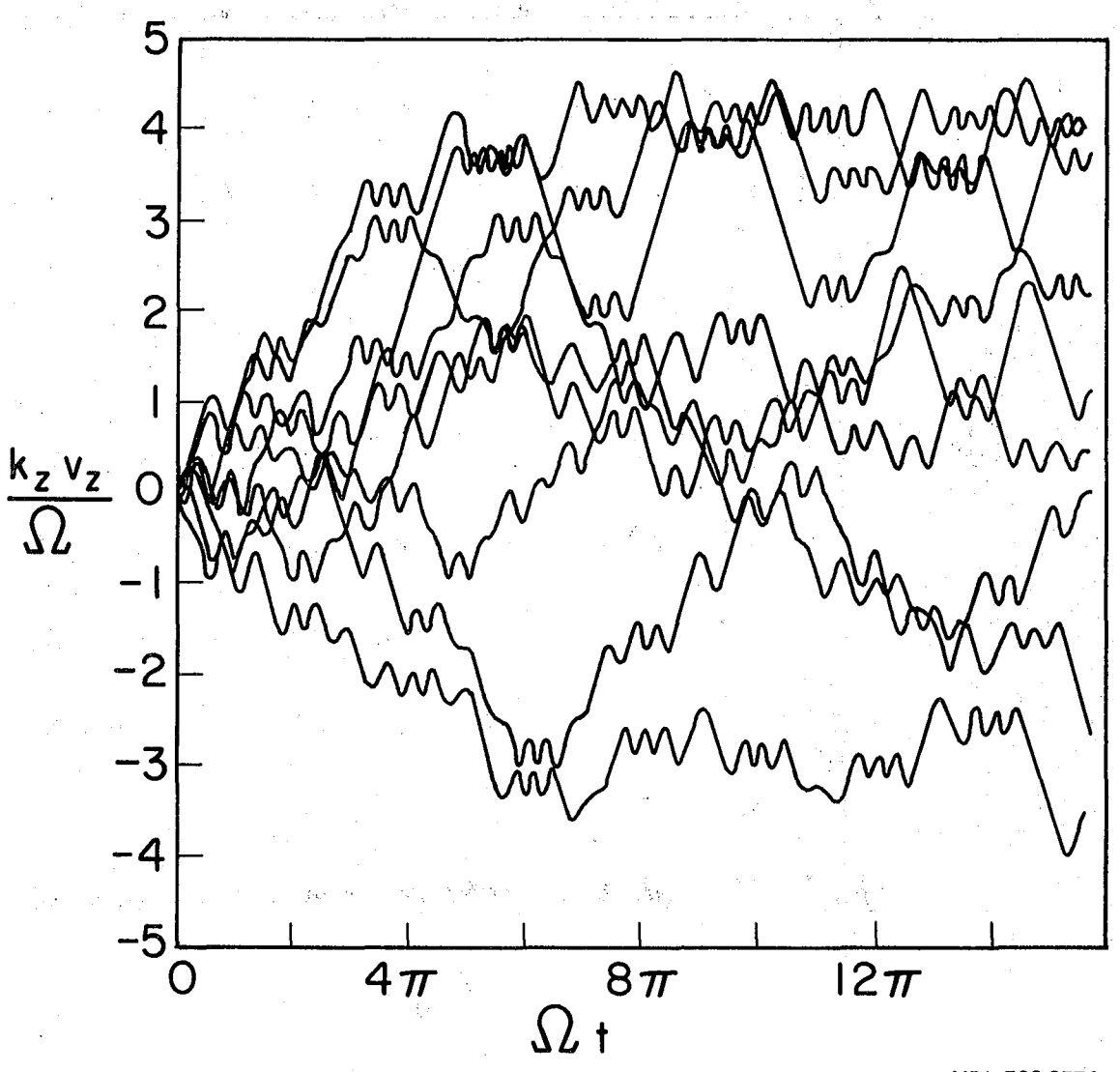

Fig. 21

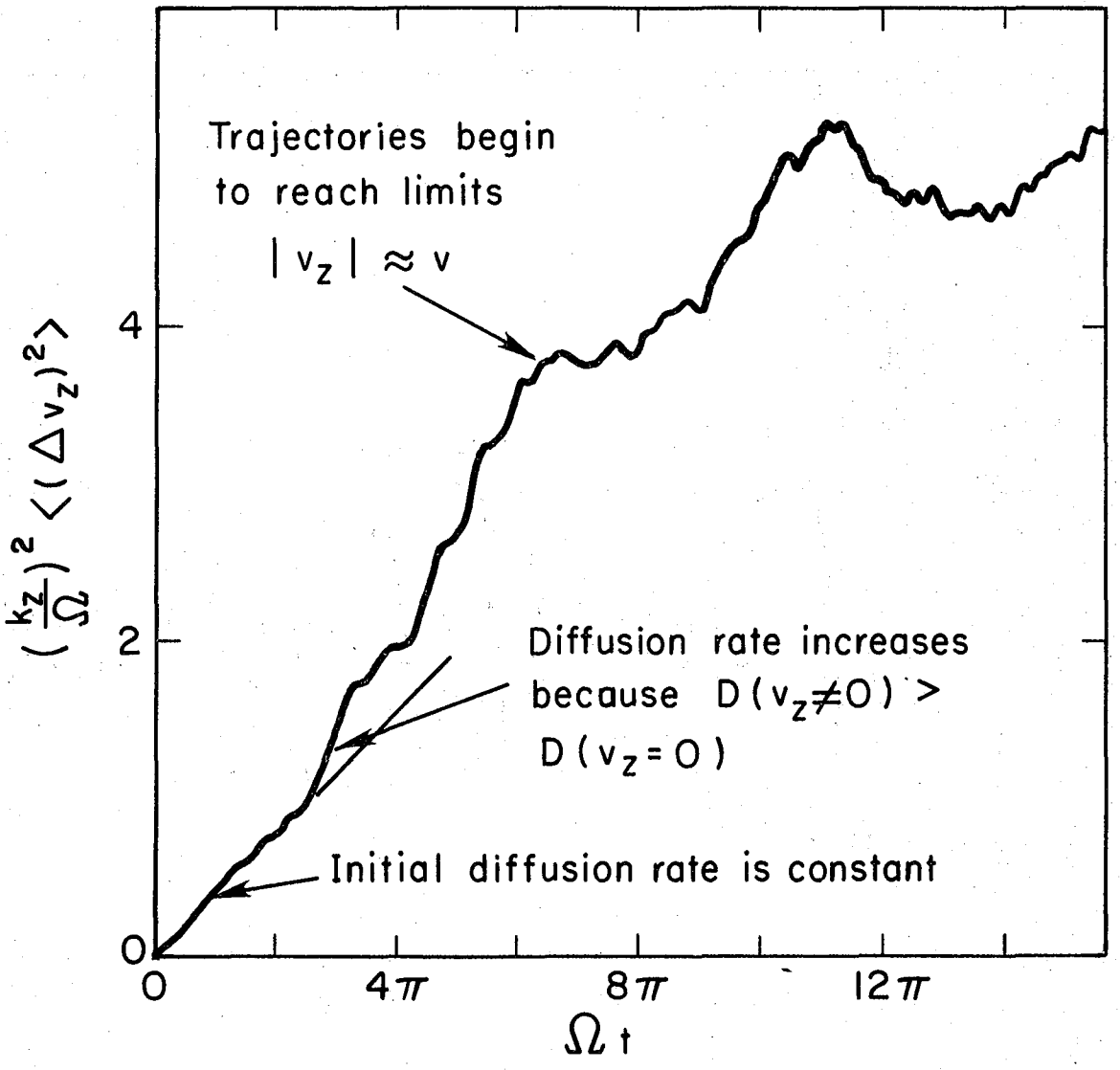

XBL 763-2577

Fig. 22

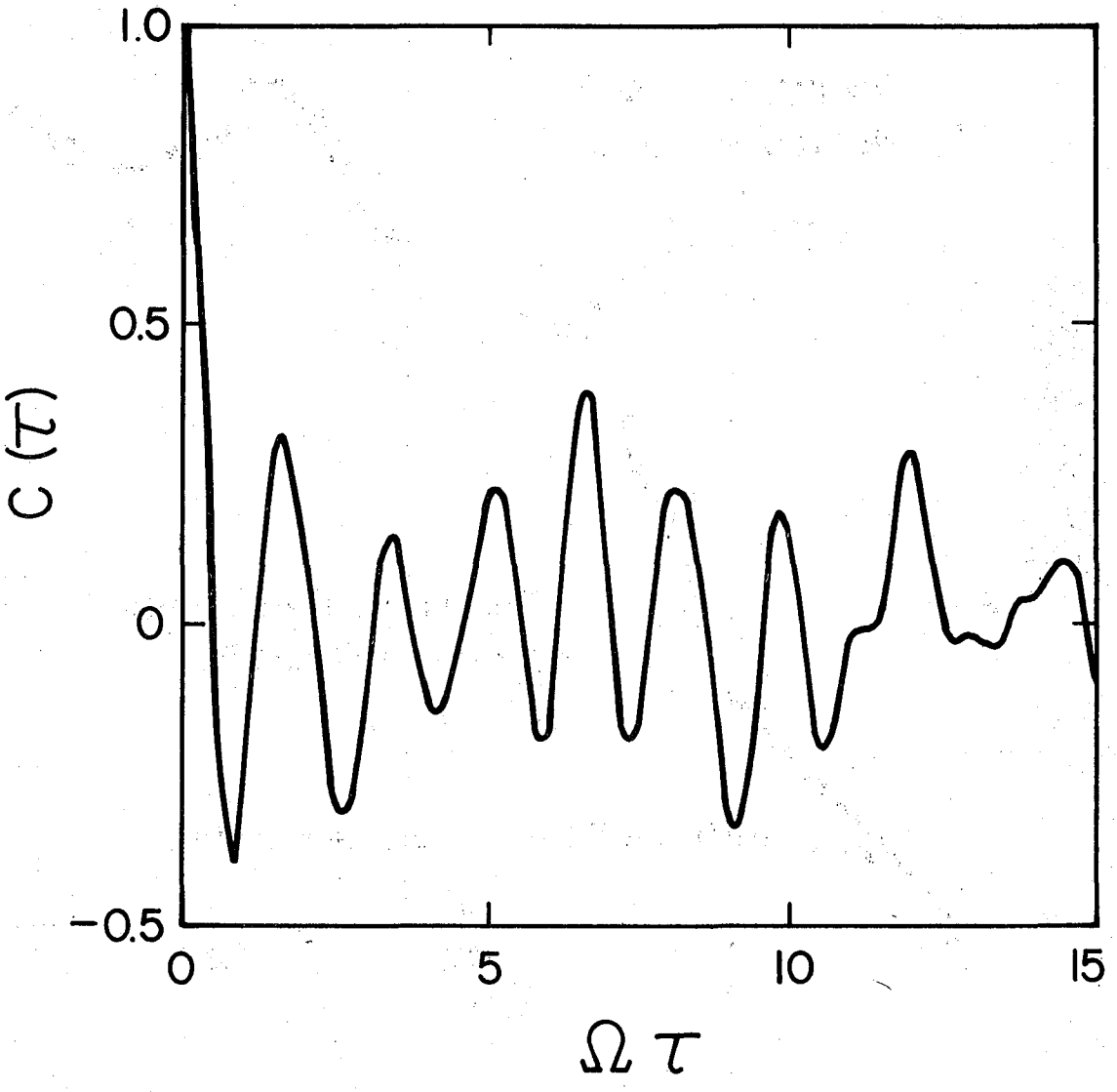

XBL777-1384

Fig. 23

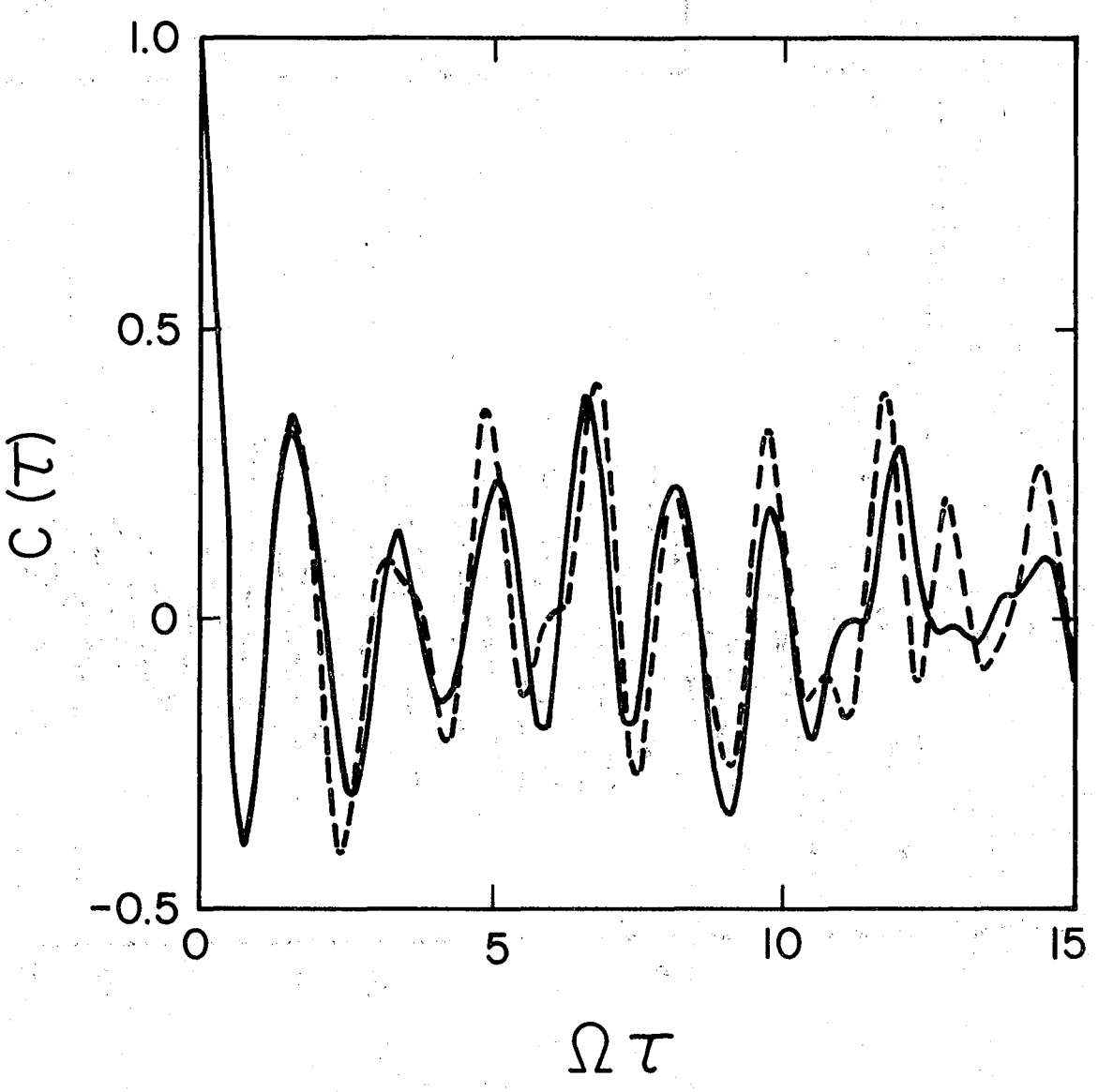

XBL 777-1385

Fig. 24

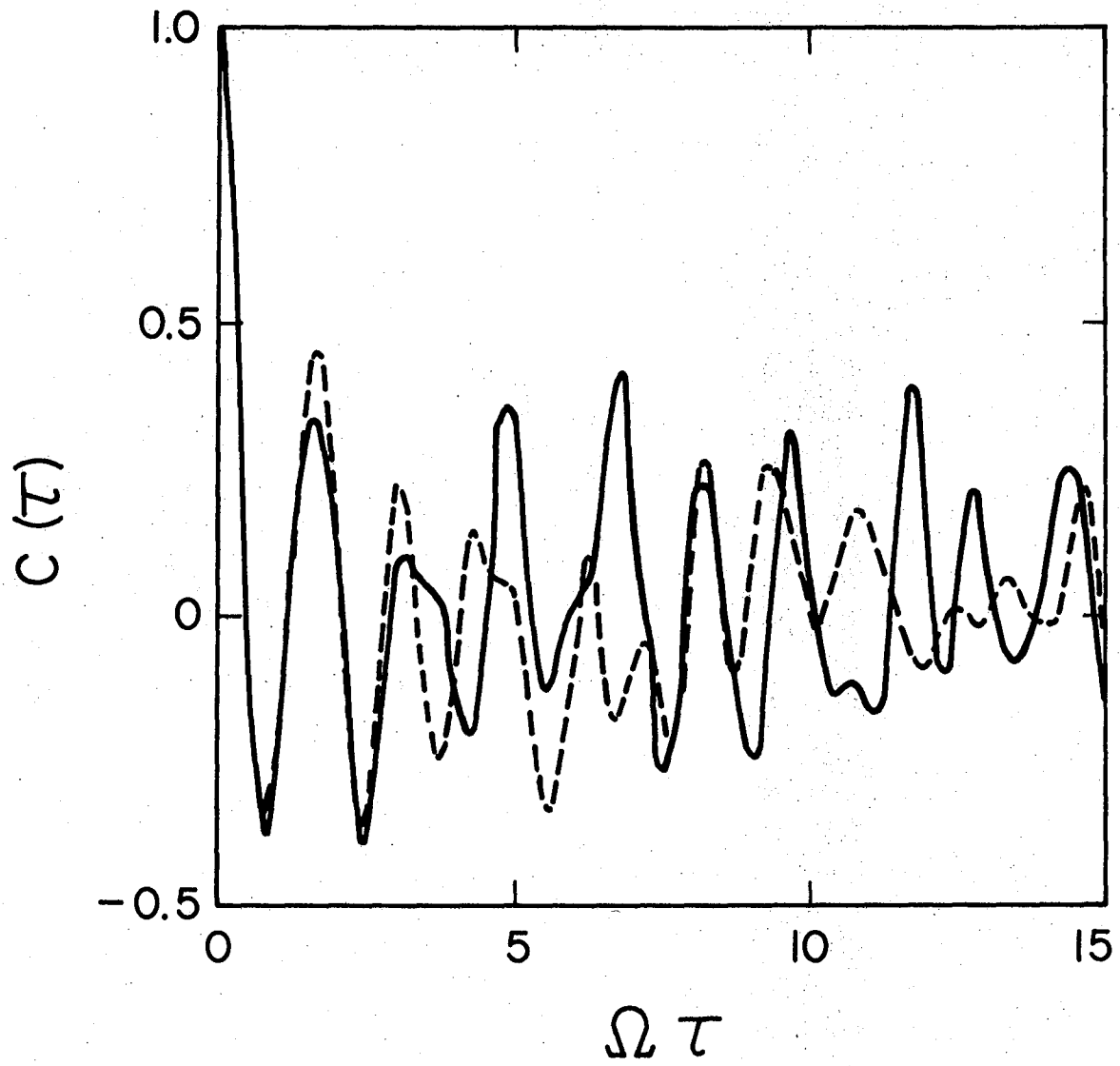

XBL 777-1383

Fig. 25

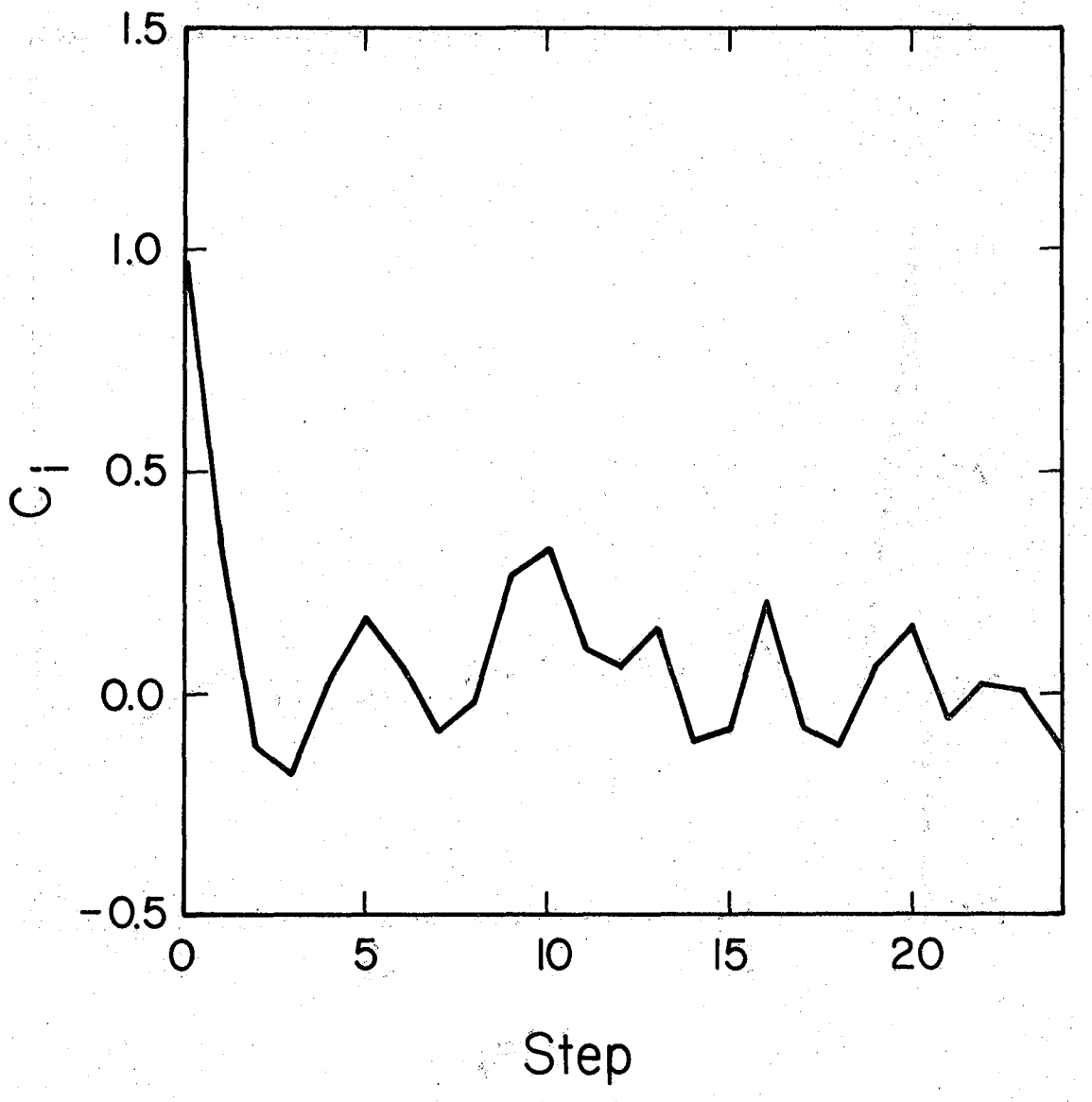

XBL777-1380

Fig. 26

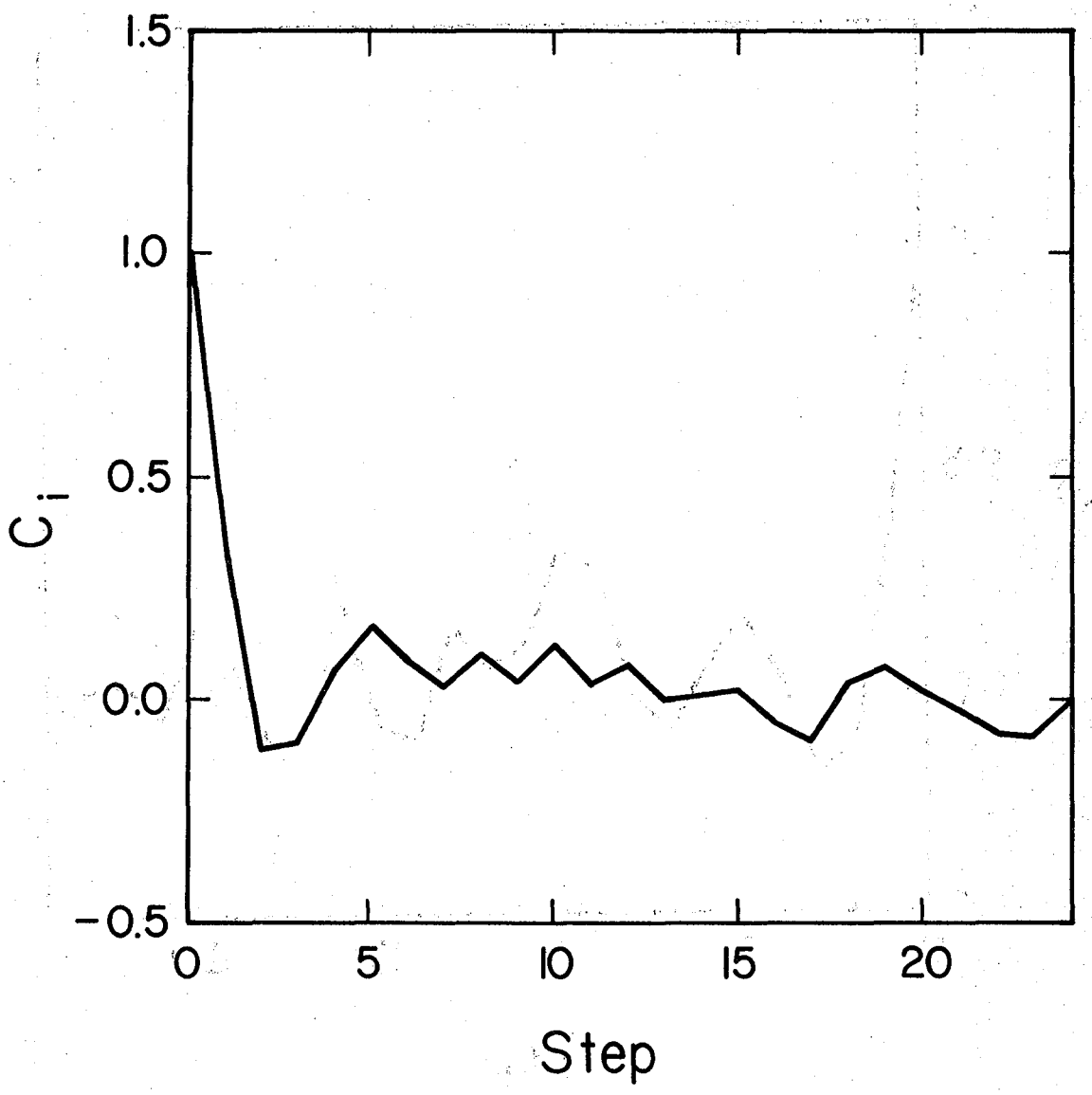

XBL 777-1382

Fig. 27

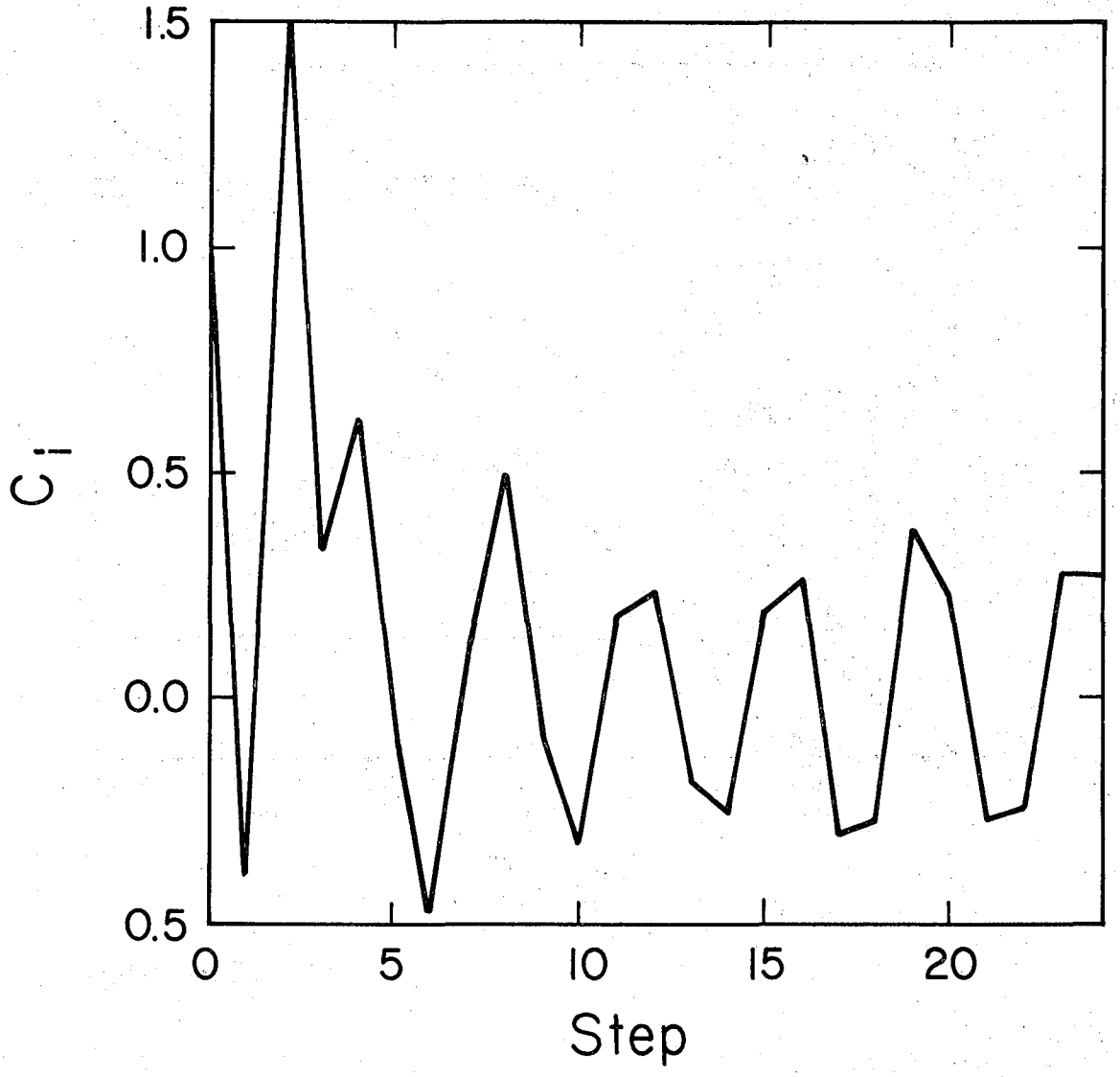

XBL 777-1381

Fig. 28

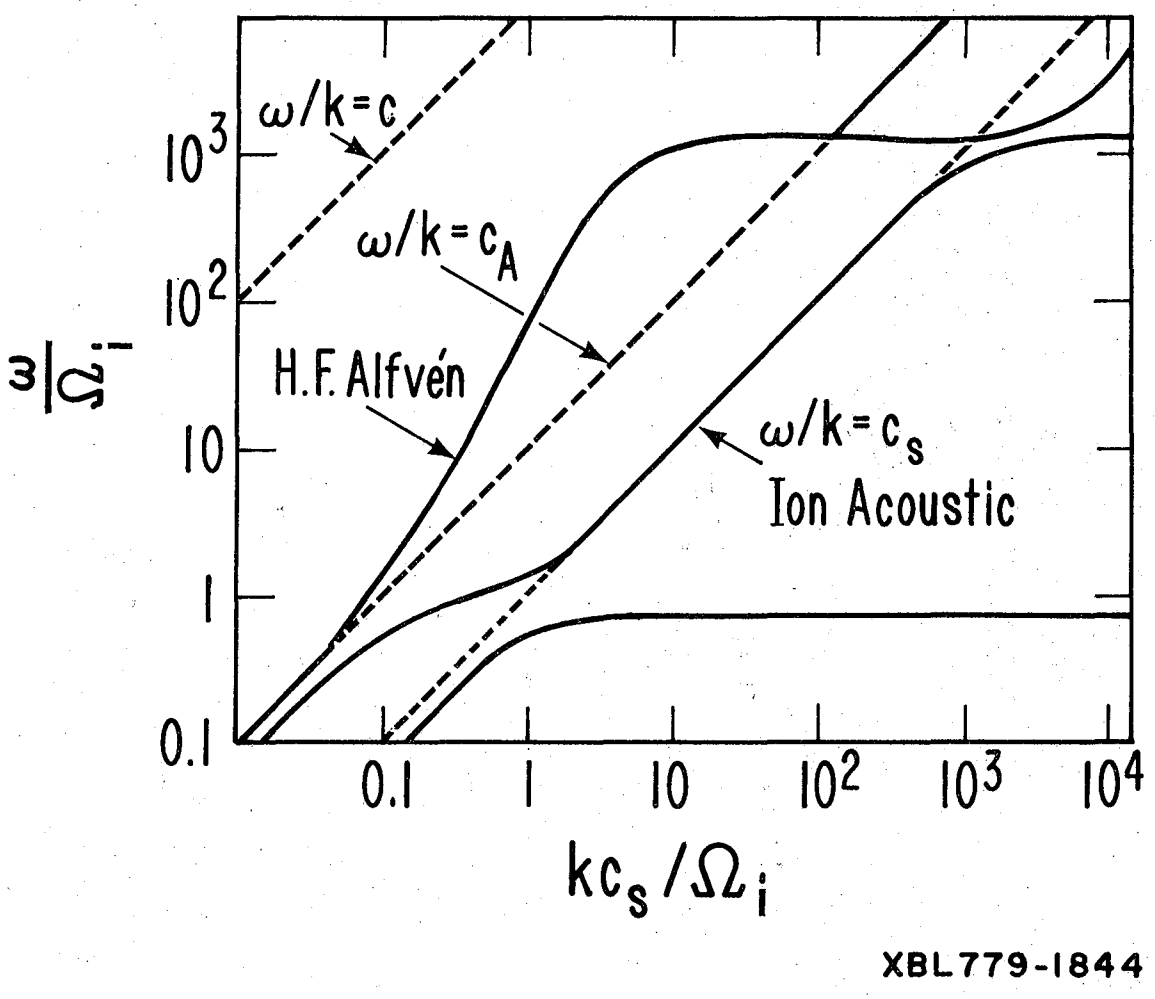
ω/k = c
ω/k = c_A
H.F. Alfvén
ω/k = c_s
Ion Acoustic
3|Ω_i|
10^3
10^2
10
1
0.1
0.1
1
10
10^2
10^3
10^4
kc_s/Ω_i
XBL779-1844

Fig. 29

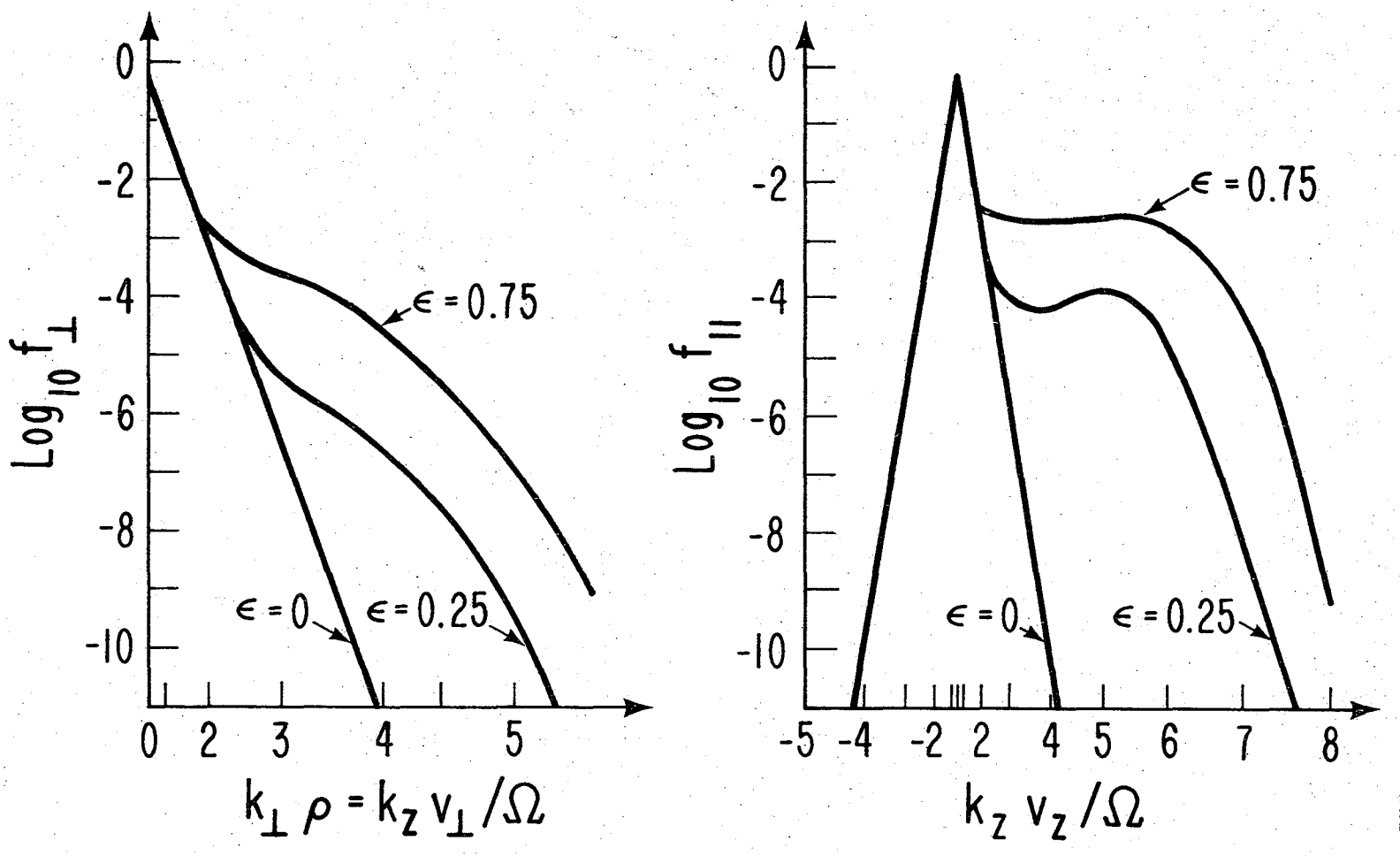

Fig. 30

XBL779-1845

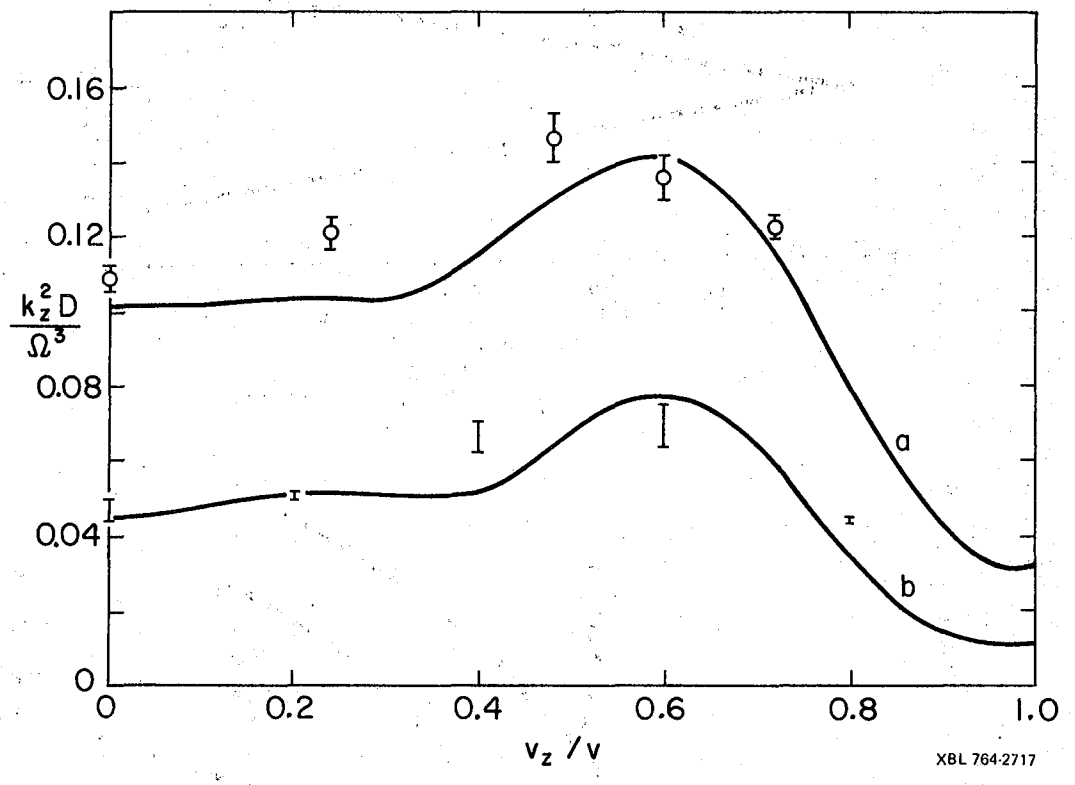
0.16
0.12
$\frac{k_z^2 D}{\Omega^3}$
0.08
0.04
0
0
0.2
0.4
0.6
0.8
1.0
v_z / v
a
b
XBL 764-2717

Fig. 31

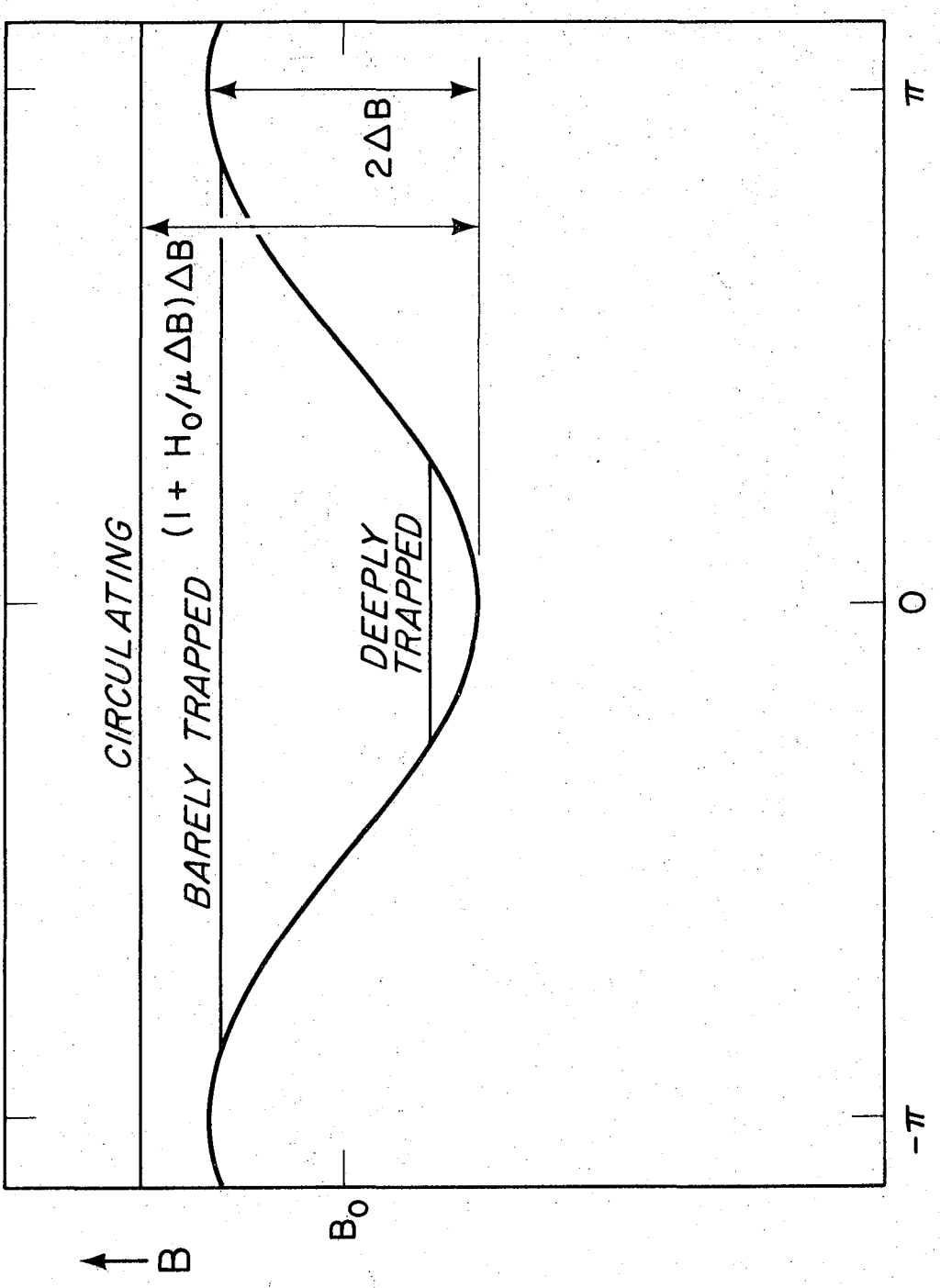
CIRCULATING
BARELY TRAPPED
$(1 + H_0/\mu\Delta B)\Delta B$
$2\Delta B$
DEEPLY TRAPPED
B
B_0
$-\pi$
0
π
$\Theta = s/qR_0$
XBL779-1842

Fig. 32

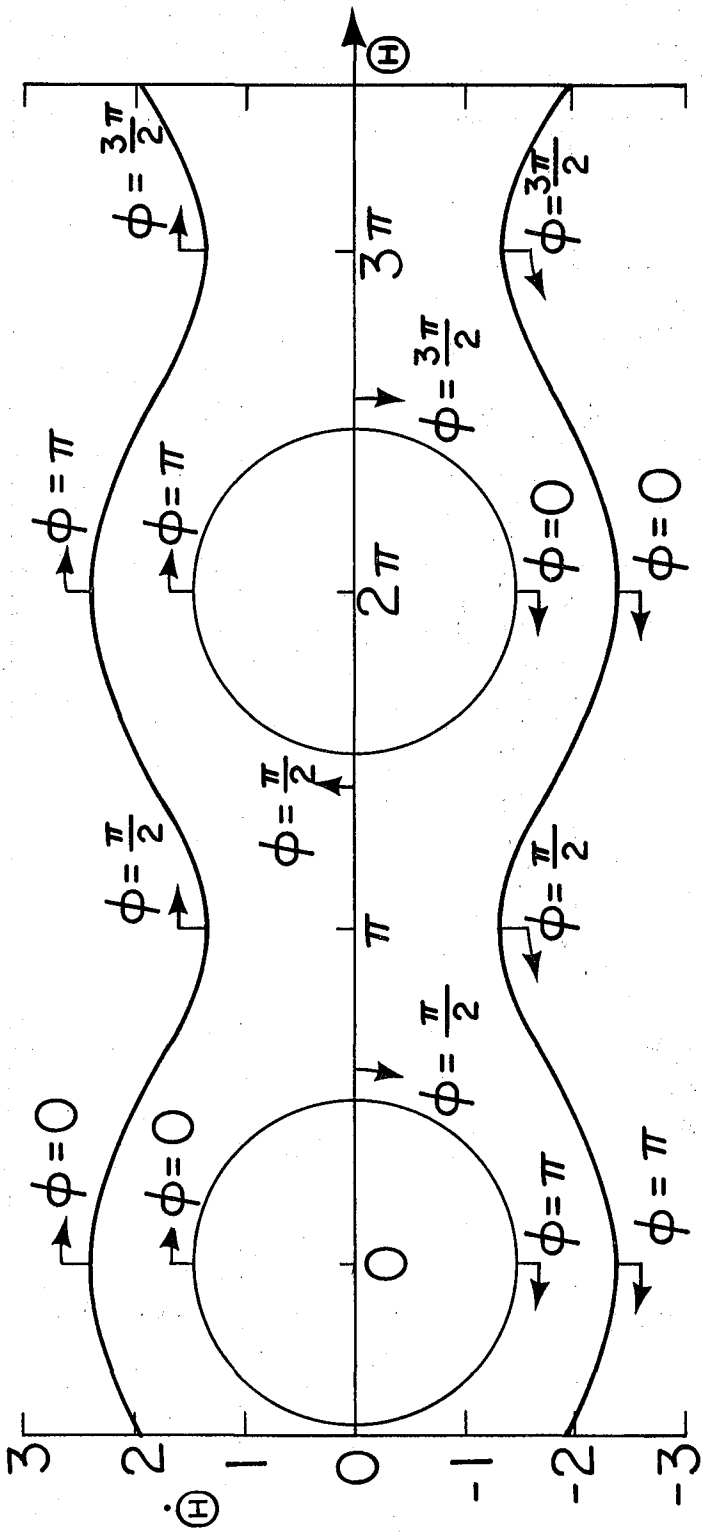

XBL771-242

Fig. 33

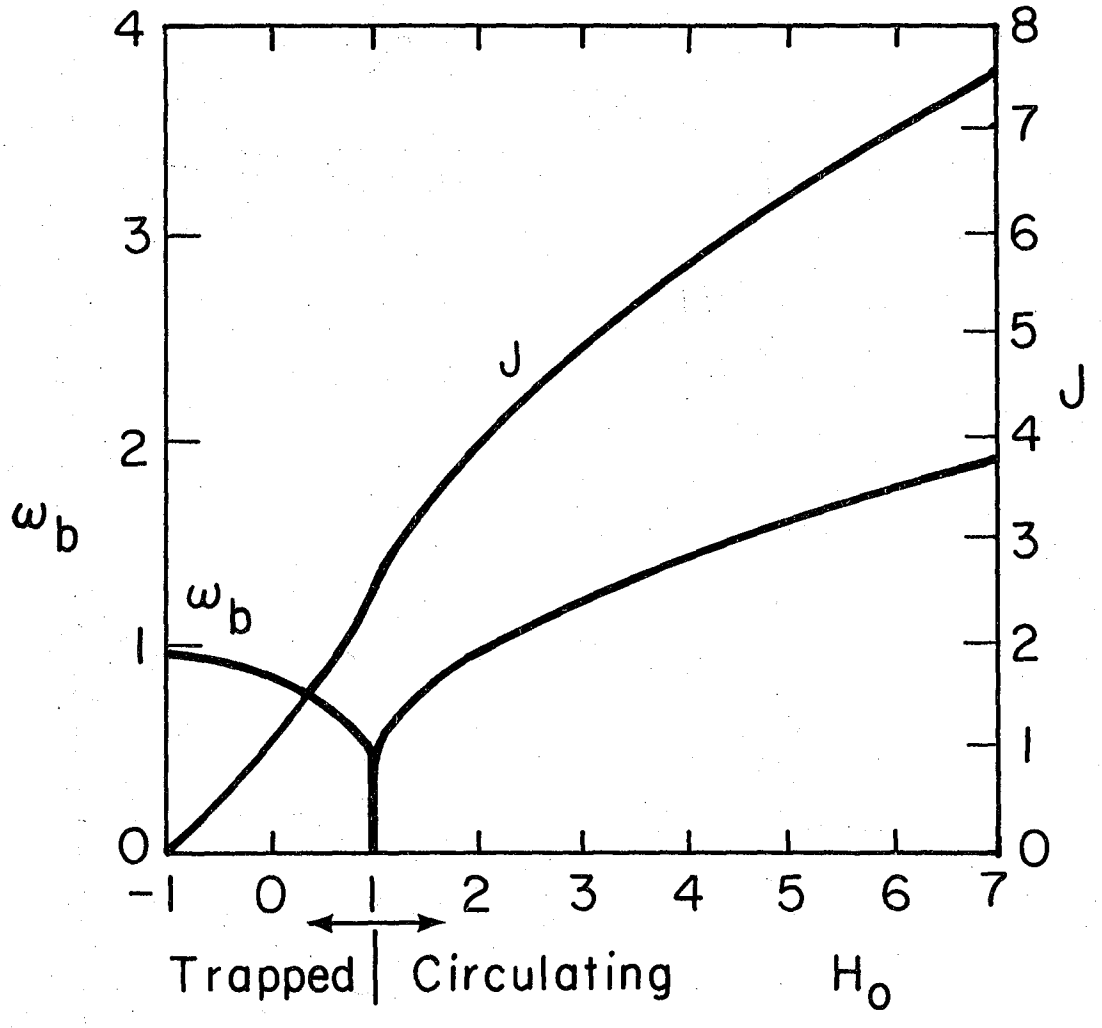
4
3
2
1
0
8
7
6
5
4
3
2
1
0
ω_b
J
ω_b
J
-1
0
1
2
3
4
5
6
7
Trapped
Circulating
H_o
XBL771-243

Fig. 34

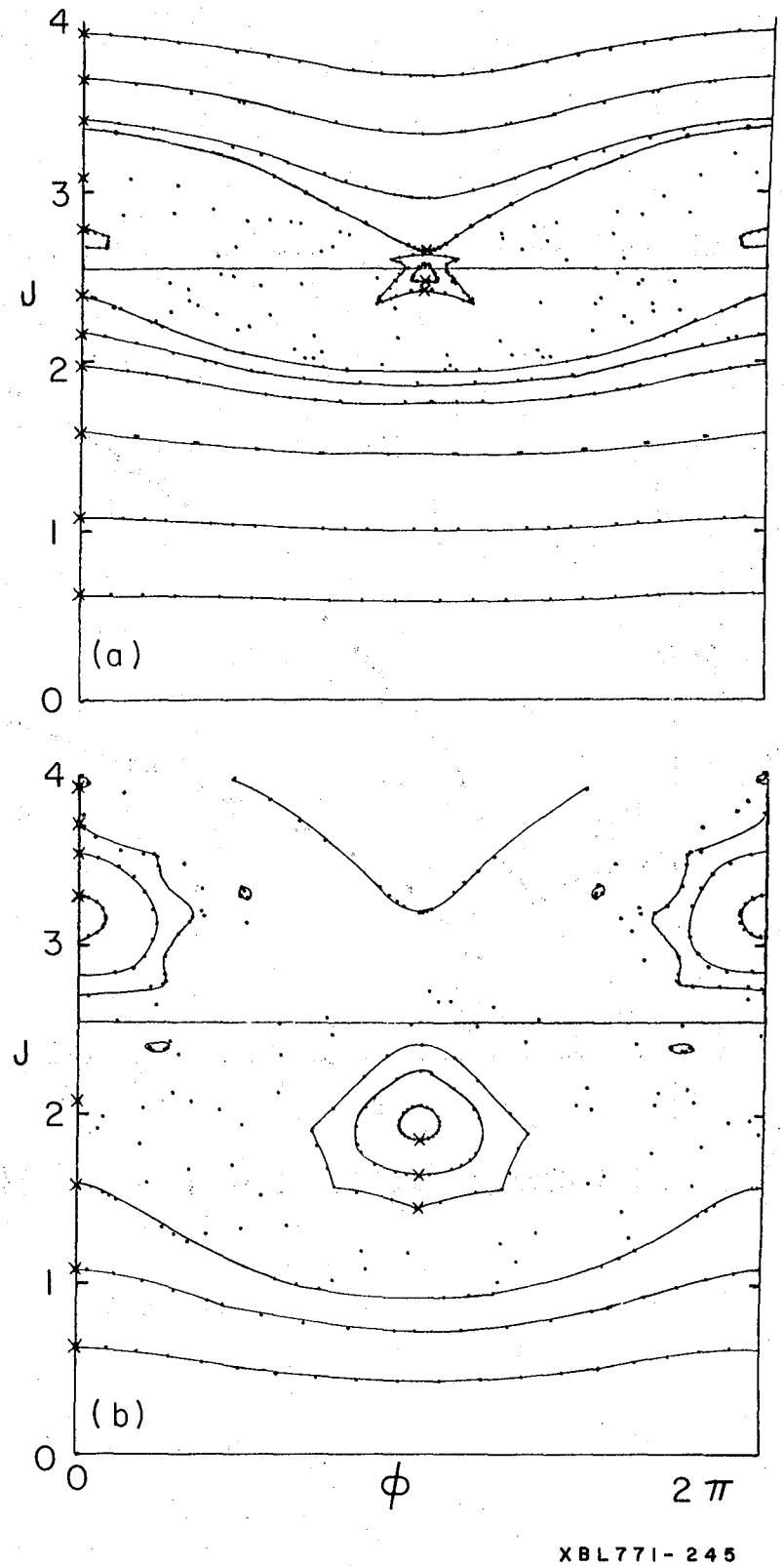

Fig. 35

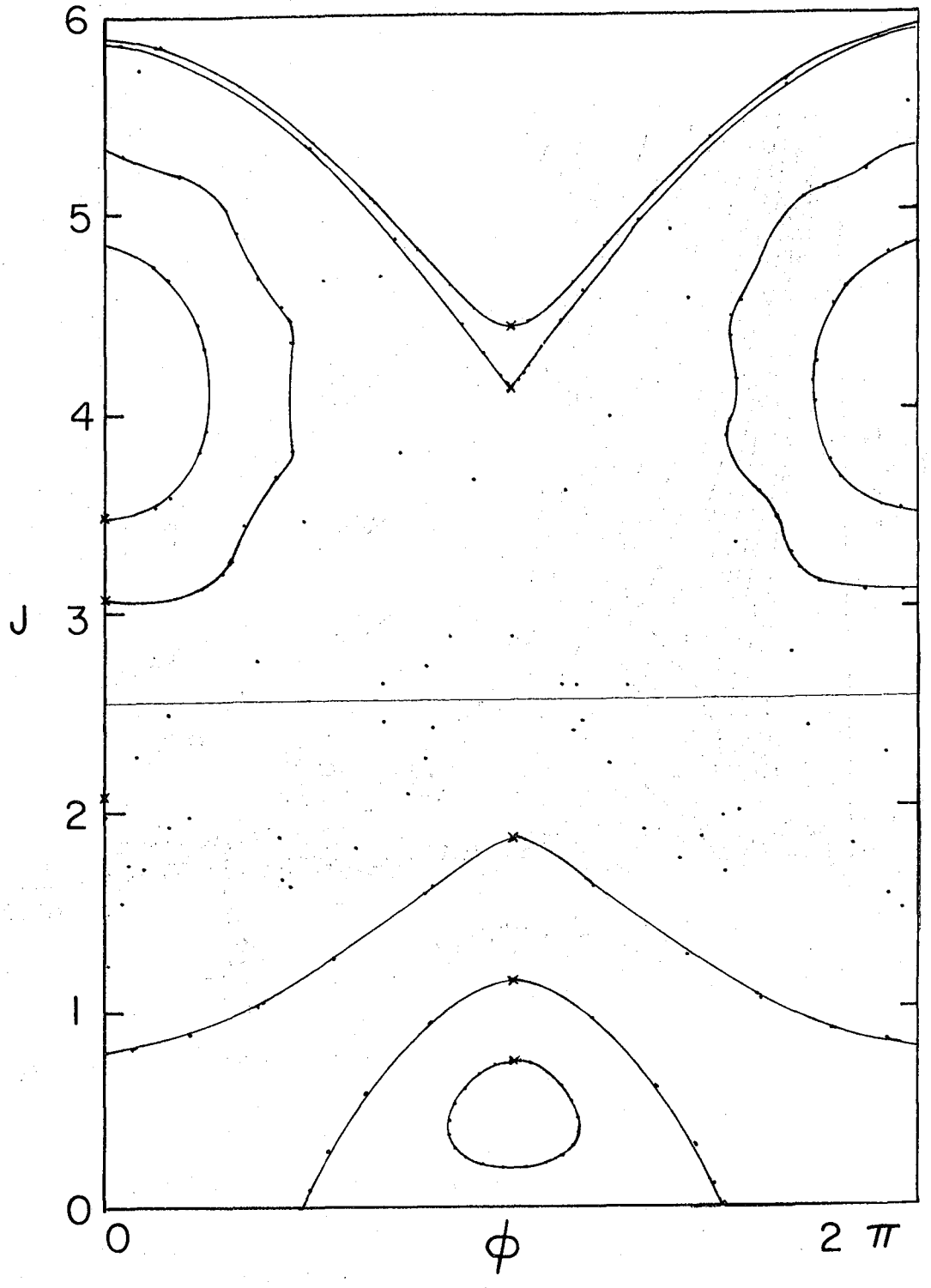

XBL 771-244

Fig. 36

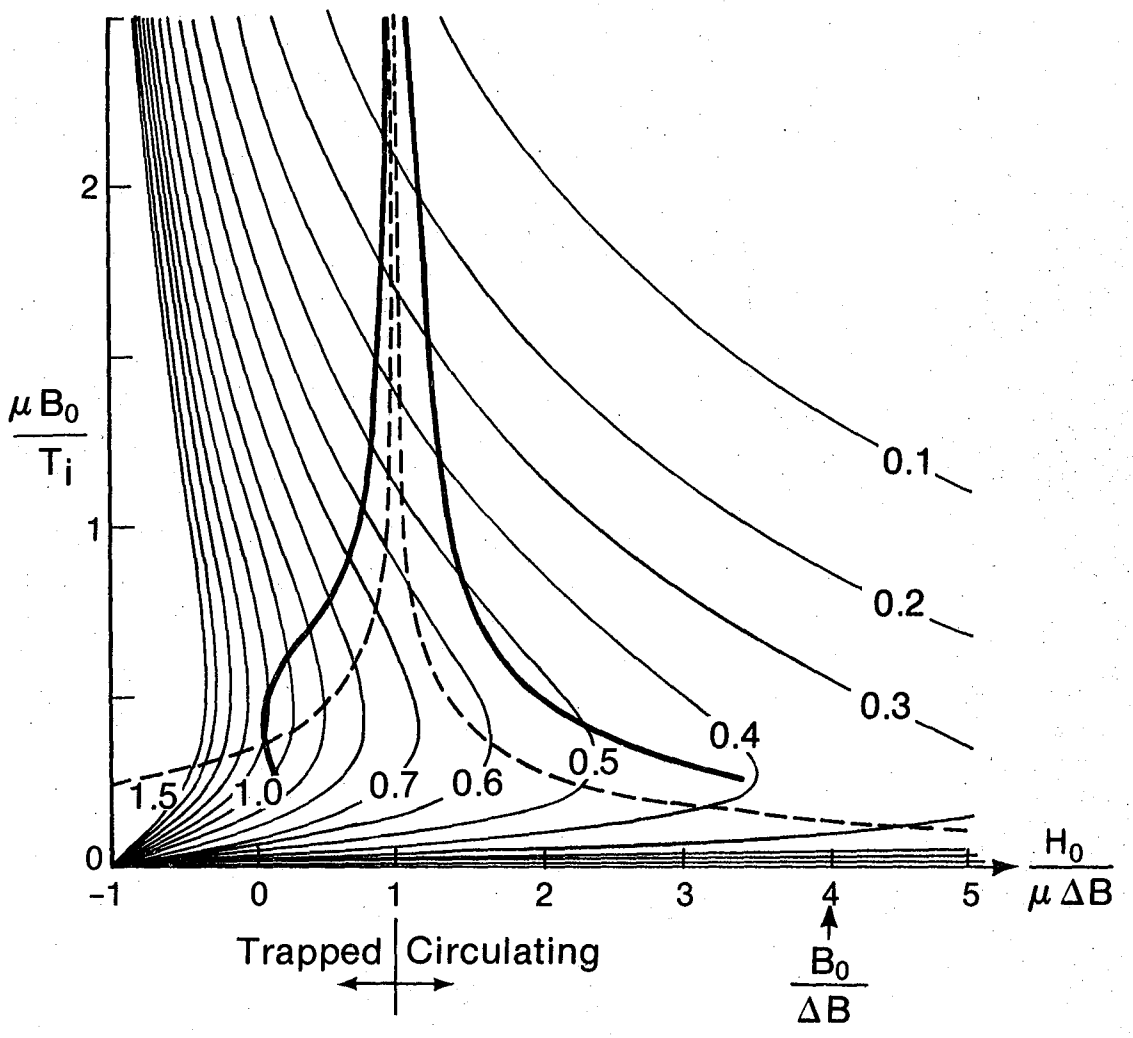

XBL772-292

Fig. 37

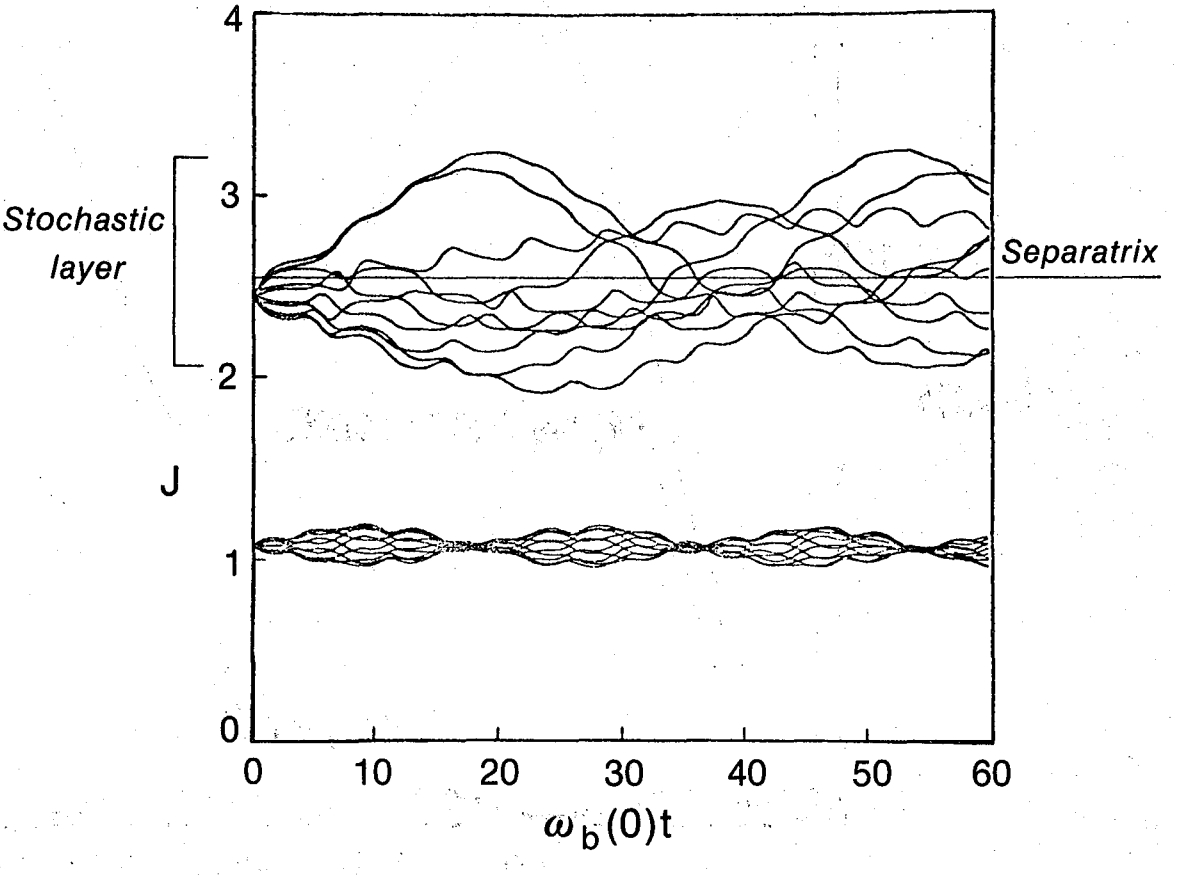

XBL 772-288

Fig. 38

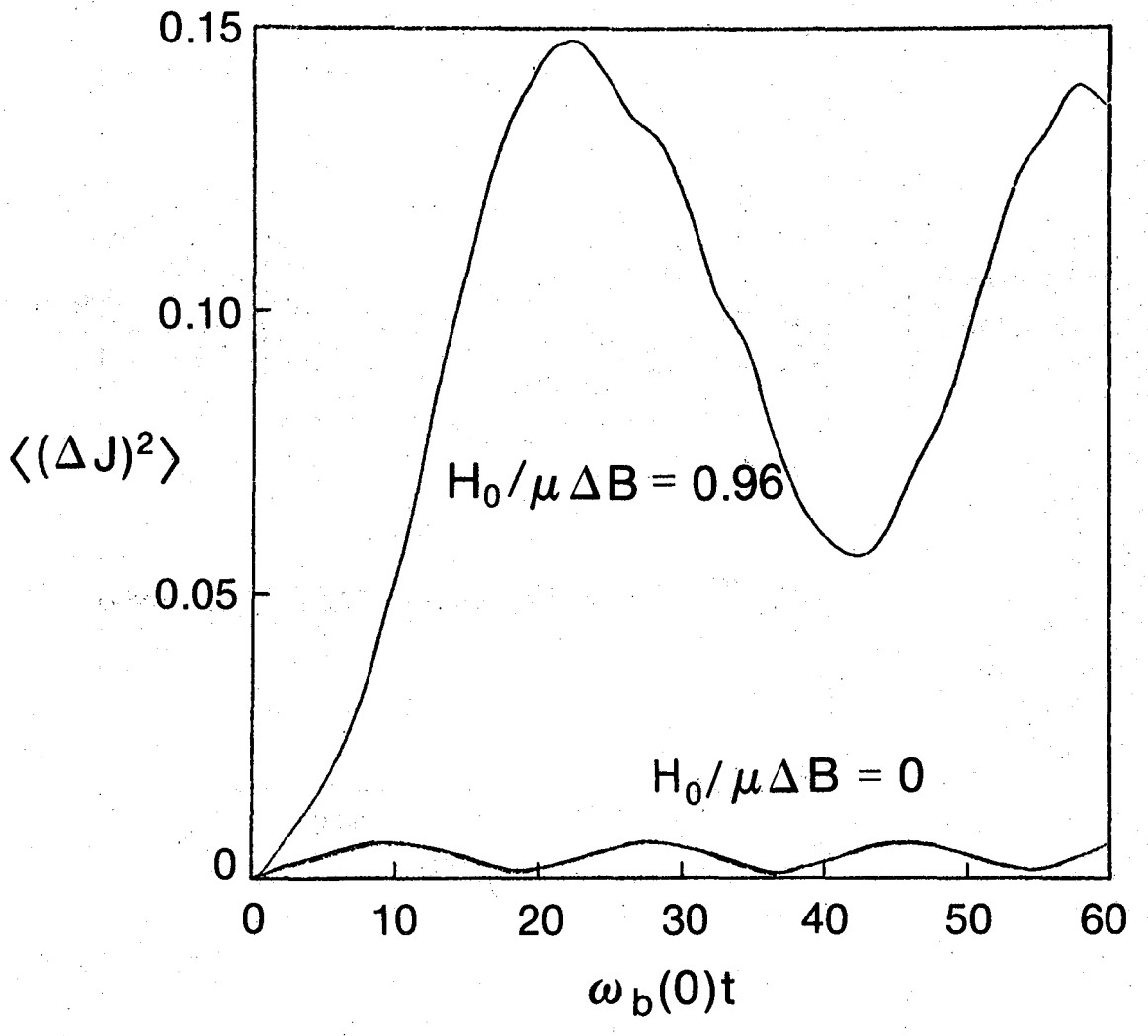

XBL 772-289

Fig. 39

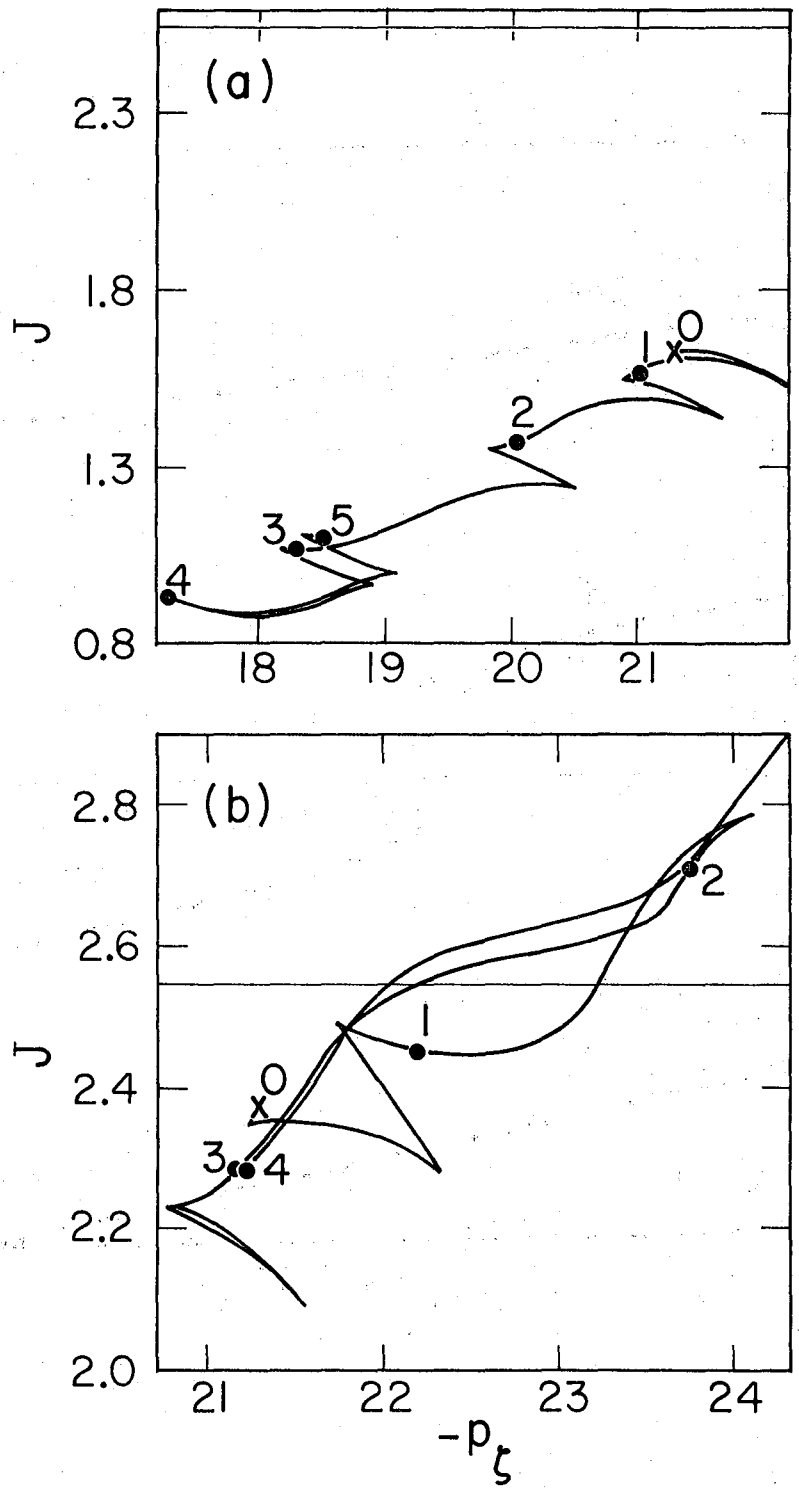
(a)
2.3
1.8
1.3
0.8
J
18
19
20
21
0
1
2
3
4
5
(b)
2.8
2.6
2.4
2.2
2.0
J
21
22
23
24
$-p_\zeta$
0
1
2
3
4
XBL779-1846

Fig. 40

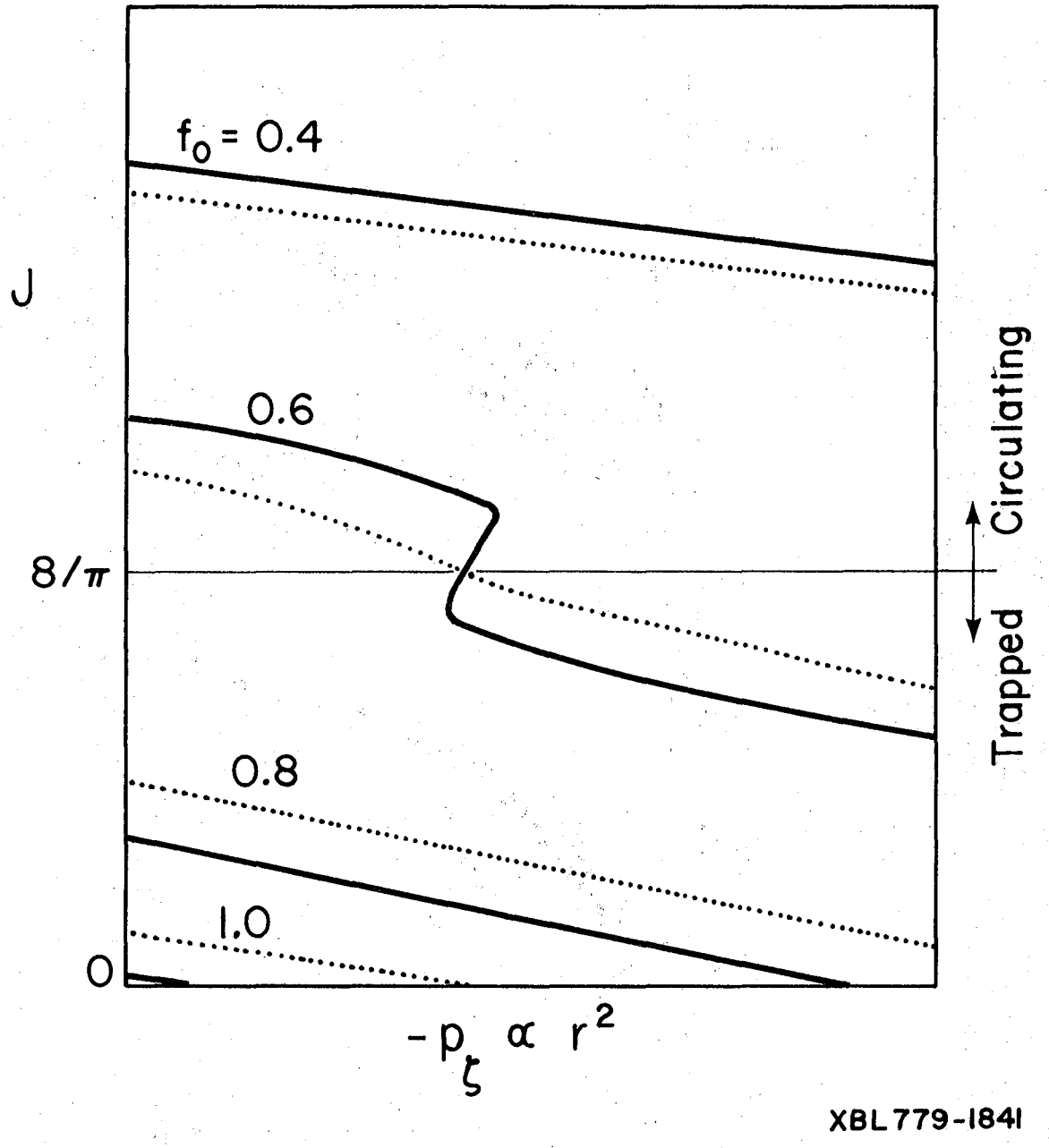
$f_0 = 0.4$
J
0.6
$8/\pi$
Circulating
Trapped
0.8
1.0
0
$-p_\zeta \propto r^2$
XBL779-1841

Fig. 41

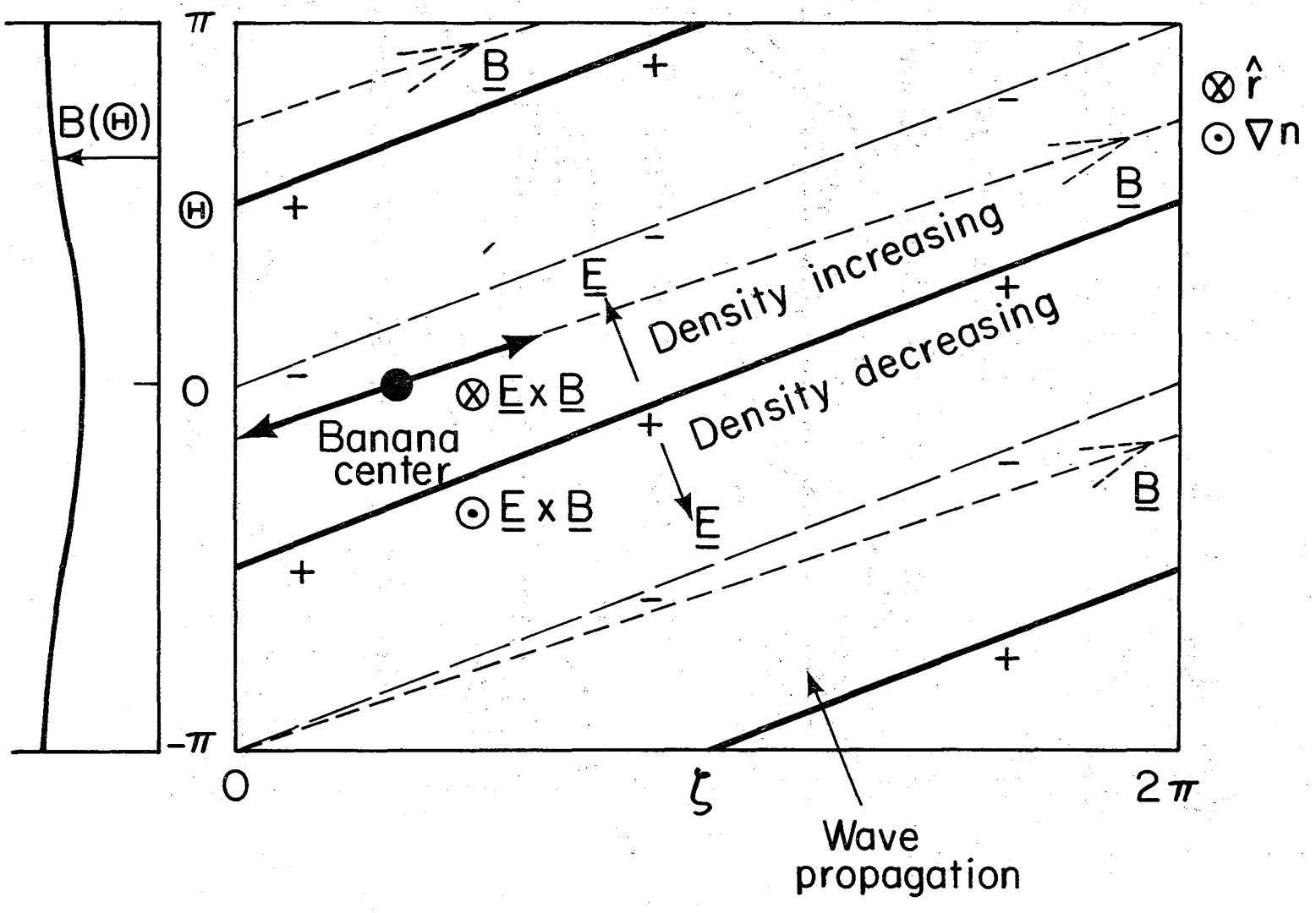

Fig. 42

XBL773-611

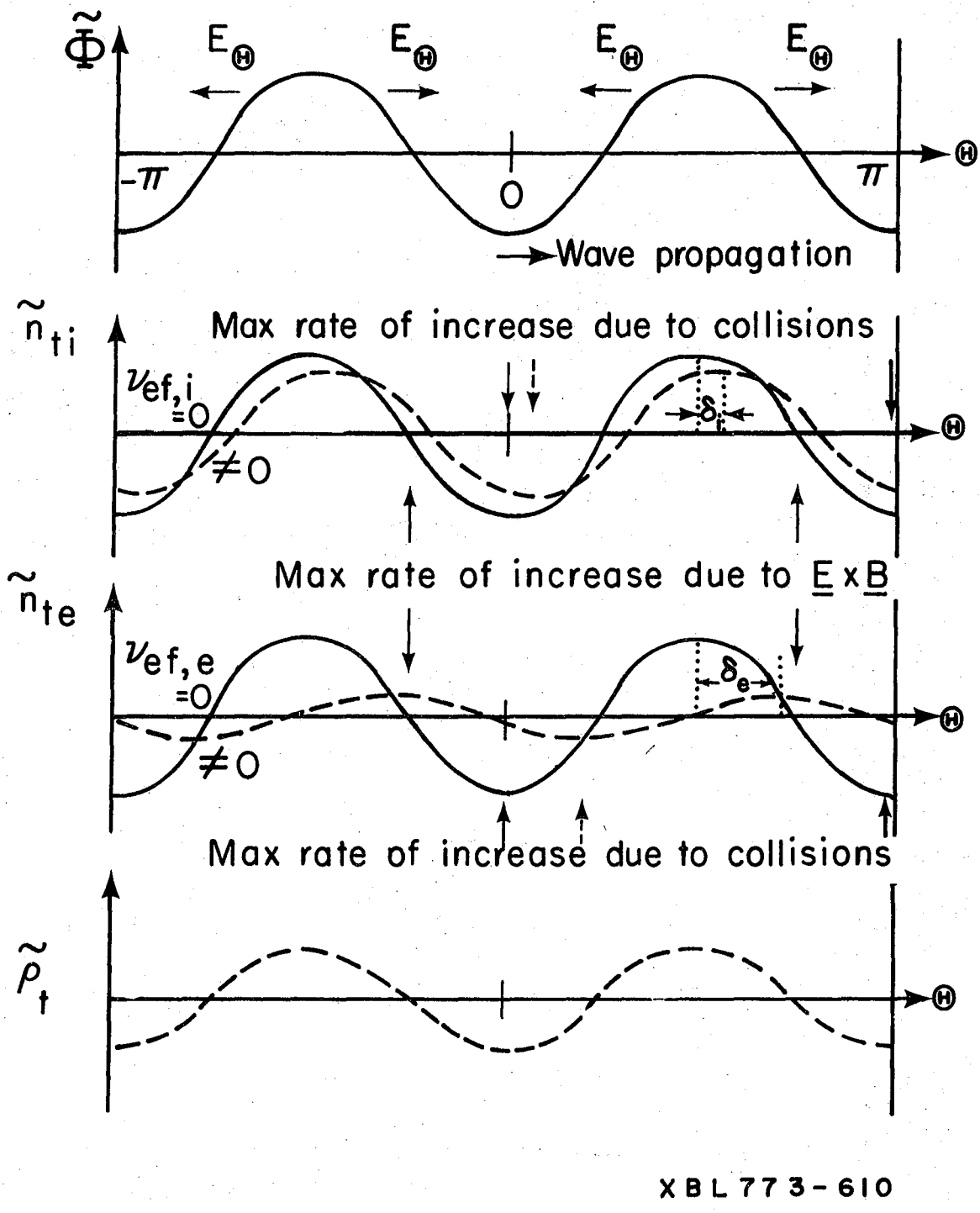
$\tilde{\Phi}$
E_Θ
E_Θ
E_Θ
E_Θ
$-\pi$
0
π
Θ
Wave propagation
$\tilde{n}_{ti}$
Max rate of increase due to collisions
$\nu_{ef,i}$
=0
≠0
δ_i
Max rate of increase due to E x B
$\tilde{n}_{te}$
$\nu_{ef,e}$
=0
≠0
δ_e
Max rate of increase due to collisions
$\tilde{\rho}_t$
XBL773-610

Fig. 43

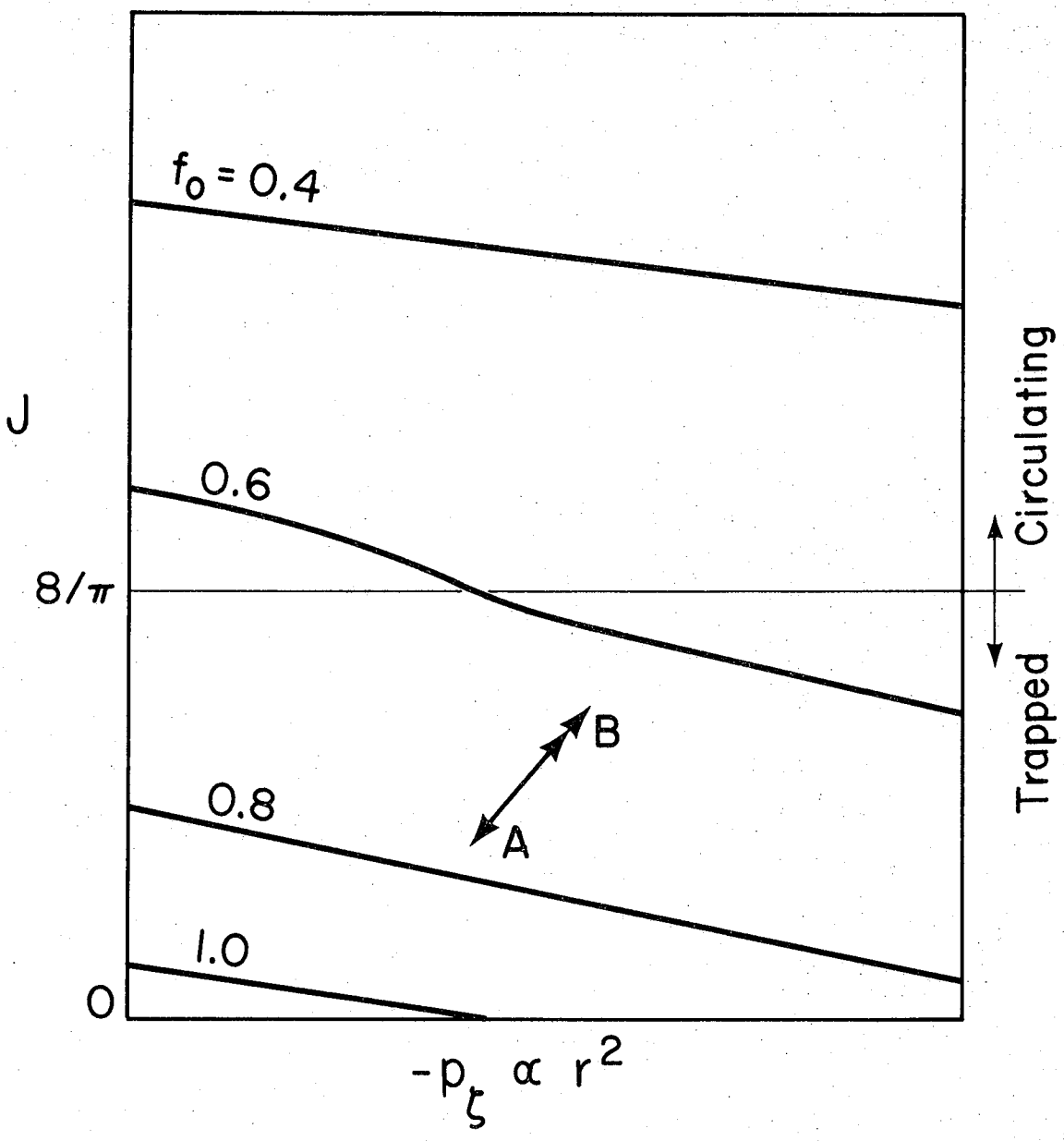
$f_0 = 0.4$
J
0.6
$8/\pi$
Circulating
Trapped
B
A
0.8
1.0
0
$-p_\zeta \propto r^2$
XBL779-1843

Fig. 44

This report was done with support from the Department of Energy. Any conclusions or opinions expressed in this report represent solely those of the author(s) and not necessarily those of The Regents of the University of California, the Lawrence Berkeley Laboratory or the Department of Energy.

TECHNICAL INFORMATION DEPARTMENT
LAWRENCE BERKELEY LABORATORY
UNIVERSITY OF CALIFORNIA
BERKELEY, CALIFORNIA 94720